STETSON1971

ARL 71-0127
AUGUST 1971

Aerospace Research Laboratories

EXPERIMENTAL RESULTS OF LAMINAR BOUNDARY LAYER SEPARATION ON A SLENDER CONE AT ANGLE OF ATTACK AT $M_\infty = 14.2$

KENNETH F. STETSON

FLUID DYNAMICS FACILITIES RESEARCH LABORATORY

PROJECT NO. 7065

see flat file for large prints of some.
- fig. 48 30° at 14° AoA several prints incl. details leeward side
- fig. 57 30° cone at 18° AoA

AIR FORCE SYSTEMS COMMAND
United States Air Force

FOREWORD

This report was prepared by Kenneth F. Stetson of the Fluid Dynamics Facilities Research Laboratory, Aerospace Research Laboratories, Wright-Patterson Air Force Base, Ohio.

The author would like to acknowledge support and suggestions of ARL personnel, particularly those of Mr. Elmer G. Johnson, Director, Fluid Dynamics Facilities Research Laboratory, Captain E. Ojdana and Mr. D. Murray. Also, the helpful discussions with and suggestions of Dr. Frank Fernandez, Aerospace Corporation, are gratefully acknowledged.

ABSTRACT

Wind tunnel experiments with a 5.6 degree half angle cone at $M_\infty = 14.2$ indicated that the three-dimensional separation bubble concept was not the correct flow field model for these data. Based on data consisting of surface pressure measurements, pitot pressure surveys, and surface oil flow patterns, a new model for hypersonic three-dimensional separation is proposed. This model contains symmetrical supersonic helical vortices with an attachment line on the most leeward ray. The vortices are in contact with the surface (at least up to $\alpha = 18°$) and there is no subsonic reverse flow or singular points associated with the vortex pattern.

TABLE OF CONTENTS

LIST OF ILLUSTRATIONS

NOMENCLATURE

C_p	pressure coefficient
L	total model surface length
M_∞	freestream Mach number
p_B	base pressure
p	cone surface pressure
p_∞	freestream pressure
p_o	wind tunnel reservoir pressure
p_{T_2}	pitot pressure
p_{st}	stagnation pressure on model
r	radial distance from center of model base
Re_∞/ft	unit Reynolds number based on freestream conditions
R_B	model base radius
R_N	nose radius
T_o	wind tunnel reservoir temperature
T_w	model surface temperature
X	distance along the cone surface from the tip or from the zero angle of attack stagnation point
α	angle of attack
θ_c	cone half angle
ϕ	cone circumferential angle, measured in a clockwise direction based on a head-on view, with the most windward ray being designated $\phi = 0$

SECTION I

INTRODUCTION

The leeward region of a slender body at angle of attack has associated with it a complex viscous-inviscid interaction and may include a three-dimensional separated flow field. Considerable progress has been made in calculating three-dimensional flow fields about cones at angles of attack up to about the cone half angle (for example, Refs 1-6); however, these techniques have not proven capable of making an adequate prediction of boundary layer separation or producing a solution downstream of separation. Limited experimental data[7-12] have only partially defined the leeward flow field characteristics.

One point that has received little attention in previous investigations is that of communication, or lack of it, between the separated flow field on the leeward region of a cone and the separated flow field associated with the base. This aspect of separation was briefly explored in Ref 13. Figure 1 shows schematically the separated flow fields associated with a cone at angle of attack. Region I represents the fluid which has separated from the leeward side of the cone and Region II represents the fluid which has separated upon leaving the trailing edge of the cone. It might logically be concluded, based upon knowledge obtained mainly from two-dimensional studies, that these two separated regions must be tied together and that subsonic communication between the two regions would result in a nearly equal pressure throughout. This is certainly the case at very high angles of attack (for example, $\alpha \rightarrow 90$ degrees) where both flow fields merge into one base flow-type region. It was found[13] that two types of separated flow situations may be associated with a cone at angle of attack. One case is where there is no communication between the two separated regions and the pressures on the leeward surface of the cone are always larger than base pressure. The leeward separated flow field for this case is analogous to that of an infinitely long cone. At angles of attack greater than that which was required to equalize base and leeward pressures a new flow feature was observed, producing the second separated flow case, the "base interference" case. This case involved an interaction of the two separated regions and the appearance of a secondary separation on the rear portion of the cone leeward surface. This case clearly represents additional complexities to an already complex flow field structure. Most experimental investigations have not provided adequate base pressure data to evaluate this aspect of separation. It is believed that the results of Tracy[7] represent an example of the "infinite cone" case and some of the data of Feldhuhn, Winkelmann and Pasiuk[12] very likely illustrates the "base interference" case.

The objective of this present investigation was to provide additional experimental data for the infinite cone-type of separation to further describe this complicated flow phenomena. The more complex, base interference-type, separation has been left for future investigations.

SECTION II

MODEL, INSTRUMENTATION AND TEST FACILITY

1. MODEL

The model used was a sting-mounted, 5.6 degree half-angle cone with three nose tip configurations; a sharp tip and nose radii equal to 10% and 30% of the base radius. The sharp tip had a tip diameter slightly over 0.001 inch. The model base diameter was three inches and the sting diameter was one inch. The cone circumferential angle (ϕ) was measured in a clockwise direction based on a head-on view, with the most windward ray being designated $\phi = 0$. The cone surface was instrumented with pressure orifices along a cone ray, with additional pressure orifices for checking aerodynamic alignment and for measuring base pressures. Complete cone surface pressure distributions were obtained by rotating the model about its axis between runs.

2. INSTRUMENTATION

Surface pressures were measured with variable reluctance differential pressure transducers that responded linearly with pressure. Repeated calibration of these transducers have indicated that they are accurate to about ±2% of measured values. These pressure transducers are discussed in detail in Ref 14.

A simple pitot probe was constructed for pitot pressure surveys and a photograph of the probe mounted in the tunnel is shown in Fig 2. This probe was made with 0.072 O.D. pressure tubing (0.054 I.D.) with a one-inch knife edge for support and streamlining. The tube extended two inches beyond the knife edge and had a 10 degree internal bevel at the open end. The probe was mounted on the wind axis system (i.e., the axis of the probe was parallel to the direction of the free stream velocity vector and the probe traverses were made in a plane normal to the free stream velocity vector).

The oil formula used for the oil flow experiments was as follows:

Silicone oil:	7cc - 10 centistokes 3cc - 100 centistokes
Titanium dioxide:	3cc
Oleic acid:	2 drops

3. TEST FACILITY

The experiments were conducted in the ARL 20-inch wind tunnel at a Mach number of 14.2 and a free stream Reynolds number per foot of 0.62×10^6. The ratio of wall-to-total temperature was approximately 0.29 for most of these experiments. Average test conditions were as follows:

$$p_o = 1600 \text{ psia}$$

$$T_o = 2050°R$$

$$p_\infty = 0.0032 \text{ psia}$$

$$p_{st} = 0.85 \text{ psia}$$

A few additional experiments were performed at a lower free stream Reynolds number per foot of 0.39×10^6.

A more complete description of this test facility can be found in Ref 15.

Ken - wall was cold.
11/27/04, he will look for
prints. He watched the
oil flow, no singular pt.
nose oil flowed into sep. region

SECTION III

RESULTS

Cone surface pressures and surface oil flow patterns were obtained at angles of attack up to 18 degrees and pitot pressure surveys were made at several angles, with most of the pitot pressure data being obtained at 10 degrees angle of attack. Cone surface pressure

distributions along rays and circumferentially are shown for a number of conditions and representative samples of oil flow results and pitot pressure surveys are included.

As will be discussed in more detail later, the pressure data may be intuitively interpreted as a separated flow condition, but these data, per se, do not verify that the flow is actually separated nor do they permit the location of the separation lines. Additional information is required for such separation determinations. The surface oil flow technique was found to be a simple and easy method of obtaining this important three-dimensional separation information. The surface oil flow technique is a well established method of flow visualization in wind tunnels. Since the skin friction force causes the oil to flow, the patterns produced indicate skin friction lines or surface streamlines. The validity of this technique has been analytically evaluated by Squire[16] and he concluded that: (1) the oil follows the boundary layer surface streamline except near separation where it tends to form an envelope upstream of the true separation envelope; and (2) the effect of the oil flow on the motion of the boundary layer is very small. Experience has indeed indicated that the presence of the oil on the model surface has little effect on the boundary layer flow and that the technique provides reliable information regarding surface streamline direction, boundary-layer separation and boundary-layer transition.

The sharp cone and the blunt cone results are presented separately.

1. SHARP CONE

Figure 3 shows pressure distributions along the most leeward ray (ϕ = 180°) for several angles of attack. At zero angle of attack the cone surface pressure was constant, whereas at angle of attack a pressure gradient developed in the leeward region. Figure 4 presents an example of circumferential surface pressure distributions in the leeward region of the cone for angles of attack up to 14 degrees. The general features of these data are similar to the data obtained by Tracy,[7] Rainbird[8-9] and Feldhuhn, Winkelmann and Pasiuk[12] and are characteristic of the pressure distributions identified with symmetrical vortices. That is, there exists symmetrical minimum pressure locations off the leeward plane of symmetry, followed by an adverse pressure gradient in the cross-flow plane. At 14 degrees angle of attack, which is 2-1/2 times the cone half angle, the cone surface pressures are still greater than base pressure. This situation infers there was no subsonic communication between the cone surface and the base region and raises the question of whether such a flow situation would exist if the leeward separated flow field contained subsonic reverse flow. These data are then analogous to that which would be obtained on an infinitely long cone. Additional increases in angle of attack would produce further reductions in cone surface pressures and subsequent interaction with the base flow field.[13] The leeward base pressures were essentially constant in the angle of attack range from

zero to 14 degrees. The locations of the separation line were obtained from the oil flow photographs and are shown on Figure 4. Incipient separation occurred at approximately four degrees angle of attack, or about 70% of the cone half angle. As the angle of attack was increased the circumferential angle at which separation occurred changed from 11 to 27 degrees off the plane of symmetry. It does not appear possible to identify the separation lines with a unique feature of these pressure curves in a manner analogous to the two-dimensional case where the inflection point of the pressure distribution curve may be used.

Figures 5, 6 and 7 are examples of the circumferential pressure distributions at various positions along the cone. These data show a similarity of features throughout, which would be expected for a sharp cone. An interesting point is the tip effect which is shown most clearly by the curved separation lines.

Figures 8 through 15 are photographs of oil flow on a sharp cone. Several oil application patterns were tried (dots, circumferential strips, and longitudinal strips) and generally the best results were obtained by applying the oil with a brush in longitudinal strips in the windward region in conjunction with several circumferential strips in the leeward region. The tests were visually observed through the tunnel window to determine when to terminate the run. Run times were typically about two minutes. The pattern of converging surface streamlines from both sides of the separation line and diverging surface streamlines from the reattachment line on the leeward plane of symmetry was observed. Four degrees angle of attack appeared to be close to the incipient separation condition, with the rear portion of the cone exhibiting a fairly well developed separation line, whereas the forward half of the cone showed only an accumulation of oil in the leeward region with no definitive line. Figure 13 is a view of the leeward and side region, looking about 45 degrees off the leeward plane of symmetry. The distinctive cross-flow pattern on the side of the cone resulted from oil from the windward side of the cone flowing past the pressure orifices. Figures 11, 12, 14 and 15 show oil flow on a thin plate in the leeward plane of symmetry. The plate had a sharp leading edge and was sized to keep it within the aerodynamic shadow. The flow toward the cone surface is consistent with the concept of twin vortices with an attachment line on the plane of symmetry. Figure 16 contains separation angle data obtained from the oil flow photographs. The separation lines exhibited curvature for all of these tests, indicating considerable tip effect from the sharp tip.

Pitot pressure surveys were made of the leeward region to obtain information about the flow field. For example, supporting data was desired to confirm the previous suspicion that the vortices contained essentially supersonic flow and also to obtain general information about the size of the vortices and the existance of imbedded shocks. The pitot probe traverses were made in a plane normal to the free stream velocity vector, covering the region from free stream to the cone surface. Since this involved measuring a wide range of pressures

(for example, from less than a millimeter of mercury to over 100 millimeters of mercury) the following procedure was used. The pitot probe was made relatively large to reduce the response time; two pressure transducers were used (one that would accurately measure pressures of the order of a millimeter of mercury and a second transducer to measure the higher pressures); the pitot probe was first brought in to the cone surface and left there for several seconds until a steady pressure was observed, then a slow outward traverse was made, requiring about three minutes to complete. By starting the traverses at the cone surface, it was possible to measure an increasing pressure, thus helping to reduce the response time of the probe. It was found that inward traverses, even if accomplished very slowly, presented response time problems in measuring a reducing pressure. Pitot probes of this type have been found to be relatively insensitive to small angles of attack and are accurate to within a few percent even when the axis of probe and the velocity vector are different by as much as 30 degrees. It was not possible in these experiments to access the loss of pitot pressure due to the probe angle of attack; however, such effects are believed to be small over most of the region probed, and the results are believed to be adequate for the general information desired. It was not possible to probe an attached boundary layer with this pitot probe due to the large size of probe compared to the boundary layer thickness.

Figure 17 is a sample of the pitot pressure profiles obtained, going from the body surface out through the bow shock and terminating in the free stream. Figure 18 shows the shock location at 10 degrees angle of attack as obtained from five pitot probe traverses. A significant point is the curvature of the bow shock in the tip region. This is consistent with the tip effects observed in the surface pressure distributions and separation lines.

Figure 19 shows lines of constant pitot pressure, obtained by making a number of pitot probe traverses. Significant points are the large displacement of the inviscid flow, the symmetrical valleys of high-energy fluid which are presumably associated with the downward flow of the twin vortices, the region of lower energy fluid in the plane of symmetry between the vortices, and the absence of imbedded shocks.

In order to make approximate Mach number calculations of the leeward flow field, with particular interest in the region where the vortices would be expected, a constant static pressure equal to the surface pressure was assumed. Using the data of Fig 19 produced the Mach number contour lines shown in Fig 20. Supersonic flow is indicated throughout the region. Even with an allowance for a reasonable error in static pressure this general conclusion of supersonic flow is not altered, thus further substantiating the concept of a supersonic vortex. The existence of supersonic vortices could be the reason why there was no subsonic communication between the cone attached vortices and the base region.

A few exploratory experiments were performed to evaluate the feasibility of conducting additional experiments at lower Reynolds numbers and with variable model wall temperature. Data were obtained at a free stream unit Reynolds number of 0.39×10^6 and samples of the comparison of the data for the two Reynolds numbers are shown in Figs 21 and 22. No significant differences were noted, therefore it was concluded that a wind tunnel with a greater range of test conditions is required to evaluate Reynolds number effects on flow about a slender body at angle of attack. The existing model was not suitable for a study to investigate variable wall temperature effects and a new model would be required for such a program. However, since the model was made of brass, small changes in model temperature could be accomplished and some preliminary data could be obtained. Four thermocouples were mounted just under the surface to monitor model temperatures. The usual run procedure started the test with the model at room temperature and aerodynamic heating during the test produced some heating of the model. Typical temperature increases would be about 50 degrees on the rear portion of the model and about 100 degrees near the nose. A colder model surface (approximately 475°R) was obtained by cooling the model with liquid nitrogen and making short runs in order to obtain the data before any appreciable increase in model temperature occurred. The hotter model surface (approximately 750°R) was obtained by first making a run of about five minutes to heat the model, then shutting down for a few minutes to allow the model to arrive at a uniform temperature, then making the data run. Figure 23 contains a sample of the data obtained. There was a noticeable effect of wall temperature, with the cooler wall showing a reduced tip effect at six degrees angle of attack. Additional data showing the effects of model wall temperature will be shown later with the 10% bluntness results.

2. BLUNT CONE

The two blunt nose tips used (R_N/R_B = .10 and .30) provided a convenient range of bluntness to investigate flow about a slender blunt cone at angle of attack. The 30% bluntness covered the range up to 25.5 nose radii downstream and was good for observing the formation of the vortices. The 10% bluntness extended the range to 94 nose radii downstream and was good for observing the transition of the leeward flow field from a nose-dominated to a cross flow-dominated flow.

Maskell[18] has identified several possible models for three-dimensional separation on a body of revolution at angle of attack. The three-dimensional separation bubble has been considered by many investigators to be the most likely flow field model for separation on a blunt cone at angle of attack. A pictorial representation of this model of separation is shown in Fig 24. Significant features of this model are a separation line which originates from a singular point on the most leeward generator and a separated layer enclosing a "bubble." Upstream of the separation bubble the leeward flow field is nose-dominated, with large favorable pressure gradients, and the boundary layer is attached. The separation bubble concept is

discussed here only for comparison purposes since the results of this present investigation indicated such a model of separation was incorrect (at least for the conditions of these experiments).

a. 30% Bluntness

Figures 25 through 30 present pressure distributions along several rays with increasing angle of attack. Significant features are the large favorable pressure gradients in the neighborhood of the nose tip and the development of large adverse pressure gradients in the windward region with increasing angle of attack.

Figures 31 through 38 are examples of the circumferential pressure distributions obtained with a 30% nose bluntness. At small X/R_N's, the boundary layer is attached and the minimum circumferential pressure occurs on the most leeward ray. At larger X/R_N's, two symmetrical minimum pressure locations occur off the leeward plane of symmetry, characteristic of vortex flow. The points shown on the curves are separation line data obtained from the oil flow photographs. At 6 degrees angle of attack separation occurs on the rear portion of the cone and the origin of separation occurs closer to the nose tip with increasing angle of attack. The initial portion of the separation line exhibits considerable curvature, developing in width (in terms of circumferential angle) to a value larger than observed on the sharp cone, followed by a gradual reduction, apparently approaching the sharp cone value. The cone surface pressures were always larger than base pressure, even at the maximum angle of attack of 18 degrees which was 3.2 times the cone half angle. Figures 39 through 41 present circumferential pressure distributions from the most windward to the most leeward ray, for three axial locations on the 30% blunt cone.

Figures 42 through 51 are photographs of oil flow on the cone with 30% nose bluntness. Oil was applied with a brush to the windward region and the nose cap. The tests were observed through the tunnel window. The oil from the windward region was observed to flow around the cone, turning toward the rear of the cone as it approached the separation line. At the separation line the oil accumulated and proceeded to travel down the separation line to the rear of the cone. The origin of the separation lines was an interesting area to observe. There was no evidence of reverse flow and a singular point. In terms of skin friction, the leeward flow was seen initially to have a lateral component in the direction toward the leeward plane of symmetry. This lateral component of skin friction then reversed its sign as the flow traveled downstream. Two symmetrical separation lines developed downstream of the region where the lateral component of skin friction passed through zero. The longitudinal component of skin friction was always finite. This fact could be verified by observing the oil flowing from the attached region behind the nose, through the region of zero lateral skin friction, and into the vortex region. The analysis of Wang[19] is the only one known to this author to be compatible with this observed phenomena. The plate in the leeward plane of symmetry is the same one shown previously with the sharp cone.

Figures 52 through 54 are pitot pressure contour maps for the blunt cone at 10 degrees angle of attack. The first location of $X/R_N = 8$ is in the region where the lateral component of skin friction is zero and the boundary layer is still attached. The second location of $X/R_N = 14.7$ is slightly downstream of the apparent origin of separation. Only small effects are observed in the pitot pressure contours. The third location of $X/R_N = 23.6$ is in the region of maximum angular width. Significant differences between these data and the previously discussed case for the sharp cone are found in the leeward plane of symmetry and the displacement of the inviscid flow. The difference between the sharp and blunt cones in the plane of symmetry is believed to be due to the physical distance between the vortices on the blunt cone, produced by the longitudinal flow from the nose region.

b. 10% Bluntness

Figures 55 and 56 show the longitudinal pressure variations on the leeward and windward planes of symmetry for several angles of attack. Figures 57 through 61 show the pressure distributions along several rays at various angles of attack. The over-expansion, recompression and return to the approximate sharp cone value is a dominant feature of the flow.

Figures 62 through 68 are examples of the circumferential pressure distributions on the cone with 10% bluntness. The data at 18 degrees angle of attack represents a situation where some base interference is experienced. This angle of attack is near the maximum angle attainable for this configuration. At this angle the test cabin pressure has increased slightly, the model support interference has increased and, as a result, the base pressure (p_B/p_∞) increased from 0.7 to approximately 1.0. The open data points indicate locations on the cone where the pressure is equal or less than base pressure. A recompression occurs on the rear portion of the cone such that the minimum pressures at the trailing edge of the cone are approximately equal to base pressure. Previous experiments of base interference[13] for a sharp cone found that the interactions were confined to the rear quarter of the cone. The cone surface pressures on the first three-quarters of the cone were similar to those of the infinite cone case, and the flow was unaware of the fact that it had expanded to pressures significantly below base pressure levels. On the rear portion of the cone where the recompression occurred, two symmetrical secondary separations were observed in the minimum pressure regions. Oil flow tests indicated some reverse flow in these secondary separation regions. The data of Figure 68 indicates in a small way these same characteristics of base interference.

An interesting point to observe is the number of nose radii required for the circumferential pressure distributions to return to an equivalent sharp cone pressure distribution. These results are

shown in Figure 69. The blunt nose, which dominated the flow field for the first few nose radii downstream, lost its influence in a relatively short distance.

Figures 70 through 77 are photographs of oil flow on the cone with 10% nose bluntness. At 4 degrees angle of attack a separated region started to develop at the rear of the cone surface, indicating incipient separation at the same angle of attack as the sharp cone. Such a similarity would be expected as the blunt cone flow field approached a cross-flow-dominated region. At 10 degrees angle of attack the separation line for the cone with 10% bluntness returned to a straight line along a cone generator, 29 degrees off the leeward plane of symmetry. The sharp cone separation line at 10 degrees angle of attack exhibited some curvature and was nearly straight at the rear of the cone, 28 degrees off the plane of symmetry.

Some differences in the over-expansion and subsequent recompression were observed between the 10% and 30% nose bluntness configurations. It was considered of interest to see how these data correlated in terms of a bluntness parameter in the manner of Cheng.[20] An equivalent cone concept was utilized which assumed the pressure distribution on the windward plane of symmetry of a cone at angle of attack is equivalent to a cone of half angle ($\theta_c + \alpha$) at zero angle of attack. The results of such a correlation are shown in Figs 78 through 80. The dashed curve was obtained from a General Electric Company inviscid solution for zero angle of attack.[21-23] These results are felt to be of interest; however, the reason for the noted differences between the 10% and 30% bluntness is not apparent to this author.

Exploratory experiments to look at model wall temperature effects were conducted with the 10% nose bluntness configuration. These experiments were performed in the same manner as discussed previously under the sharp cone results. Figure 81 shows an example of results obtained. These preliminary data indicate that cooling the wall inhibits separation since the circumferential adverse pressure gradients are diminished and first appearance of an adverse gradient occurs further downstream. The effect of wall temperature on three-dimensional separation is believed to be an area which should be pursued in future investigations.

SECTION IV

CONCLUSIONS

A new model for hypersonic three-dimensional separation on a cone at angle of attack is proposed. This model contains symmetrical supersonic helical vortices with an attachment line on the most leeward ray. The vortices are in contact with the surface (at least up to $\alpha = 18°$) and there is no subsonic reverse flow or singular points associated with the vortex pattern. Figure 82 is a conceptual drawing of this model of separation on a slender blunt cone at angle of attack, using "stream ribbons" to illustrate the vortex flow. Separation on a blunt cone, as well as the sharp cone, appears to be basically a cross-flow phenomenon.

Two types of separation on a cone at angle of attack are identified. For one type there is no subsonic communication between the cone vortices and cone base region and the pressures on the leeward surface of the cone are always larger than base pressure. This case is referred to as the infinite cone case since the cone vortex flow field is analogous to that which would be obtained on an infinitely long cone. At angles of attack greater than that which is required to equalize base and leeward pressures a new flow feature is observed, producing the second type of separated flow, the base interference case. This case involves an interaction of the two separated regions and the appearance of a secondary separation on the rear portion of the cone leeward surface.

Although the cone surface pressure may be intuitively interpreted as a separated flow condition, these data, per se, do not verify that the flow is actually separated nor do they permit the location of the separation lines. That is, it does not appear possible to identify the separation lines with a unique feature of the pressure curves in a manner analogous to the two-dimensional case where the inflection point of the pressure distribution curve may be used. The surface oil flow technique was found to be a simple and easy method of obtaining this important three-dimensional separation information.

1. SHARP CONE RESULTS

a. Incipient separation occurred at approximately 4 degrees angle of attack ($\alpha/\theta_c \simeq 0.7$).

b. At angle of attack the leeward region exhibited a tip effect which was observed in the form of a curved bow shock wave, curved separation lines, and a longitudinal pressure gradient.

c. Cooling the model wall appeared to reduce the tip effect.

d. Pitot pressure surveys indicated a supersonic vortex flow, a large displacement of the inviscid flow in the leeward region, and gave no indication of imbedded shockwaves.

e. At X/L = 0.75 the angle of the separation line varied from 11 degrees off the leeward plane of symmetry at 4 degrees angle of attack to 27 degrees at 14 degrees angle of attack.

f. At 14 degrees angle of attack, which is 2-1/2 times the cone half angle, the cone surface pressures were still greater than base pressure, inferring there was no subsonic communication between the cone surface and the base region.

2. BLUNT CONE RESULTS

a. At small X/R_N's the cone leeward region experienced a large favorable pressure gradient with an attached boundary layer. The minimum circumferential pressure occurred on the leeward plane of symmetry and there was a lateral component of skin friction in the direction toward the plane of symmetry. At larger X/R_N's two symmetrical minimum pressure locations occurred off the leeward plane of symmetry, characteristic of vortex flow. The lateral component of skin friction was now in a direction away from the plane of symmetry. Two symmetrical separation lines developed downstream of the region where the lateral component of skin friction passed through zero. The longitudinal component of skin friction was always finite. The origin of separation occurred closer to the nose tip with increasing angle of attack.

b. Incipient separation occurred at approximately 4 degrees angle of attack.

c. Pitot pressure surveys indicated a supersonic vortex flow and differed from the sharp cone results by less displacement of the inviscid flow and higher energy fluid in the plane of symmetry.

d. The blunt nose, which dominated the flow field for the first few nose radii downstream, lost its influence in a relatively short distance. Distances to return to an equivalent sharp cone pressure distribution varied from 88 nose radii at 5 degrees angle of attack to 35 nose radii at 18 degrees angle of attack.

e. Preliminary data indicated that wall cooling inhibited three-dimensional separation.

REFERENCES

1. Babenko, K.I., Voskresenski, G.P., Lyubimov, A.N. & Rusanov, V.V., "Three Dimensional Flow of an Ideal Gas Past Ideal Smooth Bodies", NASA TT F-380.

2. Der, Joe Jr., "A Study of General Three-Dimensional Boundary Layer Problems by an Exact Numerical Method", AIAA Paper No. 69-138, January 1969.

3. Moretti, G., "Inviscid Flowfield About a Pointed Cone at an Angle of Attack", AIAA Journal, 5, pp 789-791, April 1967.

4. Gonidou, Rene, "Supersonic Flows Around Cones at Incidence", NASA TT F-11, 473, January 1968.

5. Fannelop, T.K., "A Method of Solving the Three-Dimensional Laminar Boundary Layer Equations with Application to a Lifting Reentry Body", AIAA Journal, 6, pp 1075-1084, June 1968.

6. Boericke, R.R., "The Laminary Boundary Layer on a Cone at Incidence in Supersonic Flow", AIAA Paper No. 70-48, January 1970.

7. Tracy, R.R., "Hypersonic Flow Over a Yawed Circular Cone", GALCIT Memo No. 69, August 1963.

8. Rainbird, W.J., "Turbulent Boundary-Layer Growth and Separation on a Yawed Cone", AIAA Journal, 6, pp 2410-2416, December 1968.

9. Rainbird, W.J., "The External Flow Field About Yawed Circular Cones", AGARD Conference Proceeding No. 30, May 1968.

10. Cleary, J.W., "Effects of Angle of Attack and Nose Bluntness on the Hypersonic Flow Over Cones", AIAA Paper No. 66-414, June 1966.

11. George, O.L., Jr., "An Experimental Investigation of the Flow Field Around an Inclined Sharp Cone in Hypersonic Flow", Sandia Laboratories SC-RR-69-577, September 1969.

12. Feldhuhn, R.H., Winkelmann, A.E. & Pasiuk, L., "An Experimental Investigation of the Flow Field Around a Yawed Cone", AIAA Paper No. 70-766, July 1970.

13. Stetson, K.F. & Friberg, E.G., "Communication Between Base and Leeward Region of a Cone at Angle of Attack in a Hypersonic Flow", Aerospace Research Laboratories, ARL 69-0115, July 1969.

14. Murray, D.H. & Ojdana, E.S., "Low Pressure Data Acquisition Techniques in a Hypersonic Wind Tunnel", Proceedings of the 15th National ISA Aerospace Instrumentation Symposium, May 1969.

15. Gregorek, G.M. & Lee, J.D., "Design Performance and Operational Characteristics of the ARL Twenty-Inch Hypersonic Wind Tunnel", ARL 62-392, August 1962.

16. Squire, L.C., "The Motion of a Thin Oil Sheet Under the Boundary Layer of a Body", AGARDograph 70, April 1962.

17. Maltby, R.L., "Flow Visualization in Wind Tunnels Using Indicators", AGARDograph 70, April 1962.

18. Maskell, E.C., "Flow Separation in Three-Dimensions", Royal Aircraft Establishment Report No. 2565, November 1955.

19. Wang, K.C., "Three-Dimensional Laminar Boundary Layer Over Body of Revolution at Incidence: Part III, Solutions Near the Plane of Symmetry", RIAS TR 69-14, September 1969.

20. Cheng, H.K., "Hypersonic Flow with Combined Leading-Edge Bluntness and Boundary-Layer Displacement Effect", CAL Report AF-1285-A-4, August 1960.

21. Clay, J.T., "Nose Bluntness, Cone Angle and Mach Number Effects on the Stability Derivatives of Slender Cones", ARL 67-0185, September 1967.

22. Rie, H., Linkiewicz, E.A. & Bosworth, F.D., "Hypersonic Dynamic Stability: Part III, Unsteady Flow Field Program", FDL-TDR-64-149, January 1967.

23. Friberg, E.G., "Pressure Distribution on a 5.6° Blunt Cone at Mach 14", ARL 68-0208, November 1968.

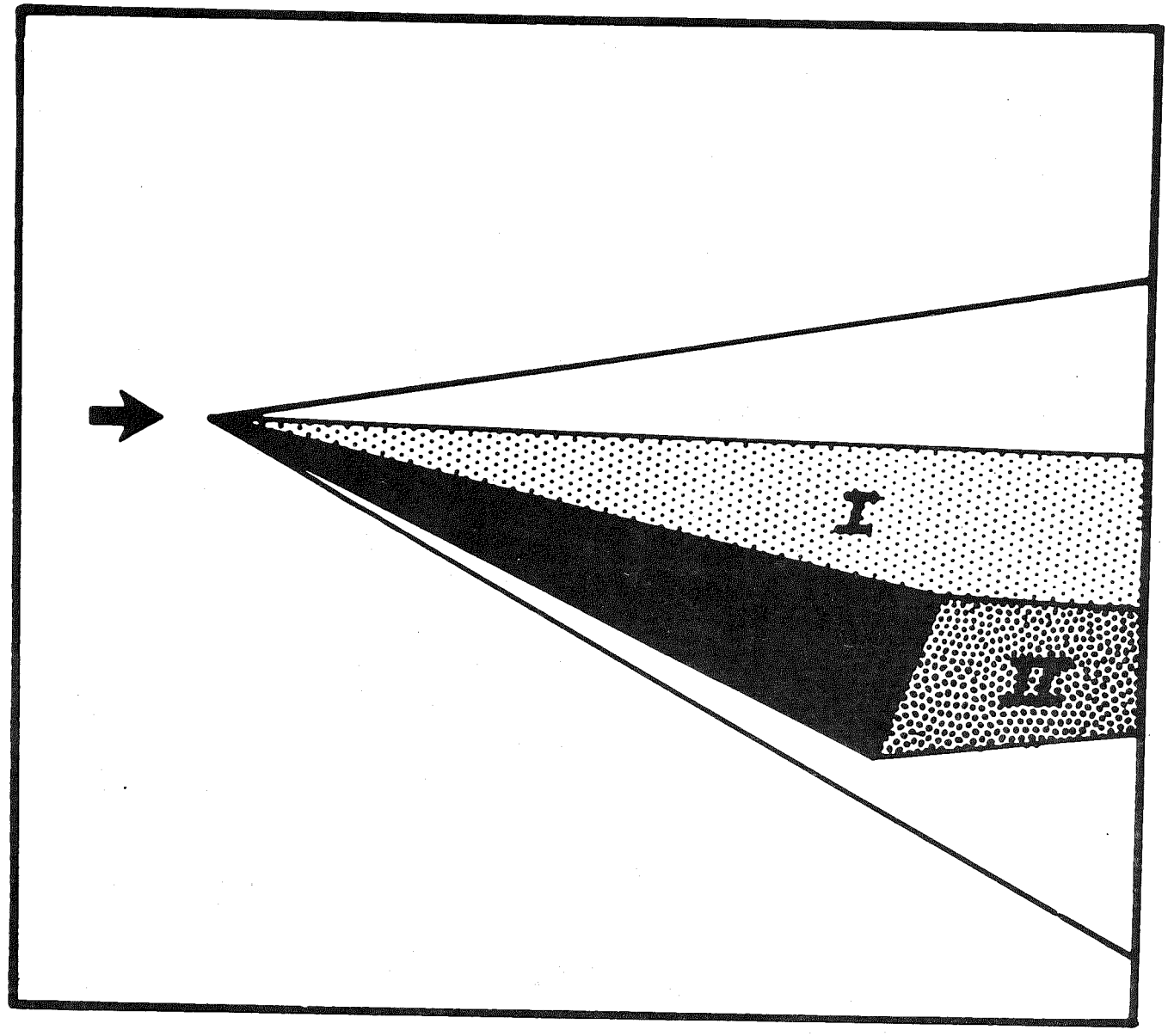

Figure 1. Schematic Representation of Separated Flow Fields Associated with a Cone at Angle of Attack

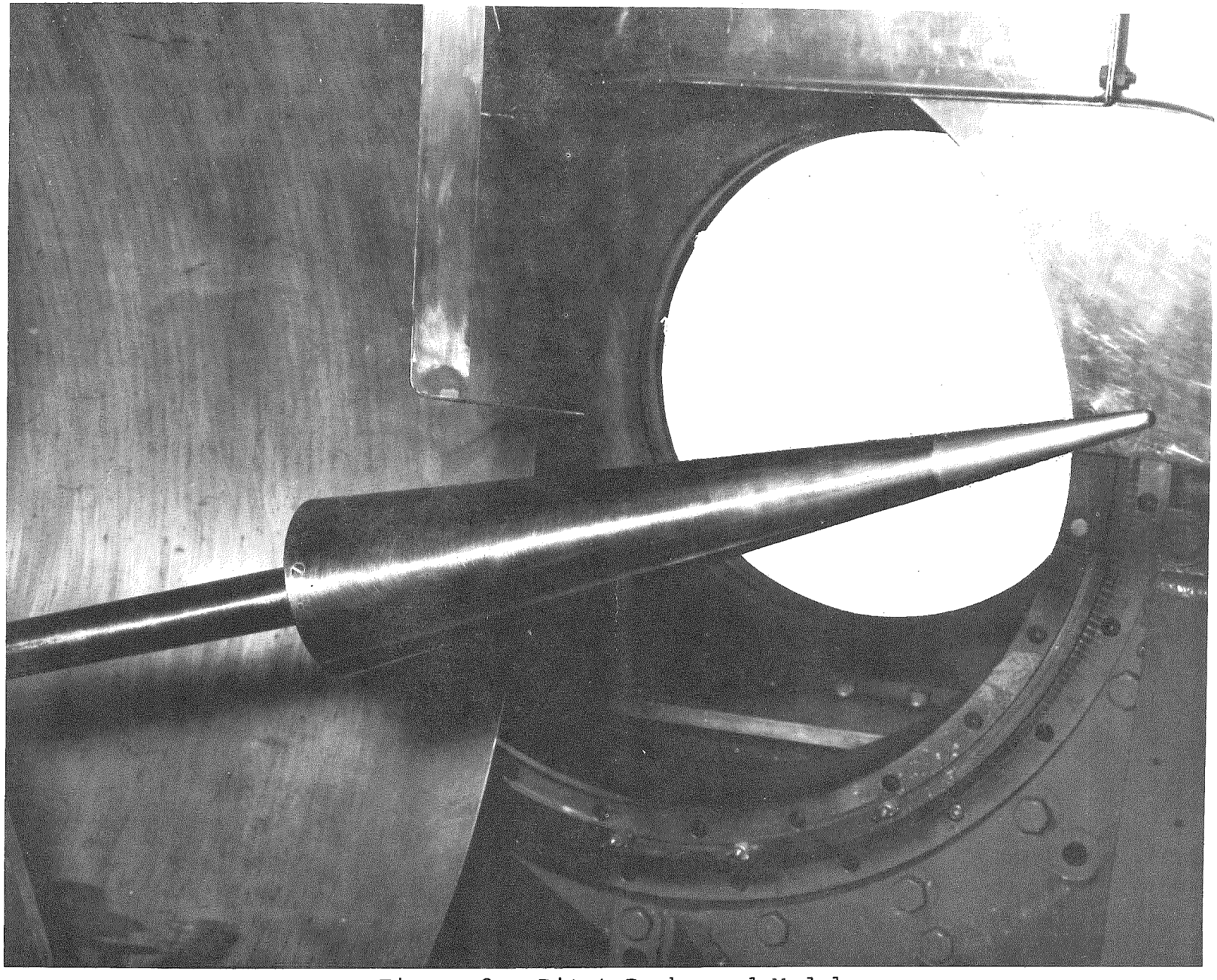

Figure 2. Pitot Probe and Model

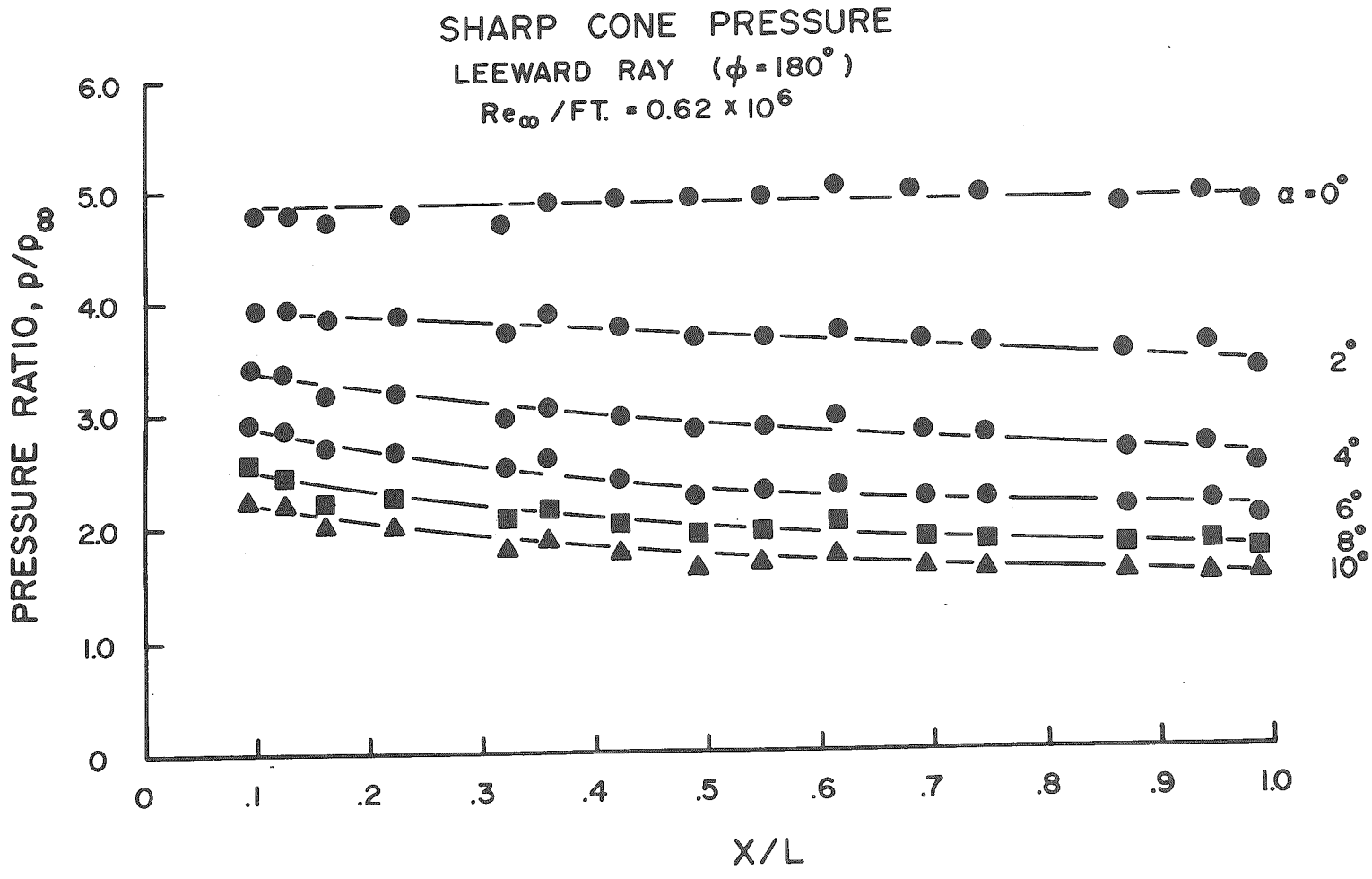

Figure 3. Sharp Cone Pressure Distributions Along Most Leeward Ray

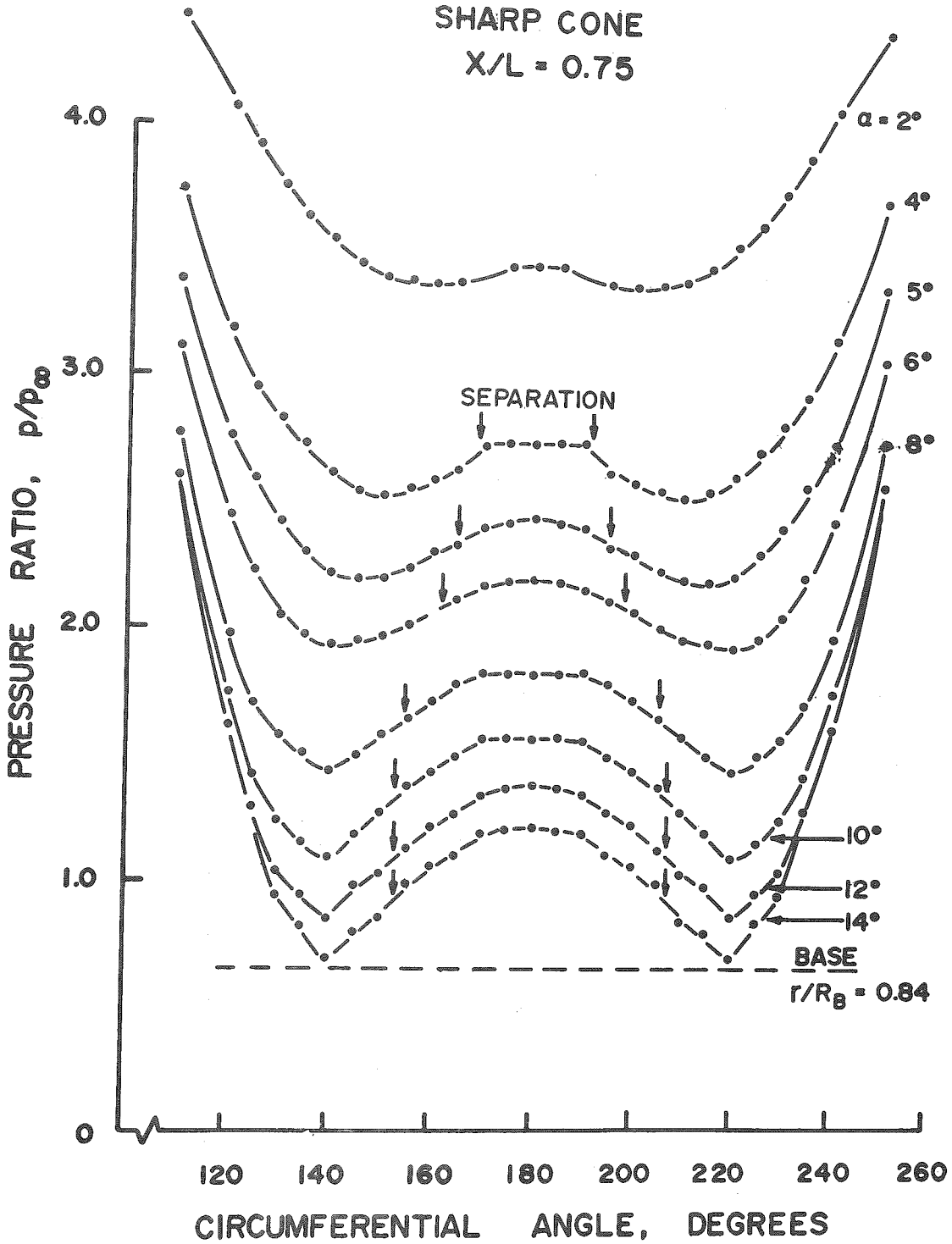

Figure 4. Sharp Cone Circumferential Pressure Distributions at X/L = 0.75

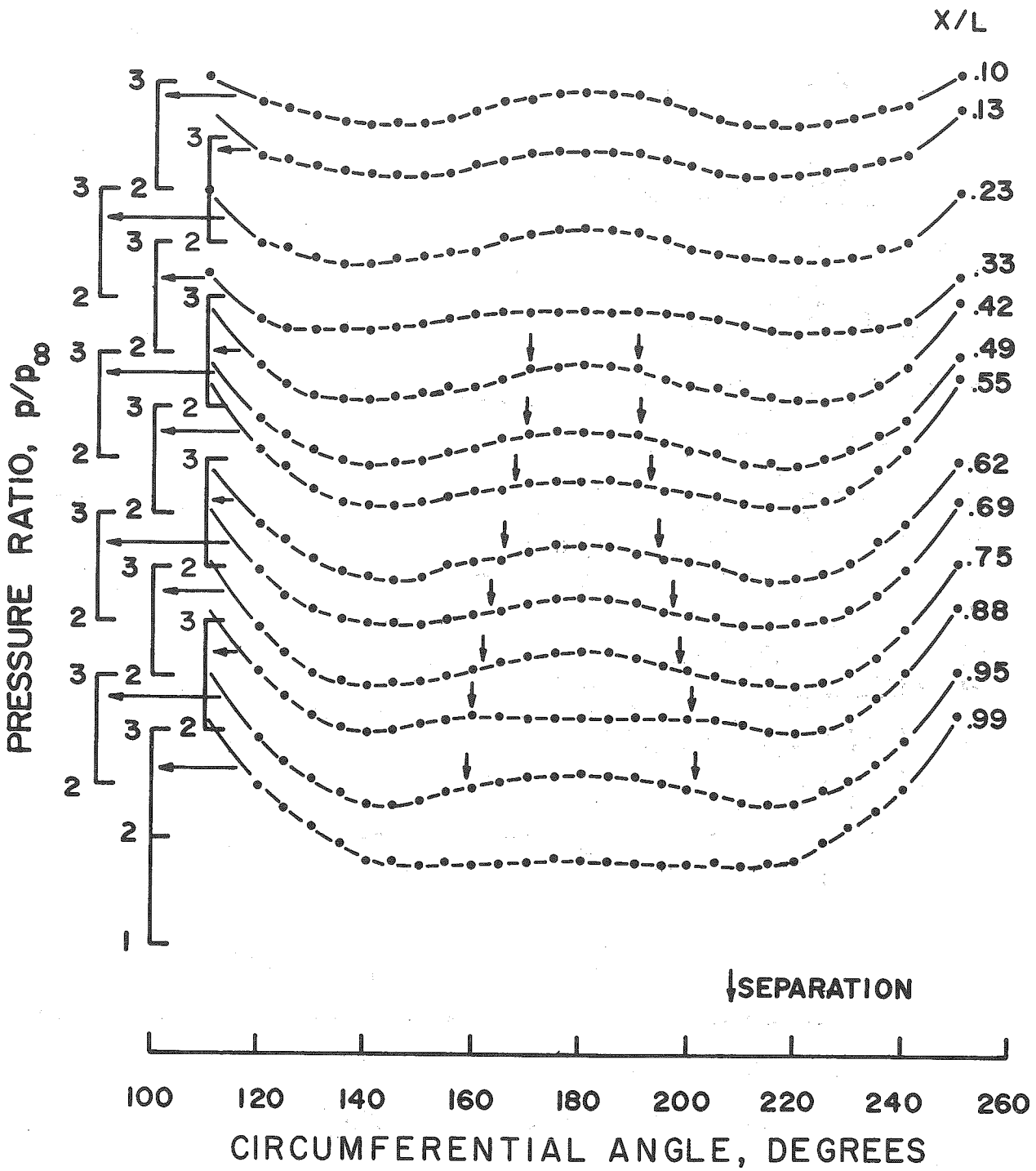

Figure 5. Sharp Cone Circumferential Pressure Distributions at α = 6 Degrees

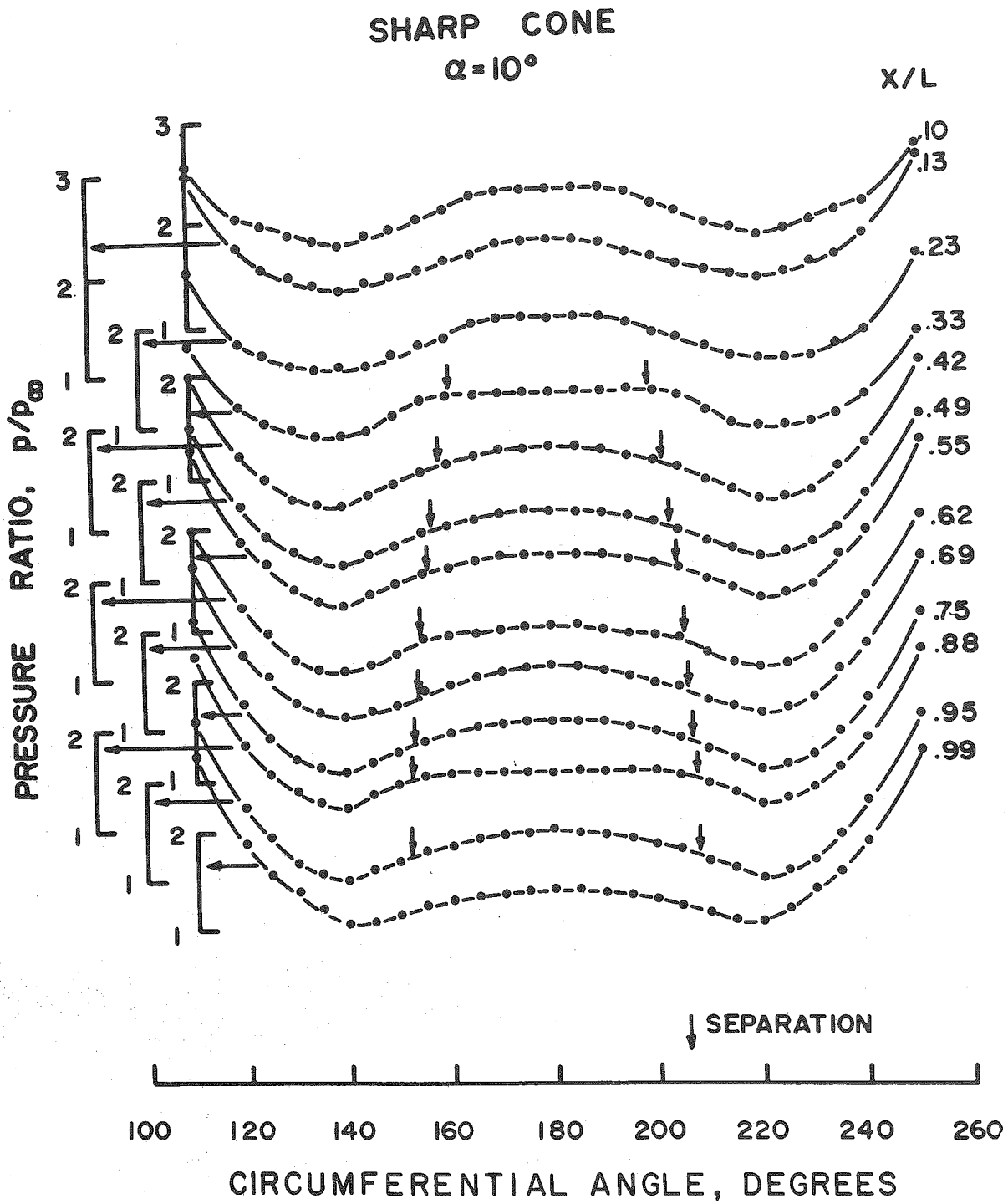

Figure 6. Sharp Cone Circumferential Pressure Distributions at α = 10 Degrees

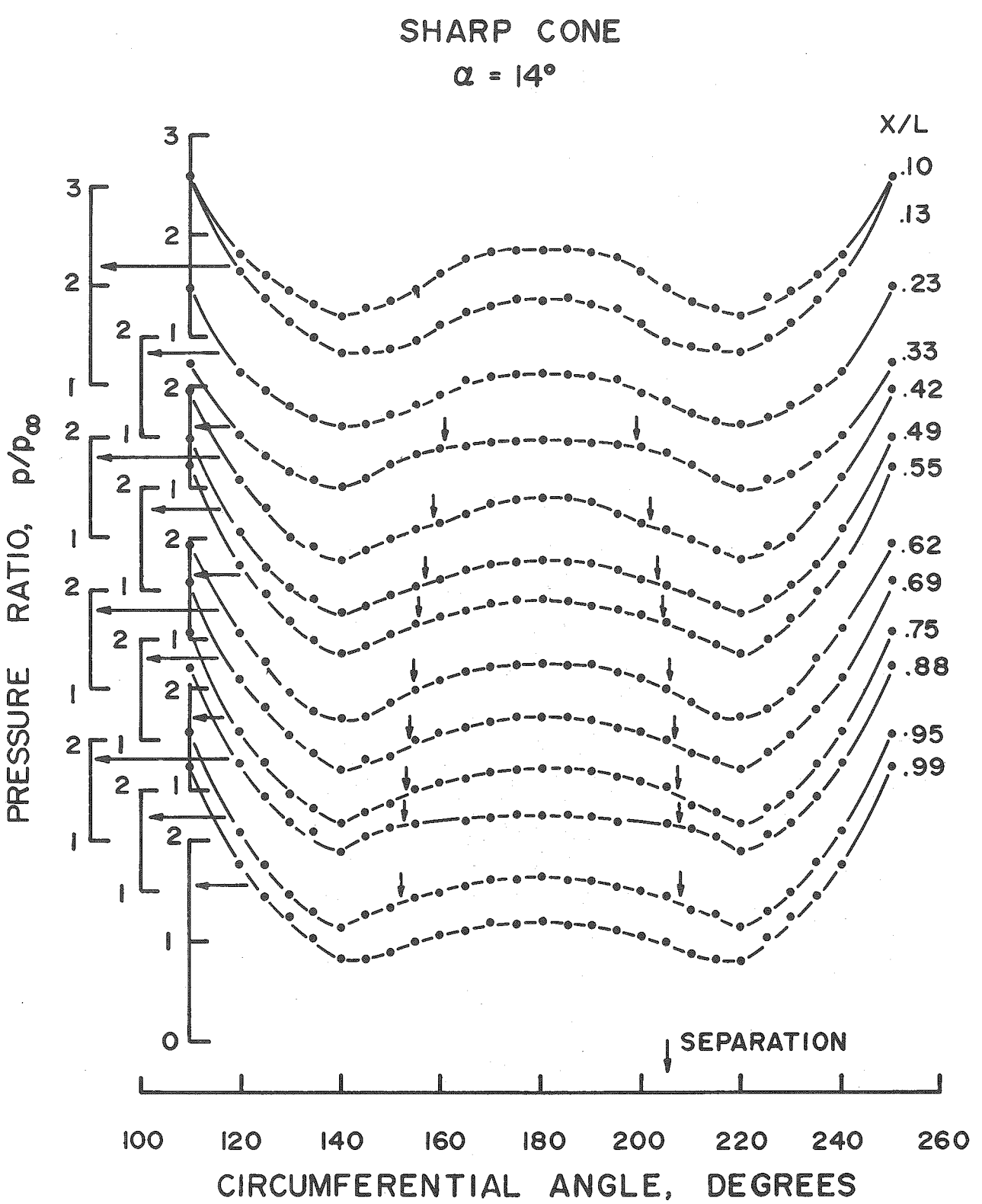

Figure 7. Sharp Cone Circumferential Pressure Distributions at α = 14 Degrees

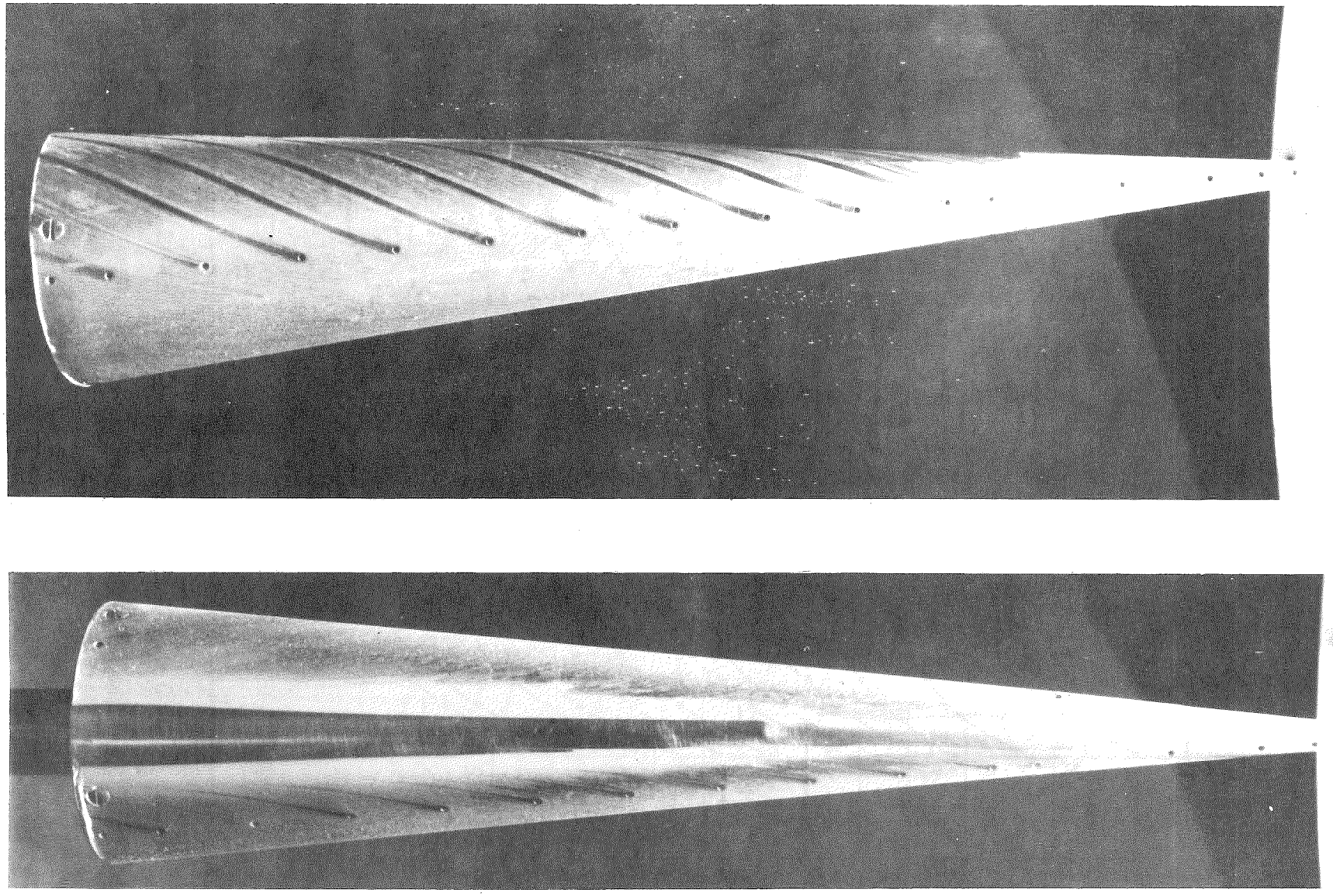

Figure 8. Oil Flow Photographs, Side and Leeward Views, Sharp Tip, α = 4 Degrees

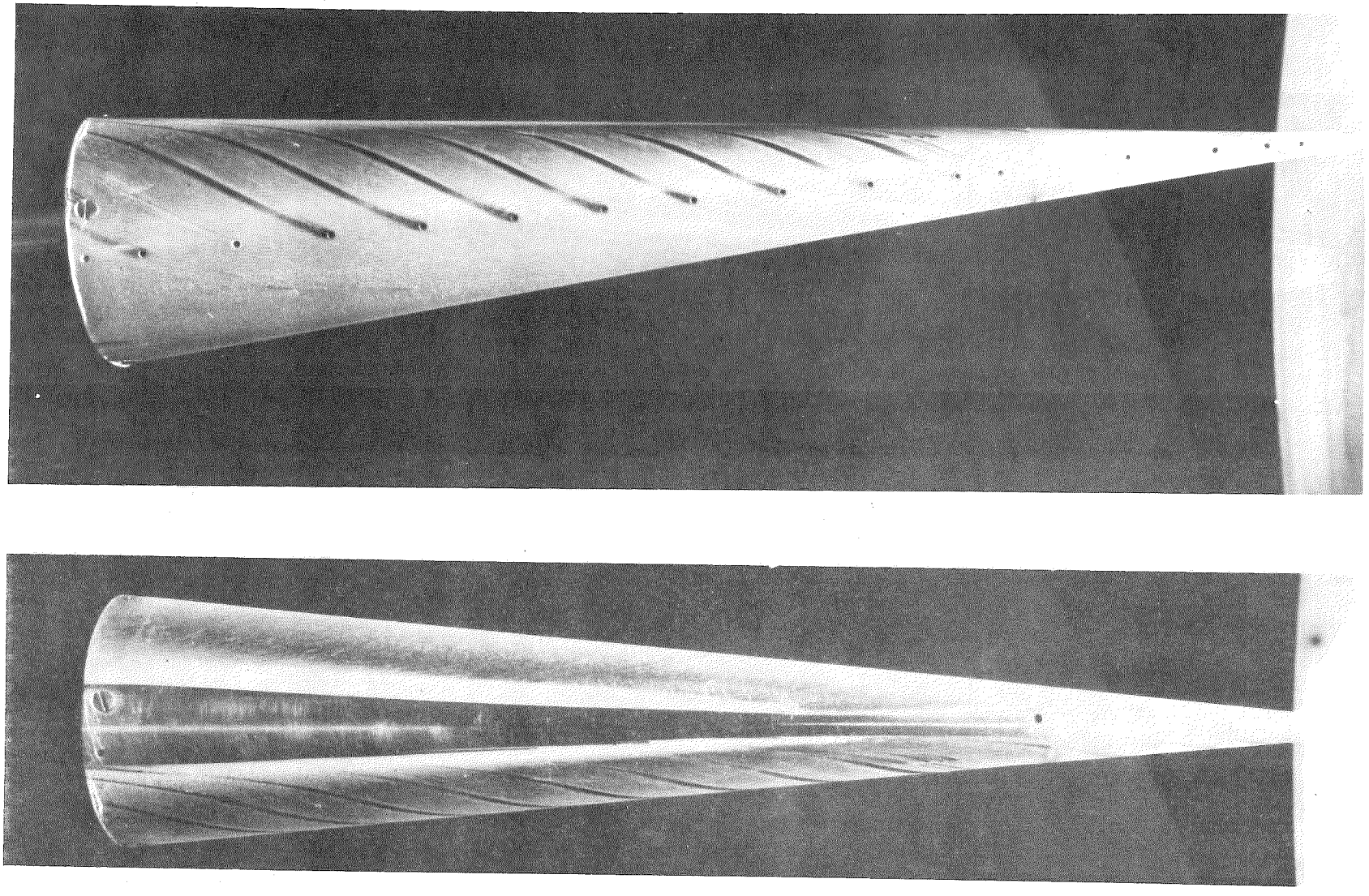

Figure 9. Oil Flow Photographs, Side and Leeward Views, Sharp Tip, α = 5 Degrees

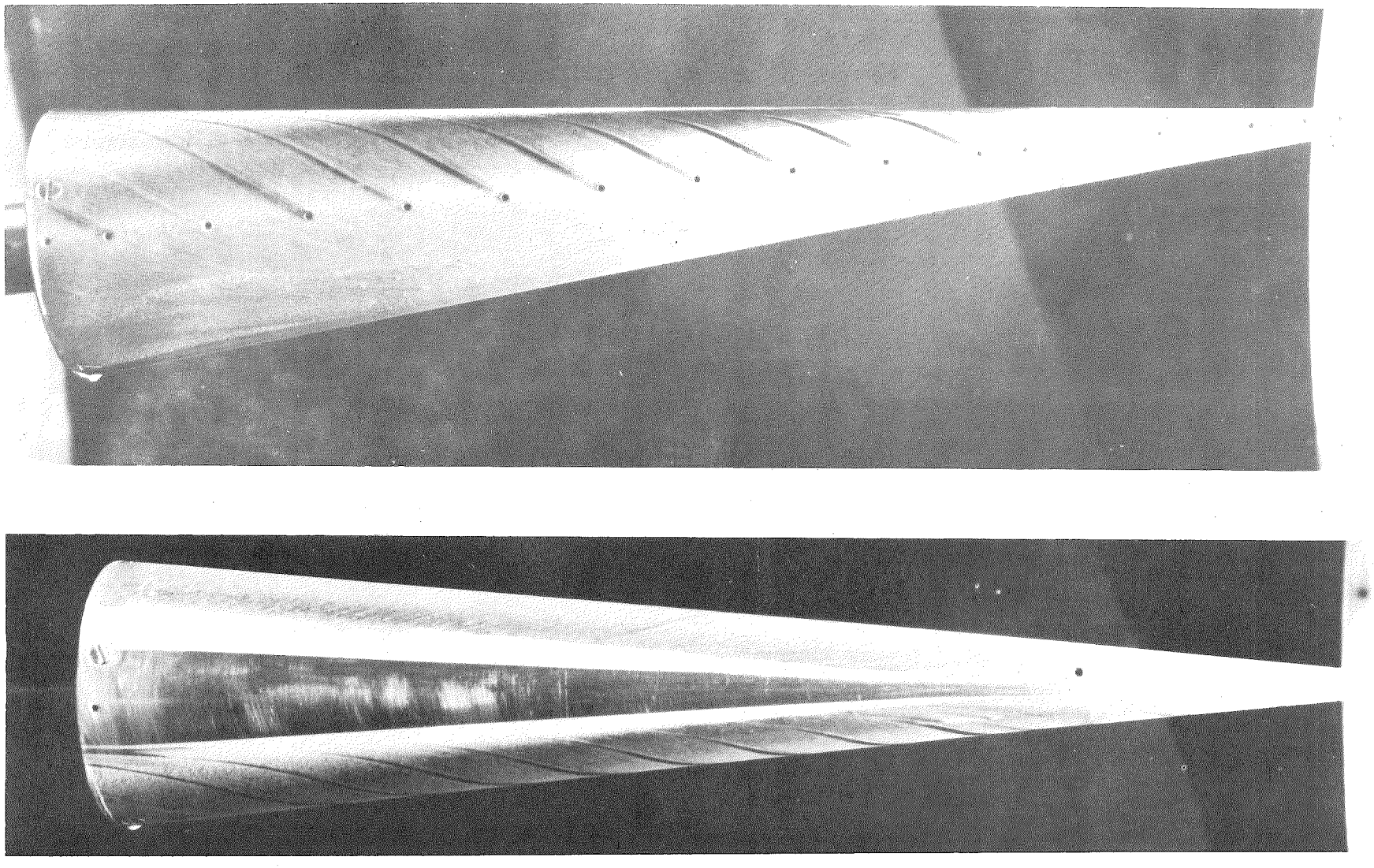

Figure 10. Oil Flow Photographs, Side and Leeward Views, Sharp Tip, α = 6 Degrees

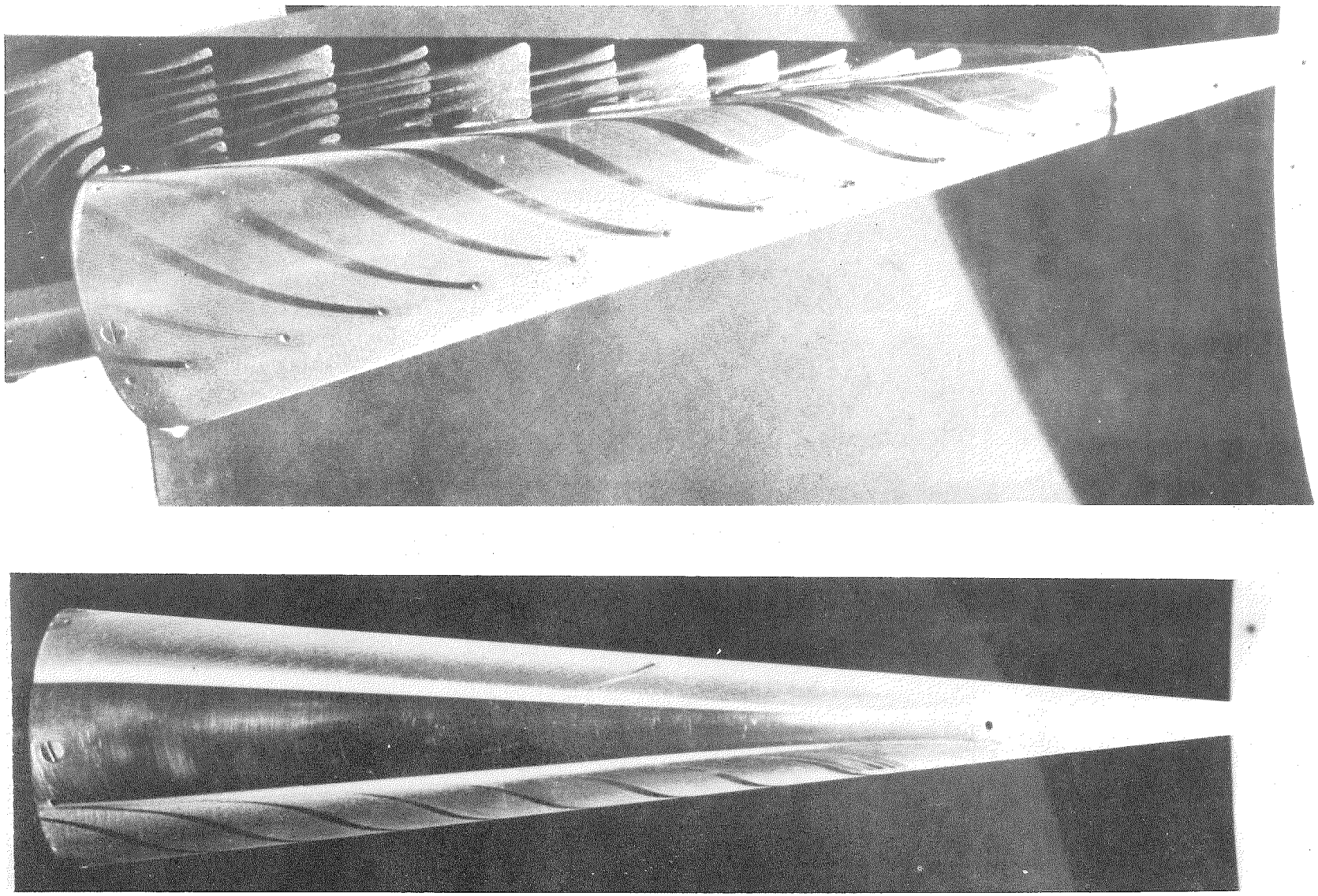

Figure 11. Oil Flow Photographs, Side and Leeward Views, Sharp Tip, α = 8 Degrees

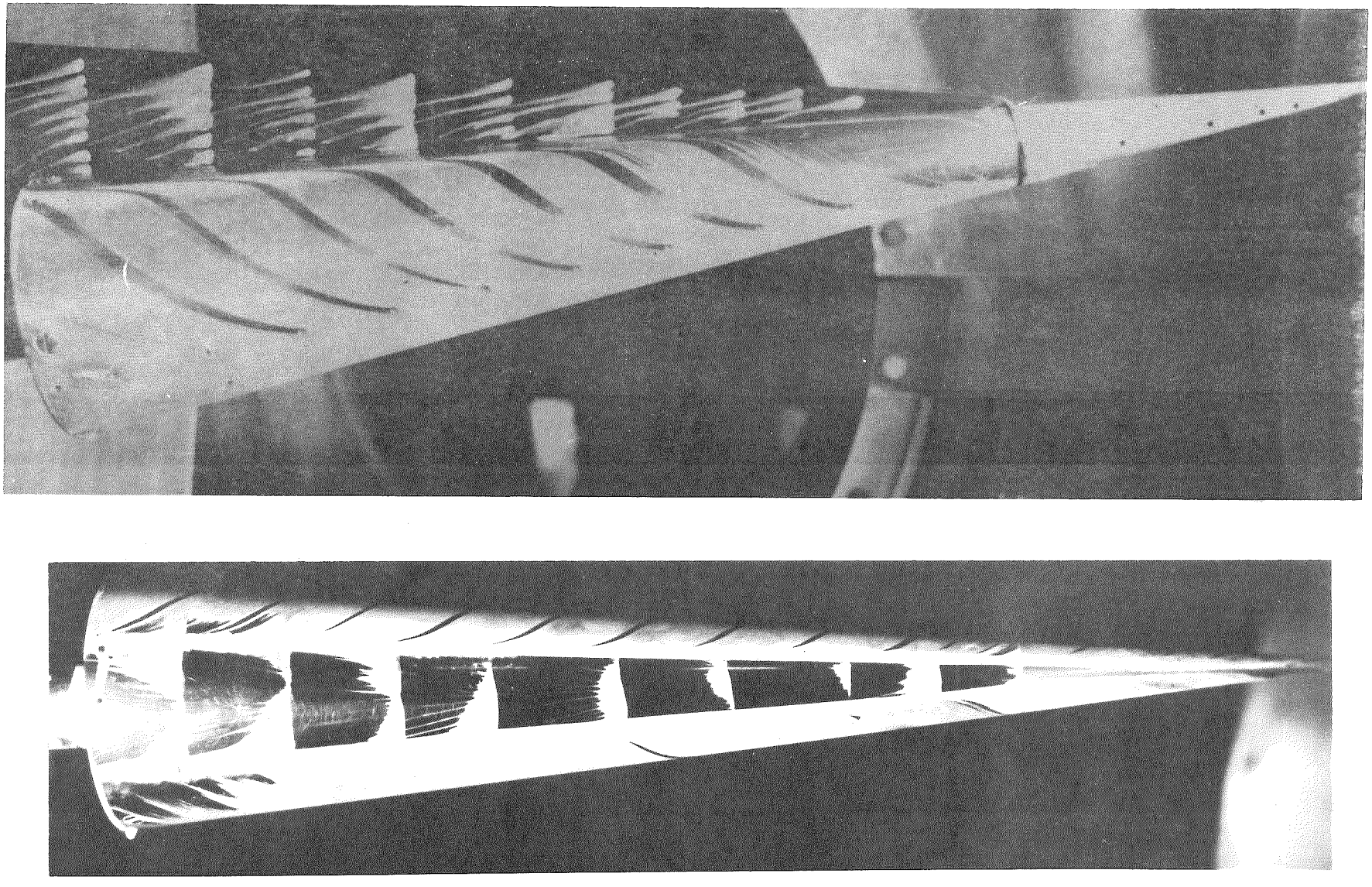

Figure 12. Oil Flow Photographs, Side and Leeward Views, Sharp Tip, α = 10 Degrees

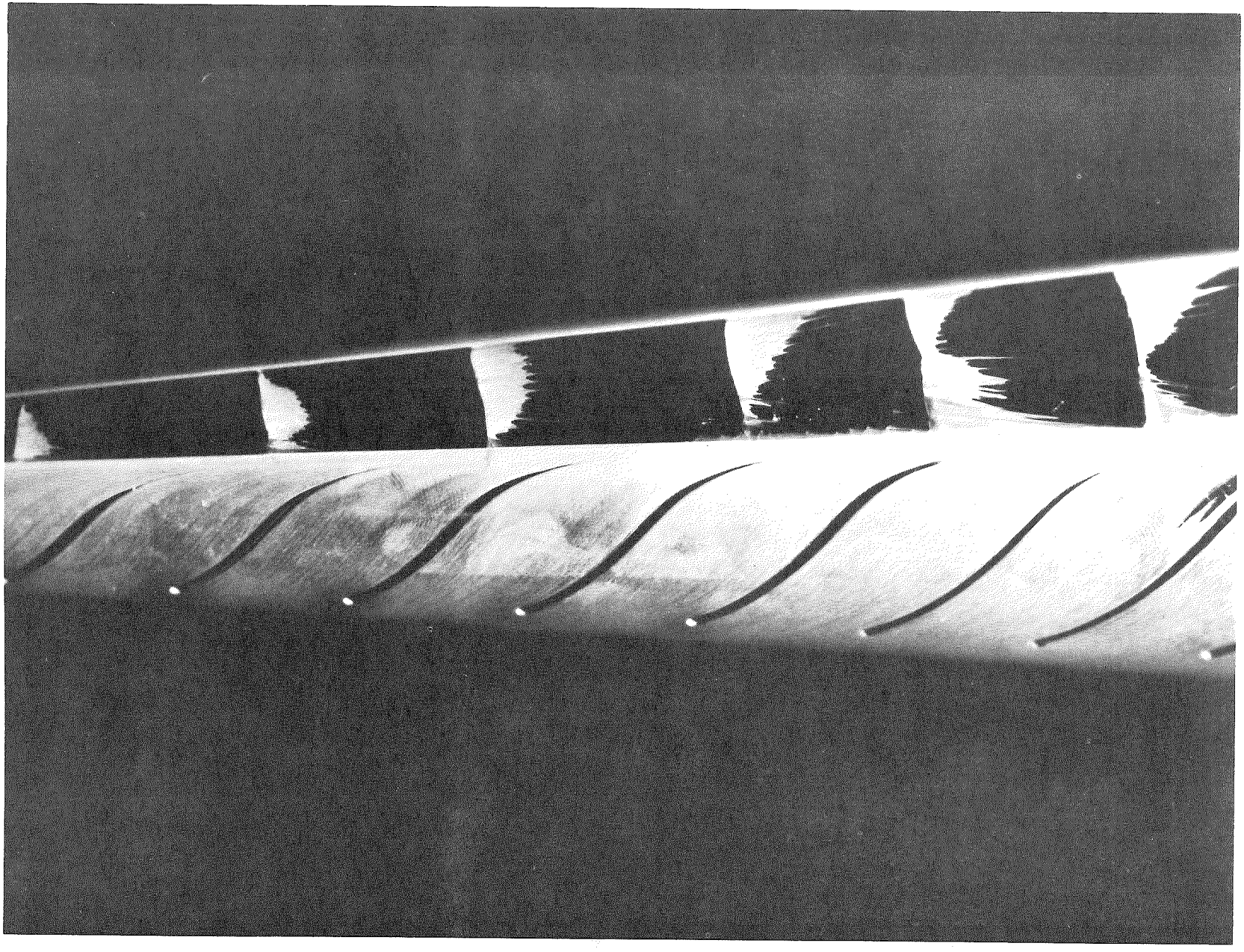

Figure 13. Oil Flow Photograph, Leeward and Side Region, Sharp Tip, α = 10 Degrees

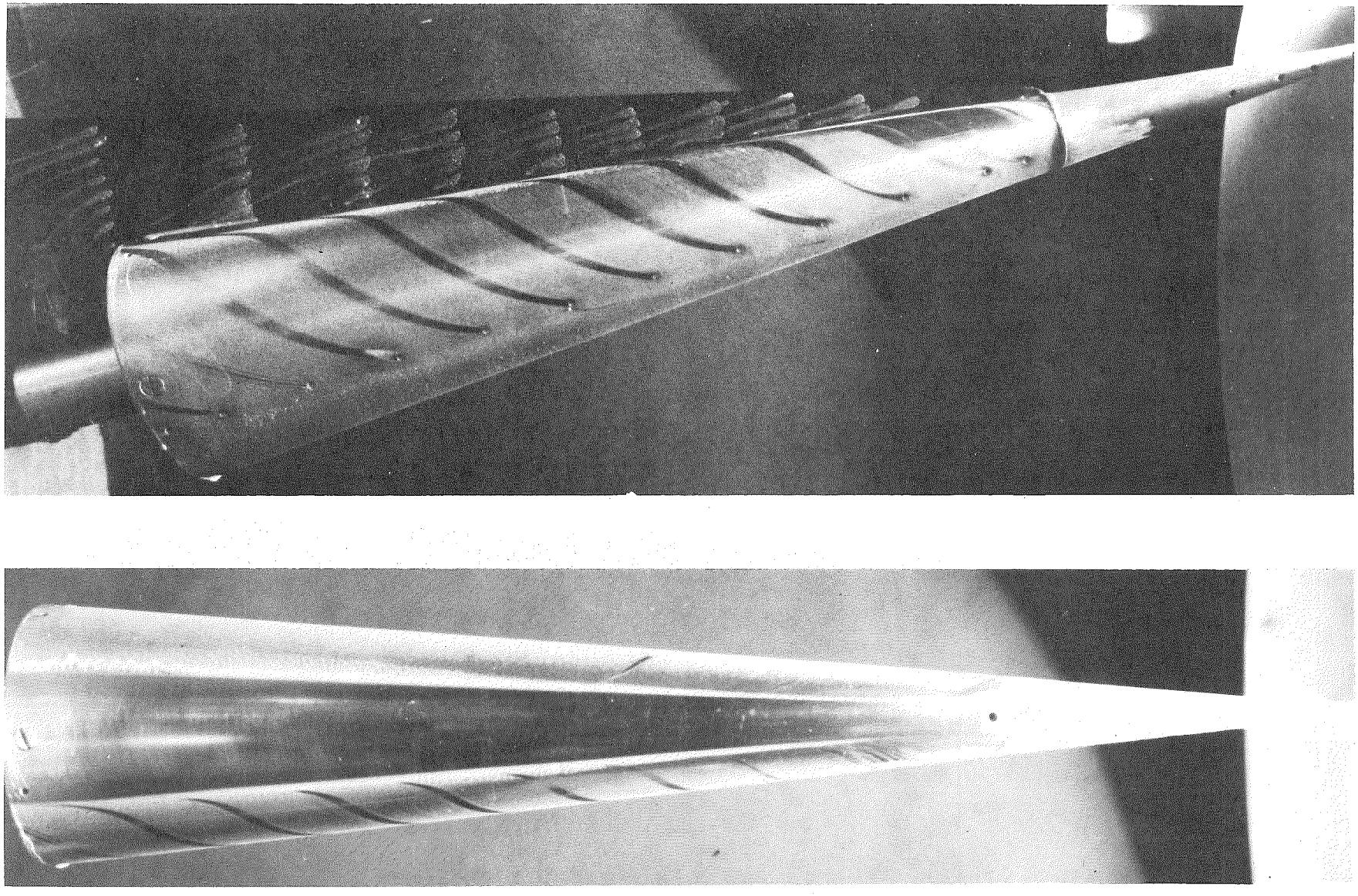

Figure 14. Oil Flow Photographs, Side and Leeward Views, Sharp Tip, α = 12 Degrees

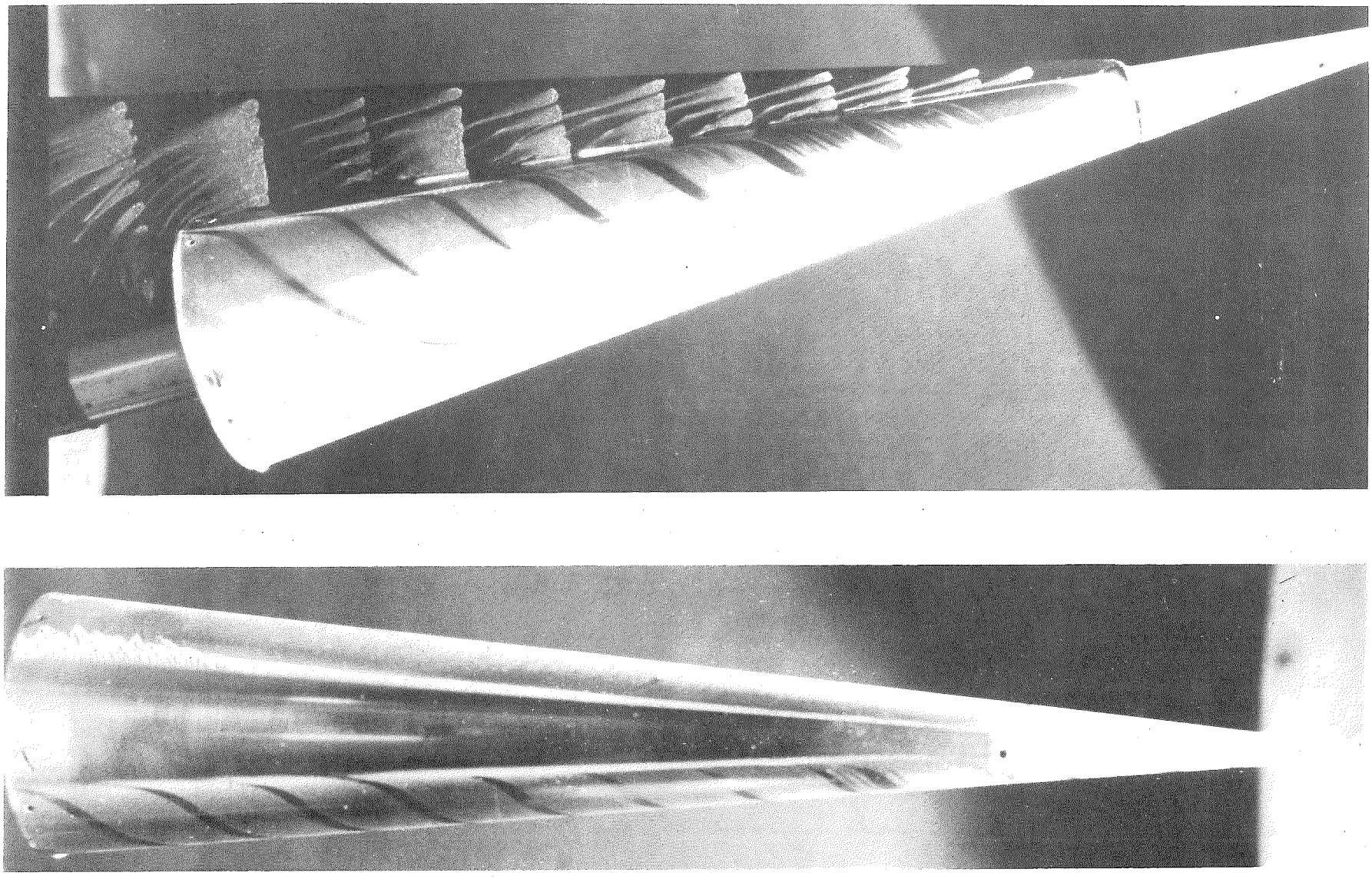

Figure 15. Oil Flow Photographs, Side and Leeward Views, Sharp Tip, α = 14 Degrees

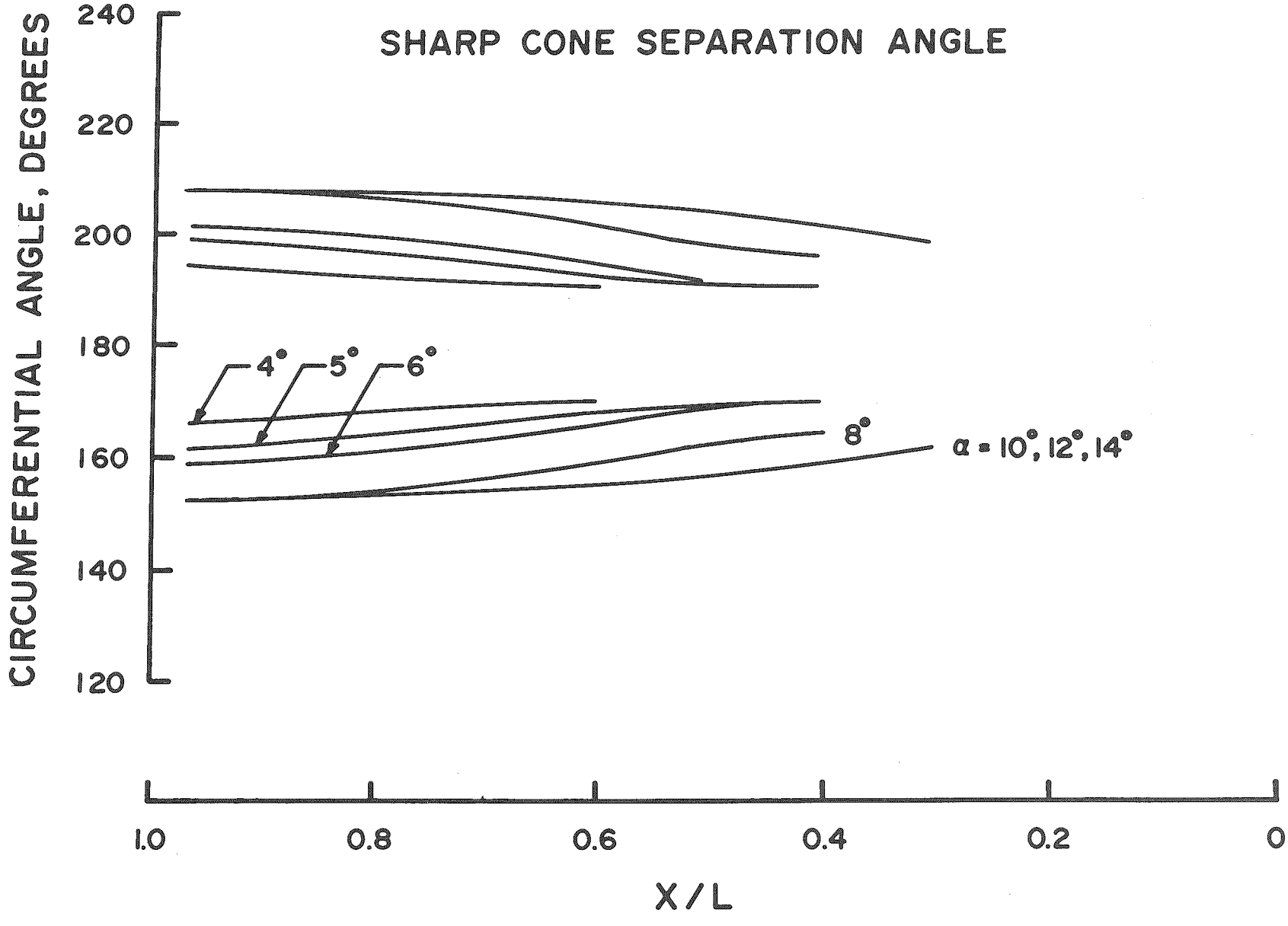

Figure 16. Sharp Cone Separation Angles

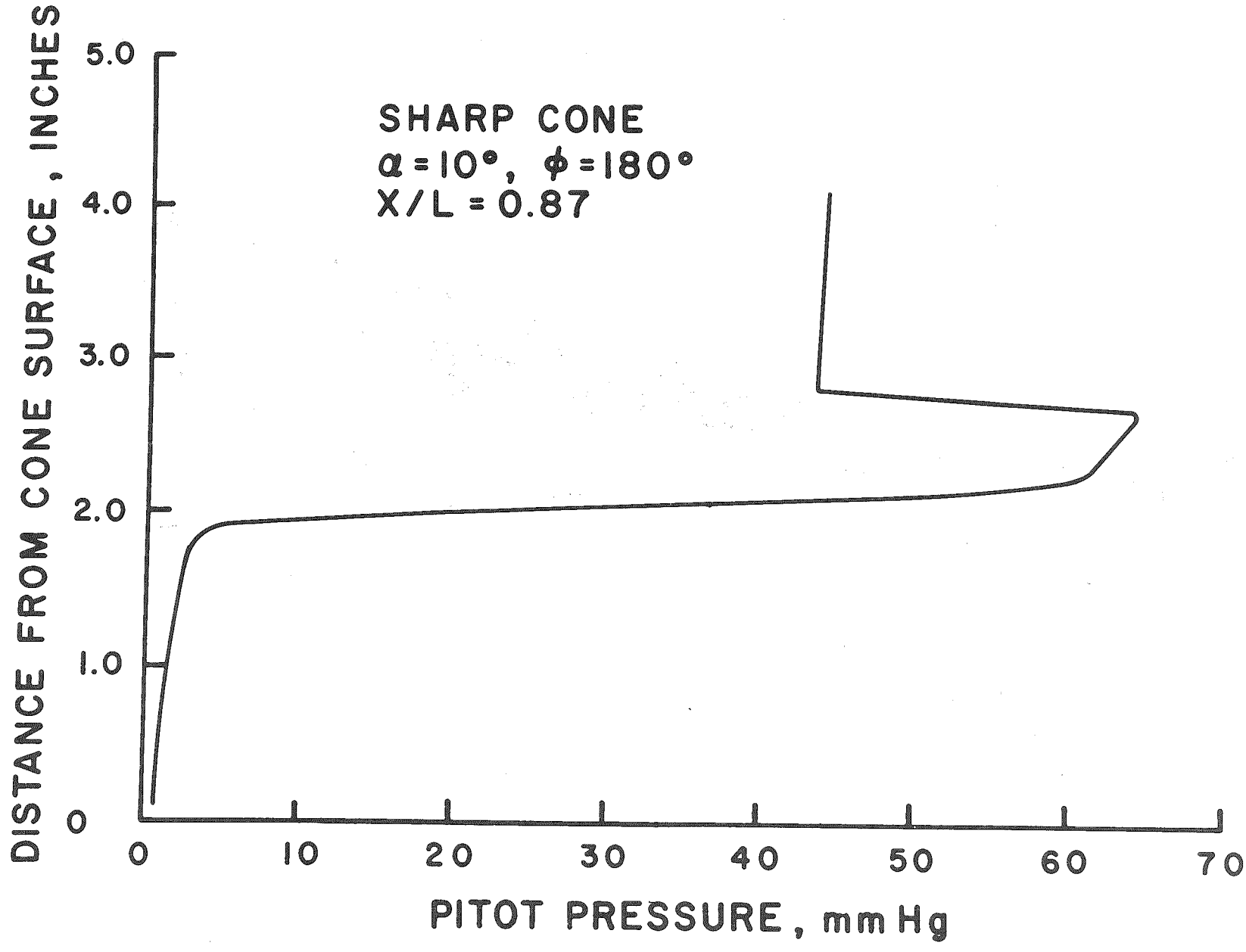

Figure 17. Sharp Cone Pitot Pressure Profile

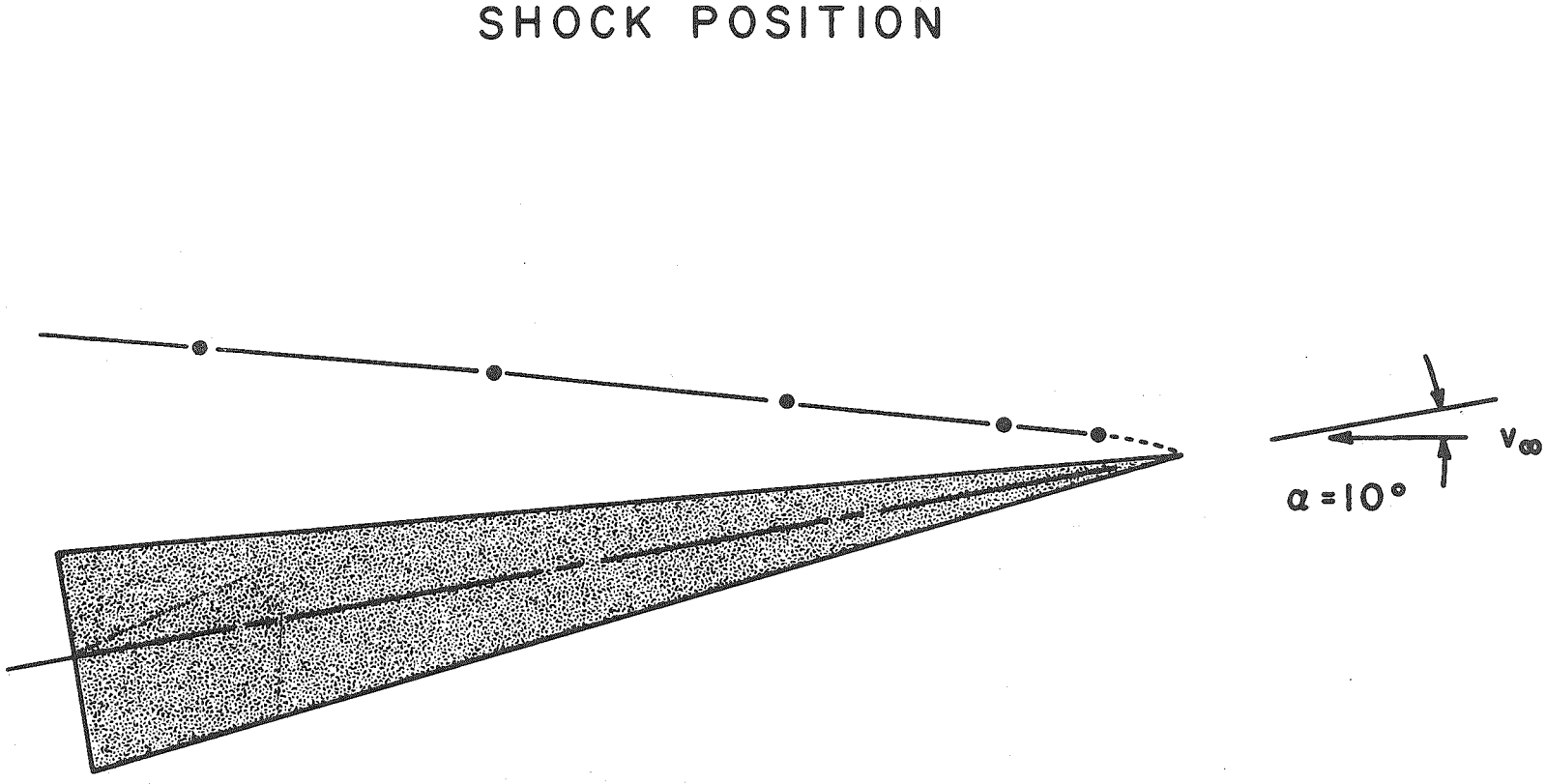

Figure 18. Sharp Cone Shock Location, α = 10 Degrees

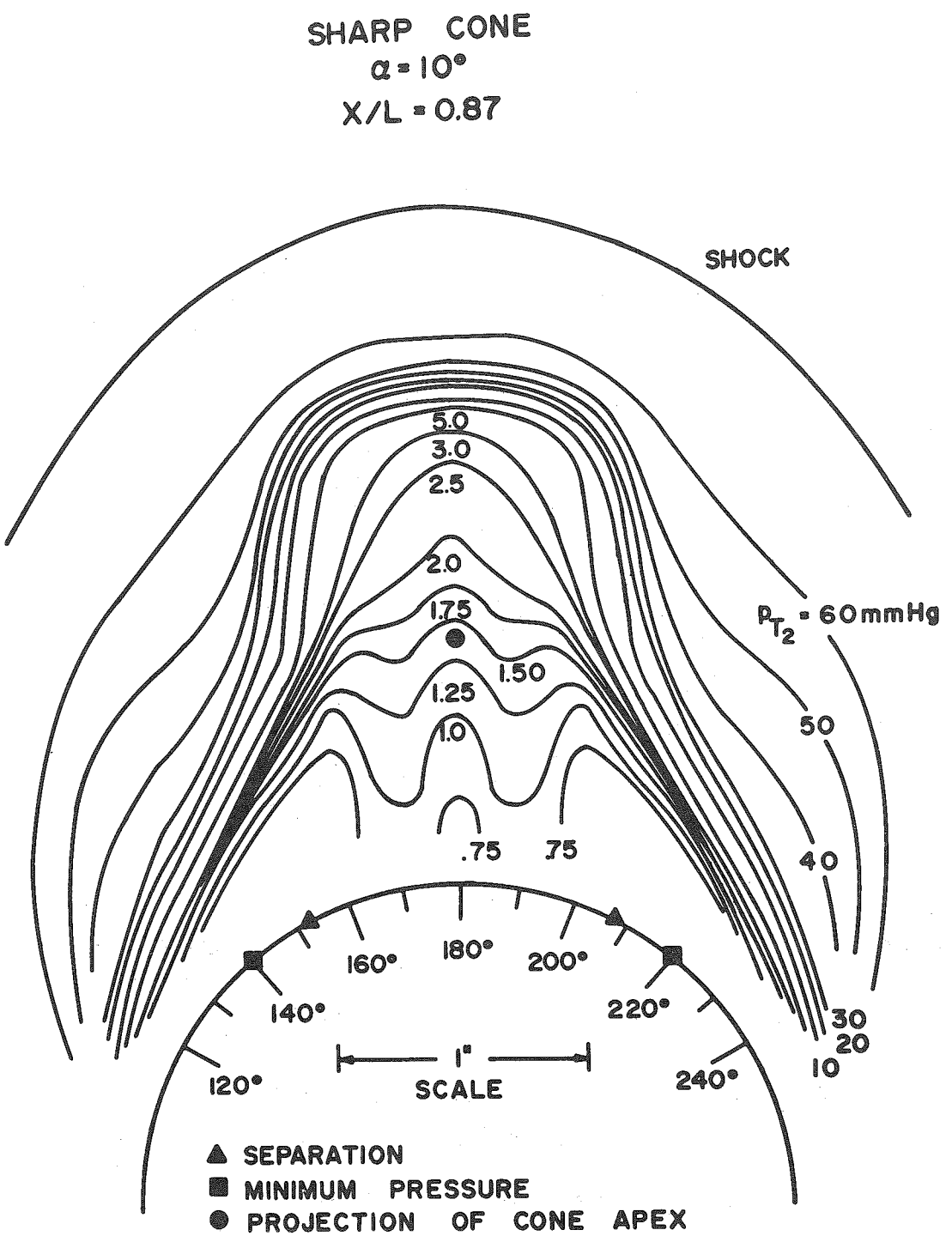

Figure 19. Pitot Pressure Contours, Sharp Cone, α = 10 Degrees

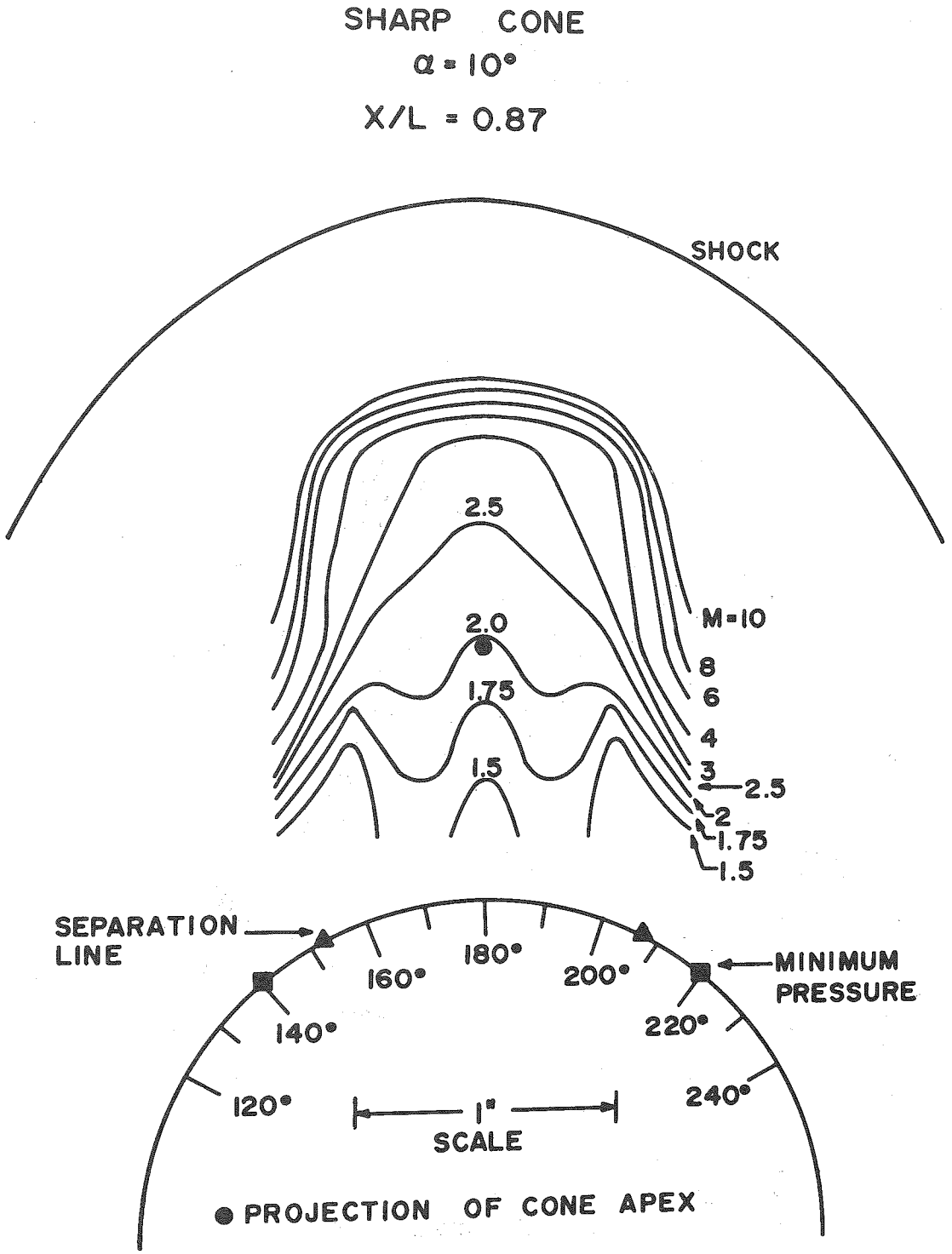

Figure 20. Approximate Mach Number Contours, Sharp Cone, α = 10 Degrees

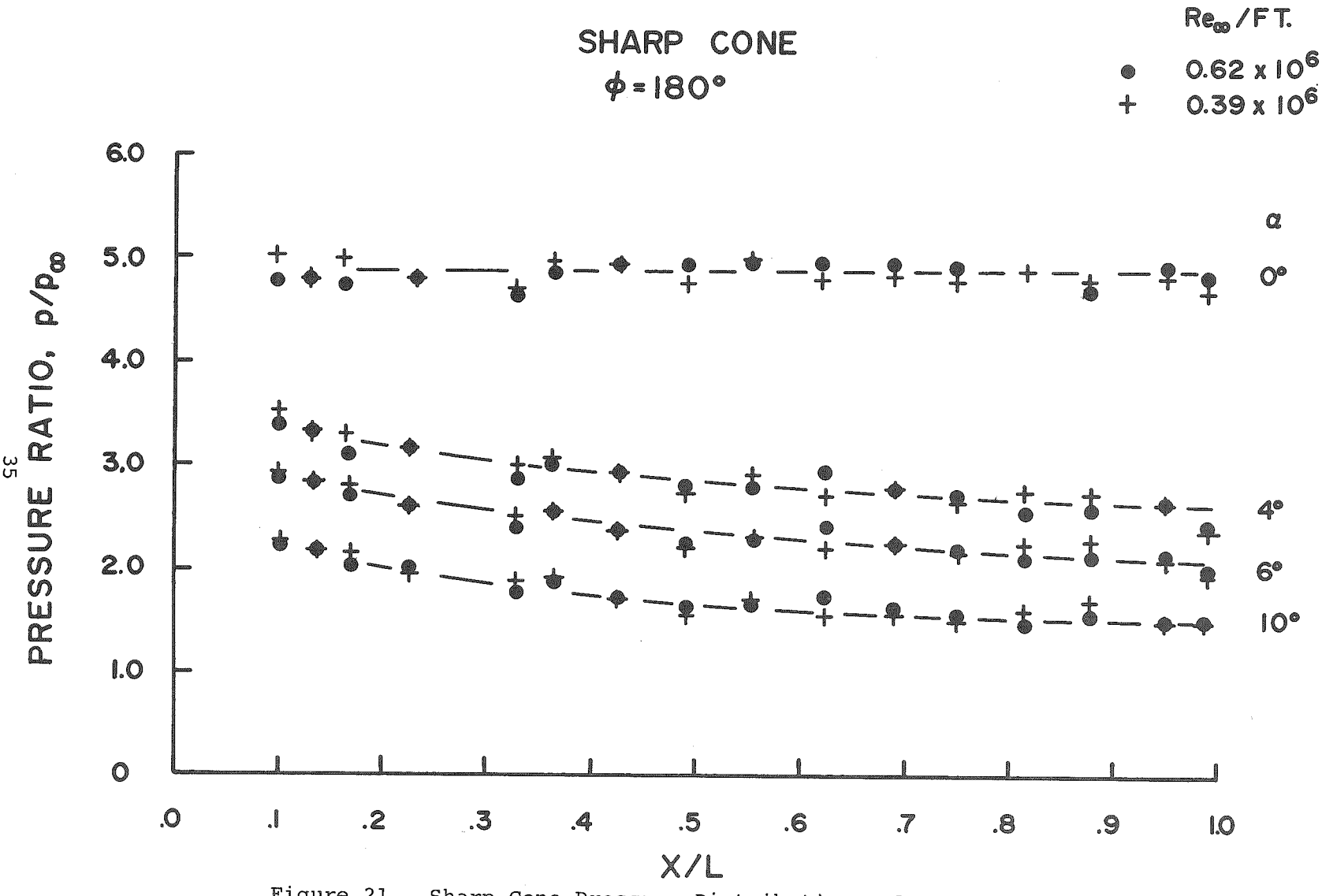

Figure 21. Sharp Cone Pressure Distributions Along the Most Leeward Ray for Two Reynolds Numbers

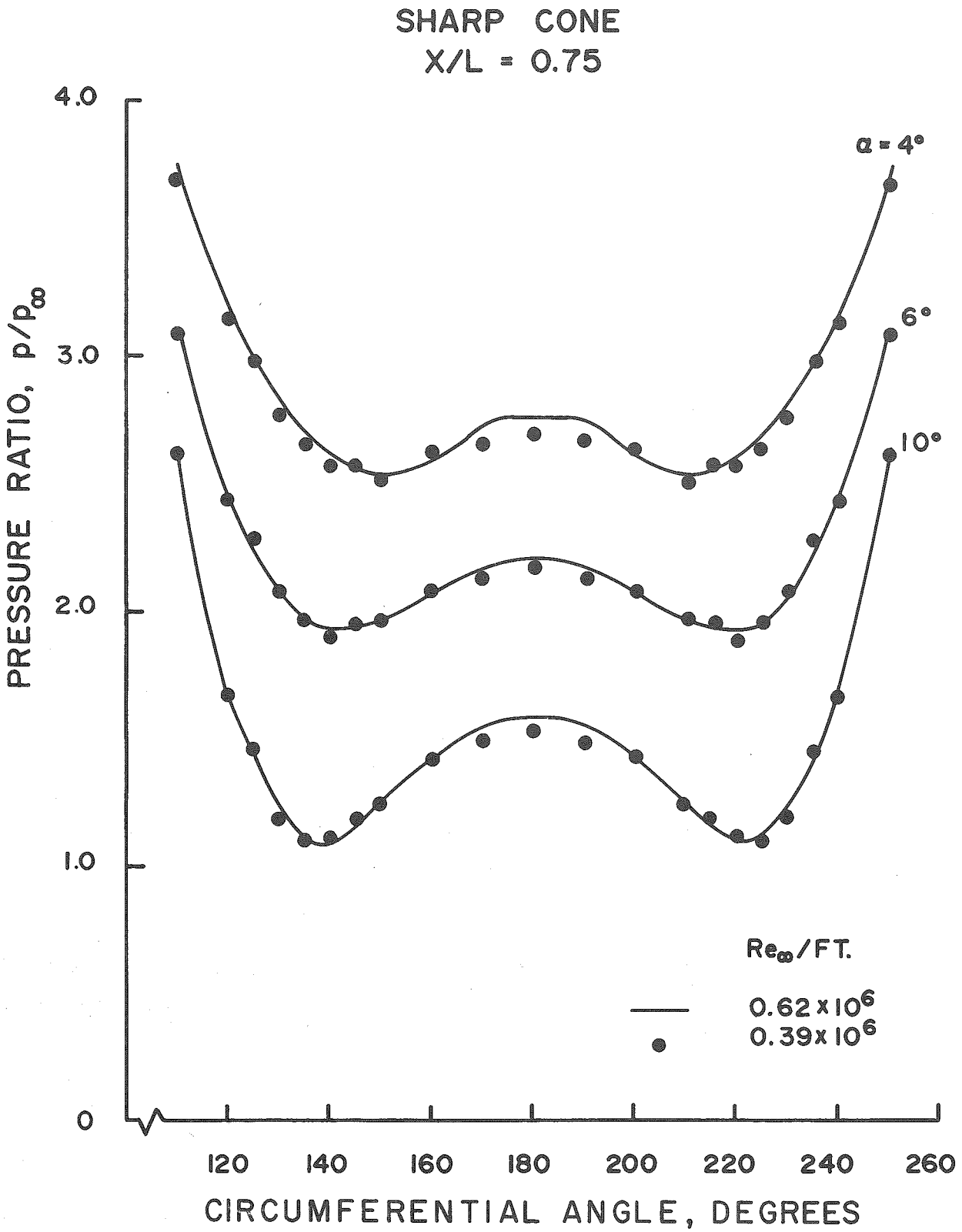

Figure 22. Sharp Cone Circumferential Pressure Distributions for Two Reynolds Numbers

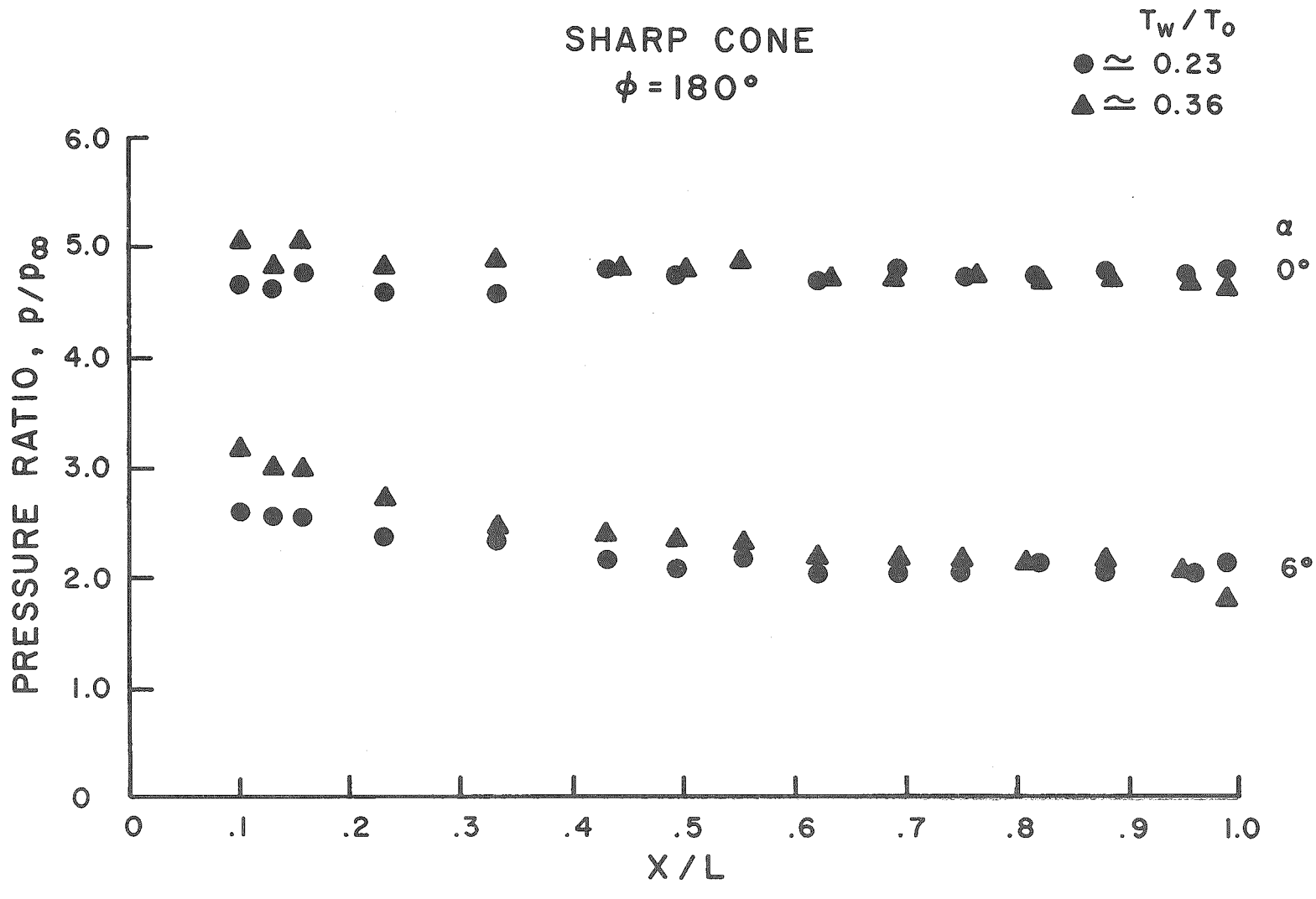

Figure 23. Sharp Cone Pressure Distributions Along the Most Leeward Ray for Two Wall Temperatures

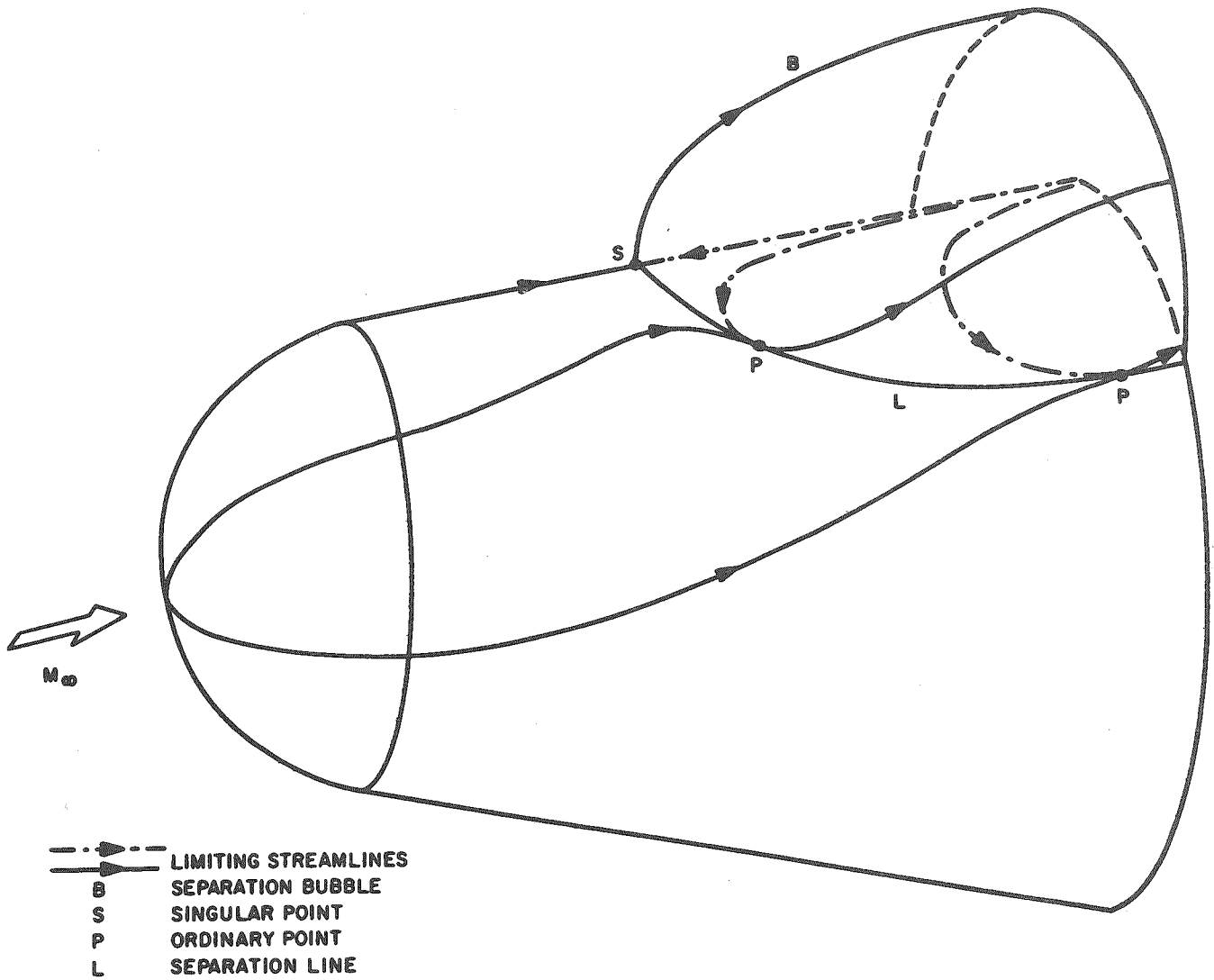

Figure 24. Separation Bubble Flow Field Model for Three-Dimensional Separation

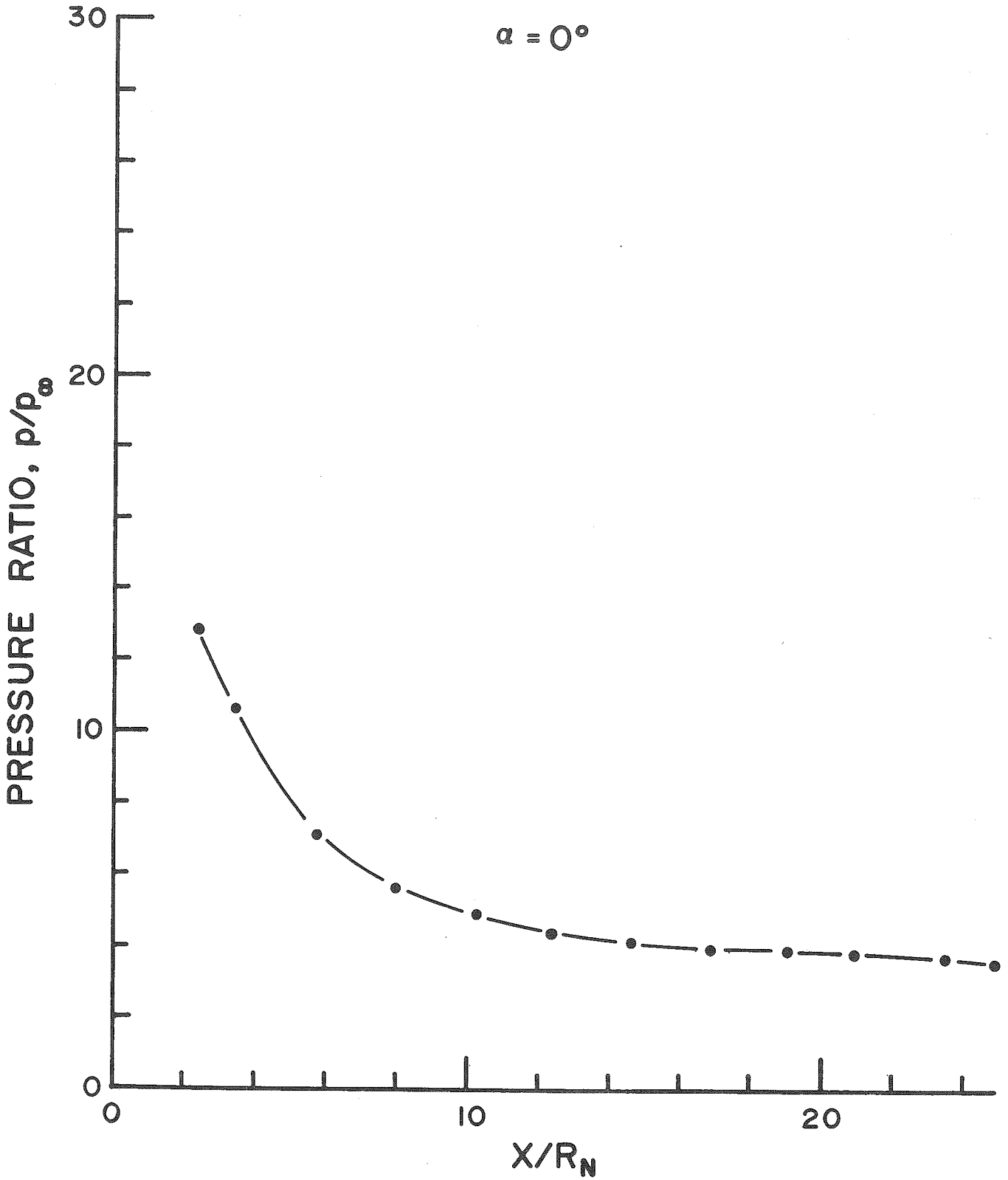

Figure 25. Longitudinal Pressure Distributions, 30% Bluntness, α = 0 Degrees

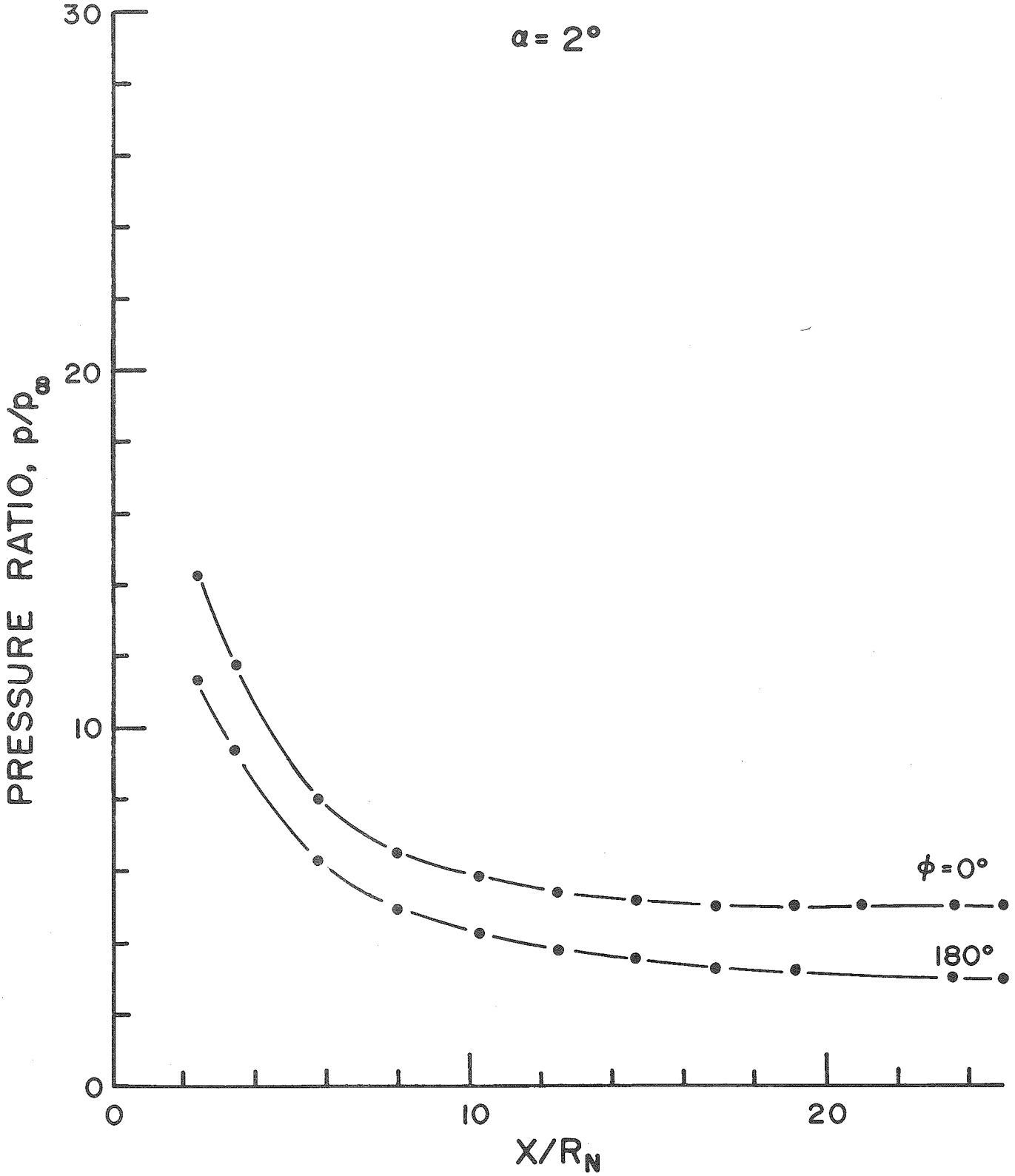

Figure 26. Longitudinal Pressure Distributions, 30% Bluntness, α = 2 Degrees

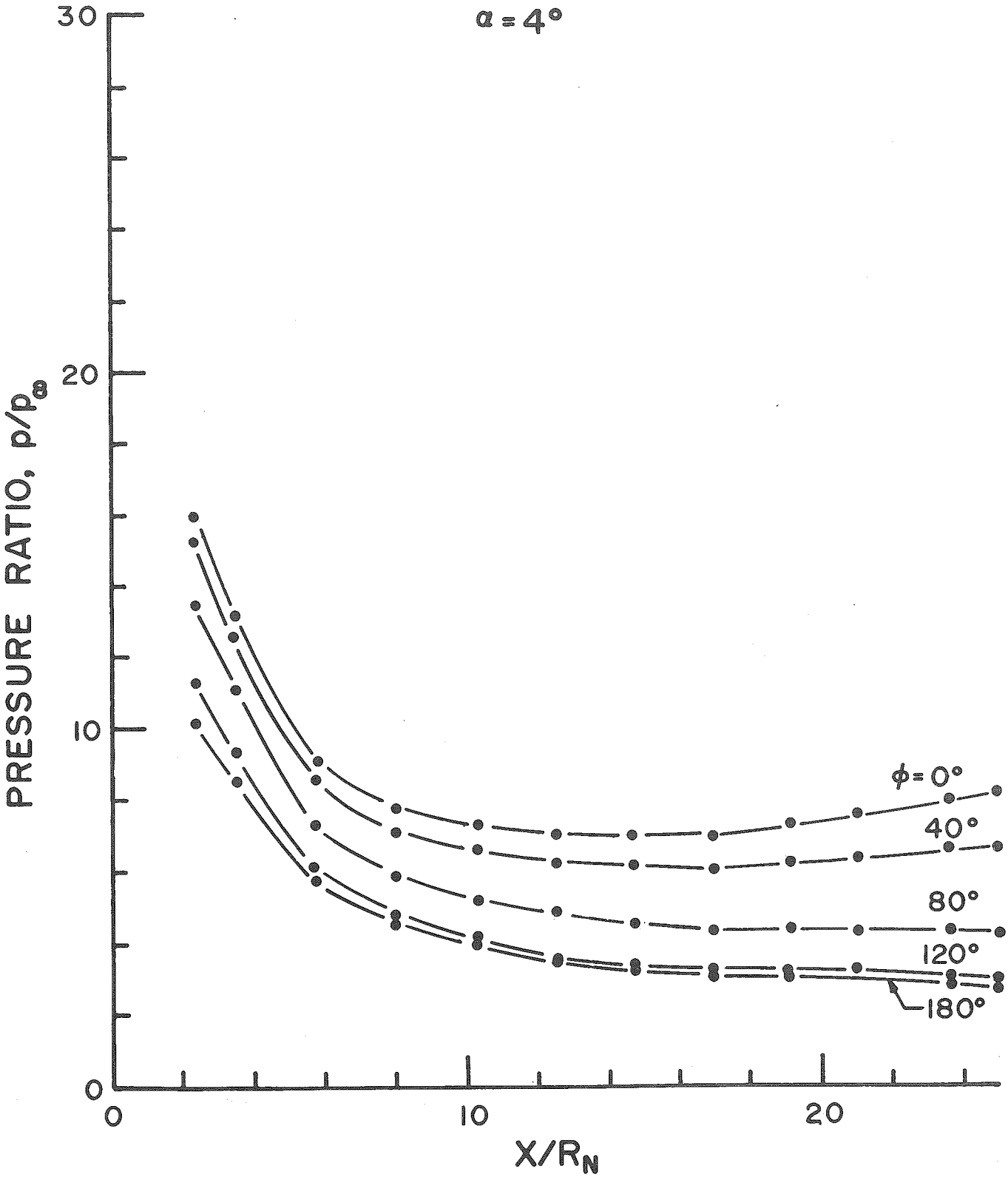

Figure 27. Longitudinal Pressure Distributions, 30% Bluntness, α = 4 Degrees

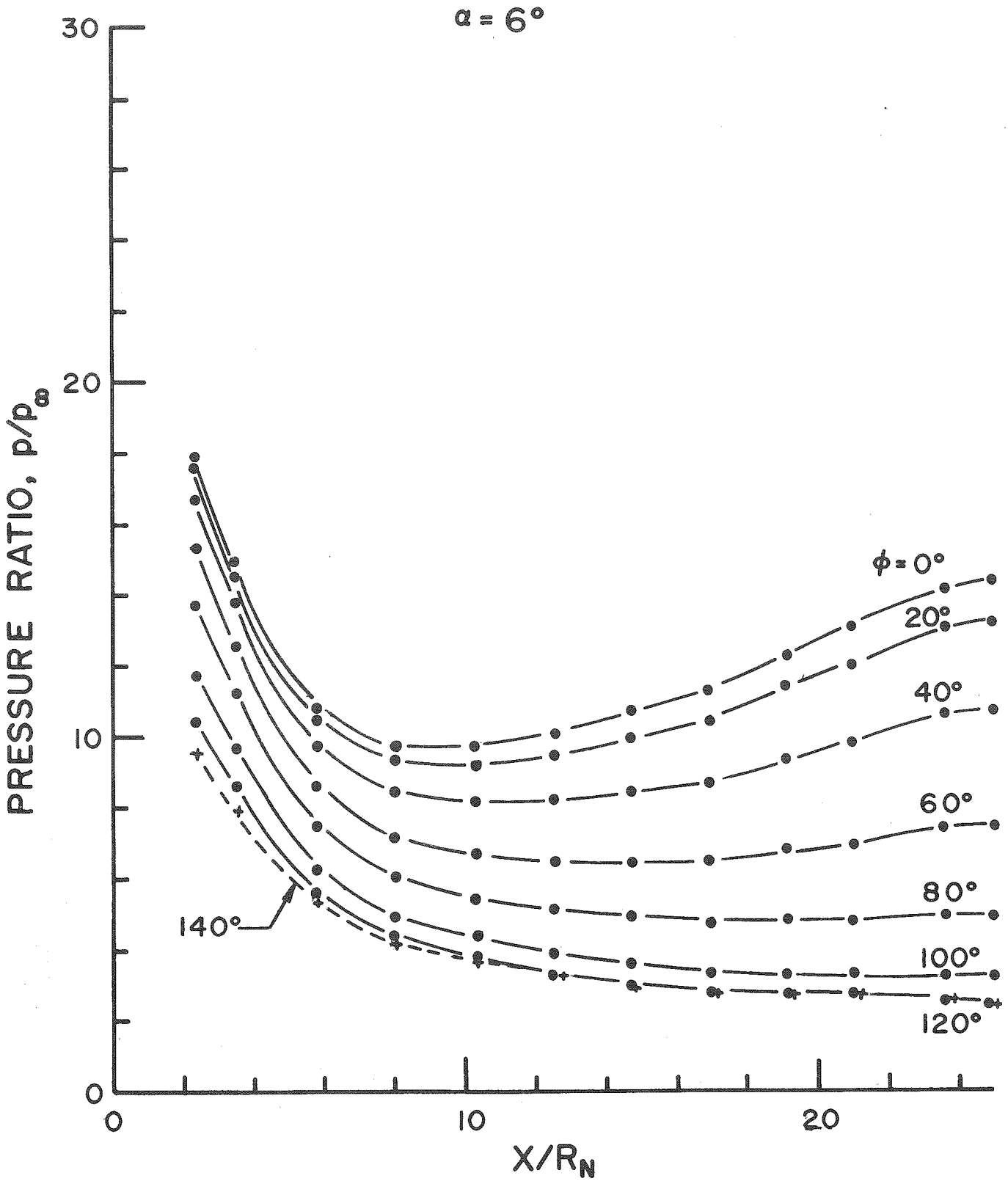

Figure 28. Longitudinal Pressure Distributions, 30% Bluntness, α = 6 Degrees

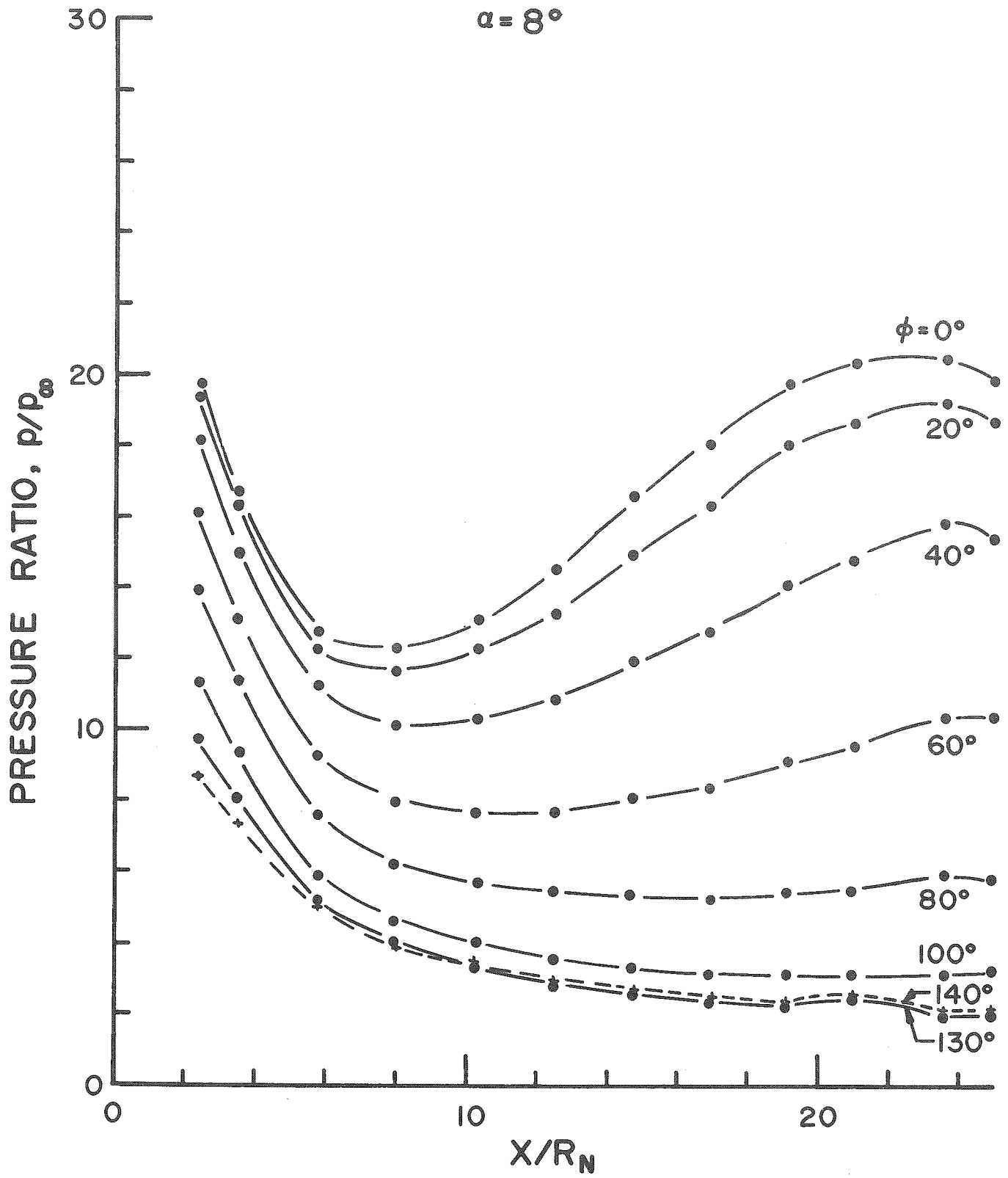

Figure 29. Longitudinal Pressure Distributions, 30% Bluntness, α = 8 Degrees

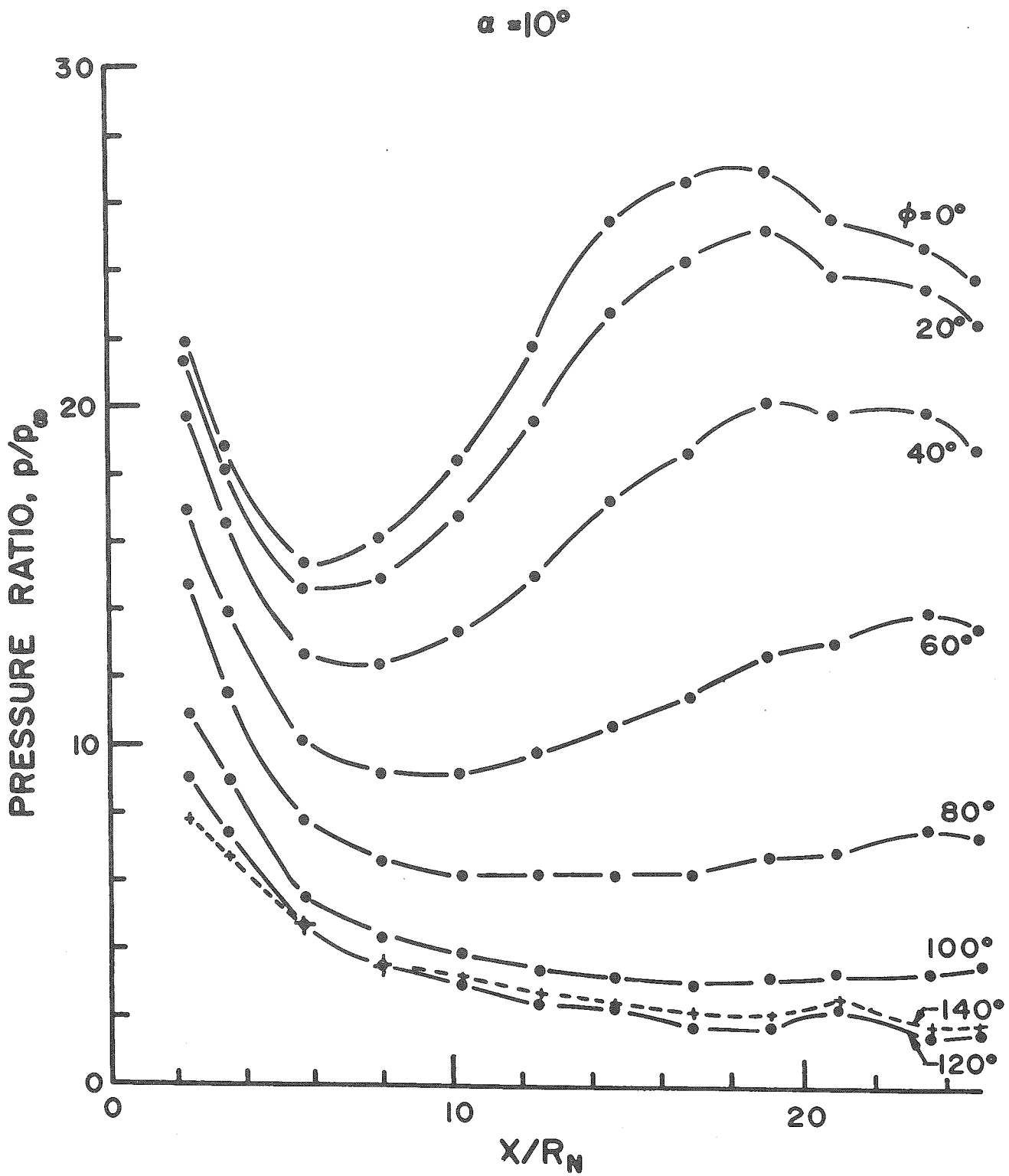

Figure 30. Longitudinal Pressure Distributions, 30% Bluntness, α = 10 Degrees

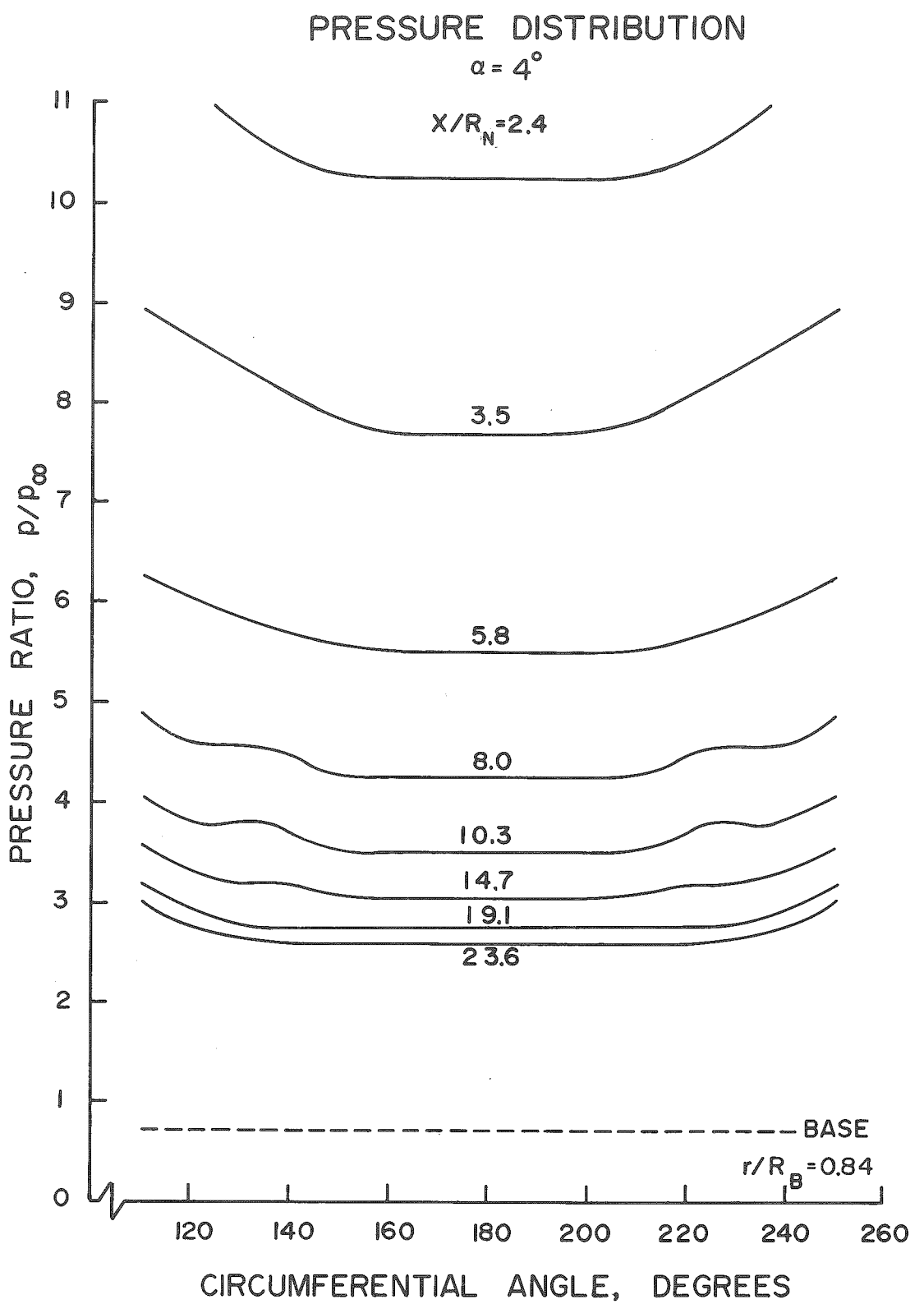

Figure 31. Circumferential Pressure Distributions, 30% Bluntness, α = 4 Degrees

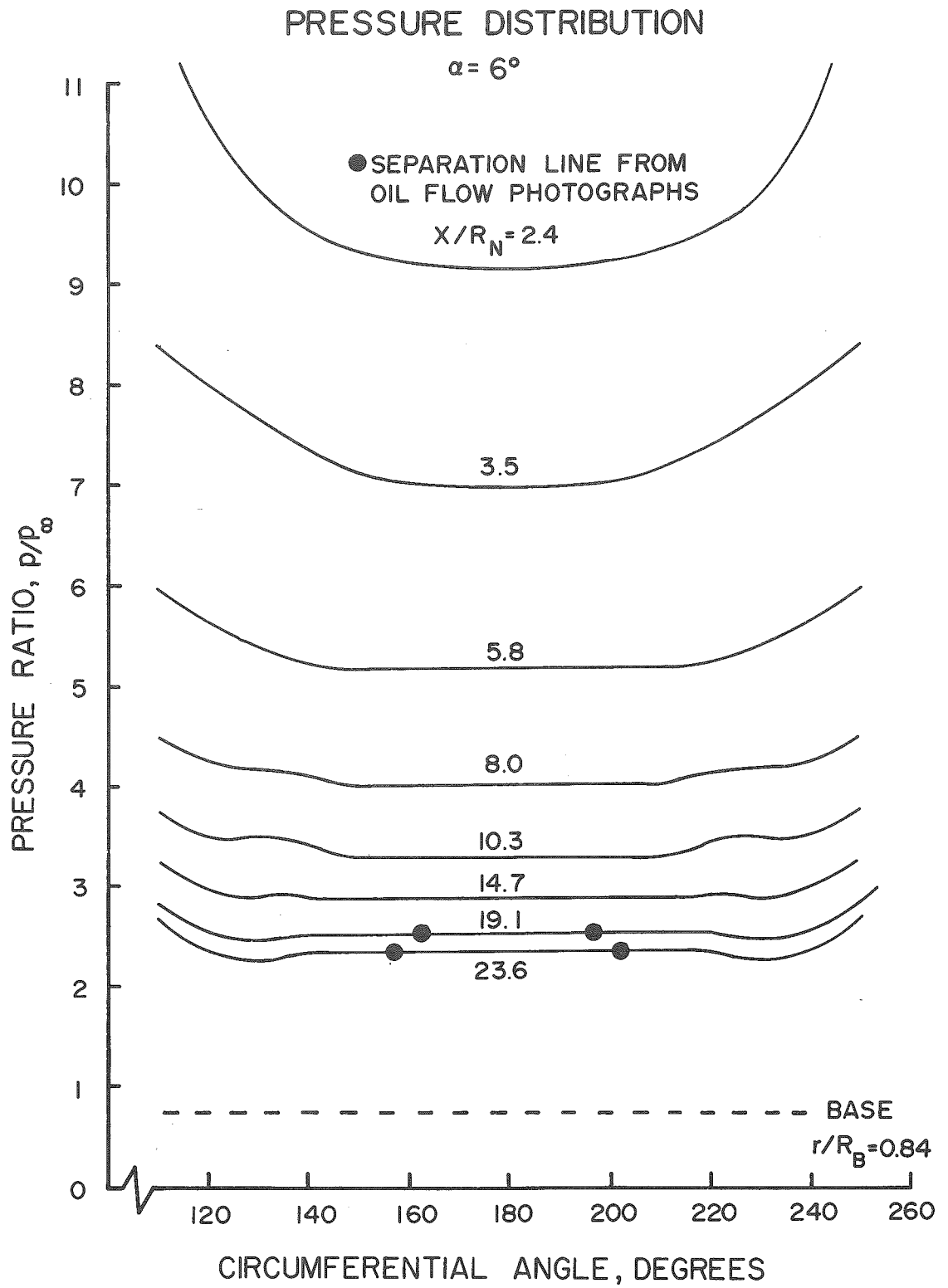

Figure 32. Circumferential Pressure Distributions, 30% Bluntness, α = 6 Degrees

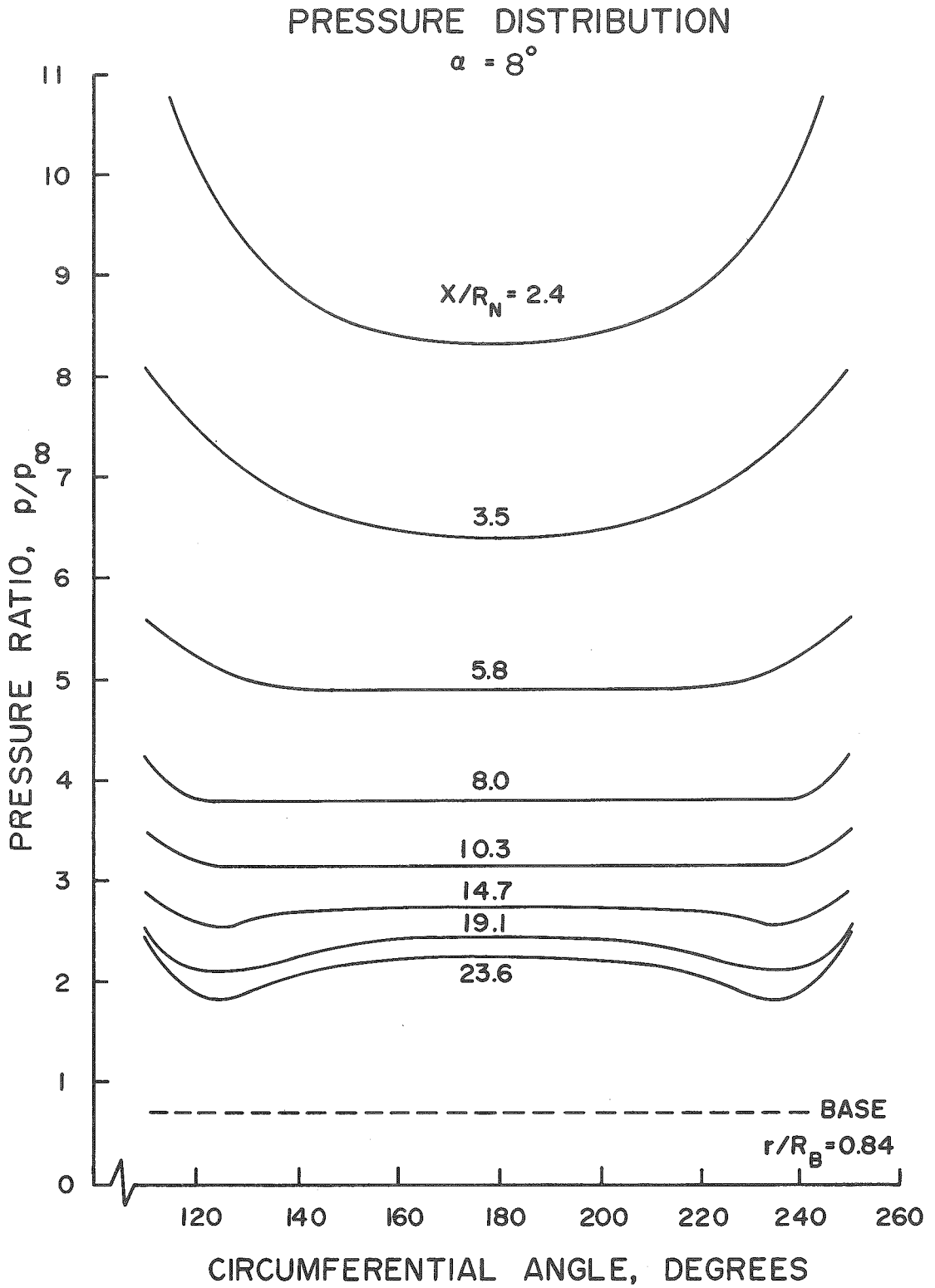

Figure 33. Circumferential Pressure Distributions, 30% Bluntness, α = 8 Degrees

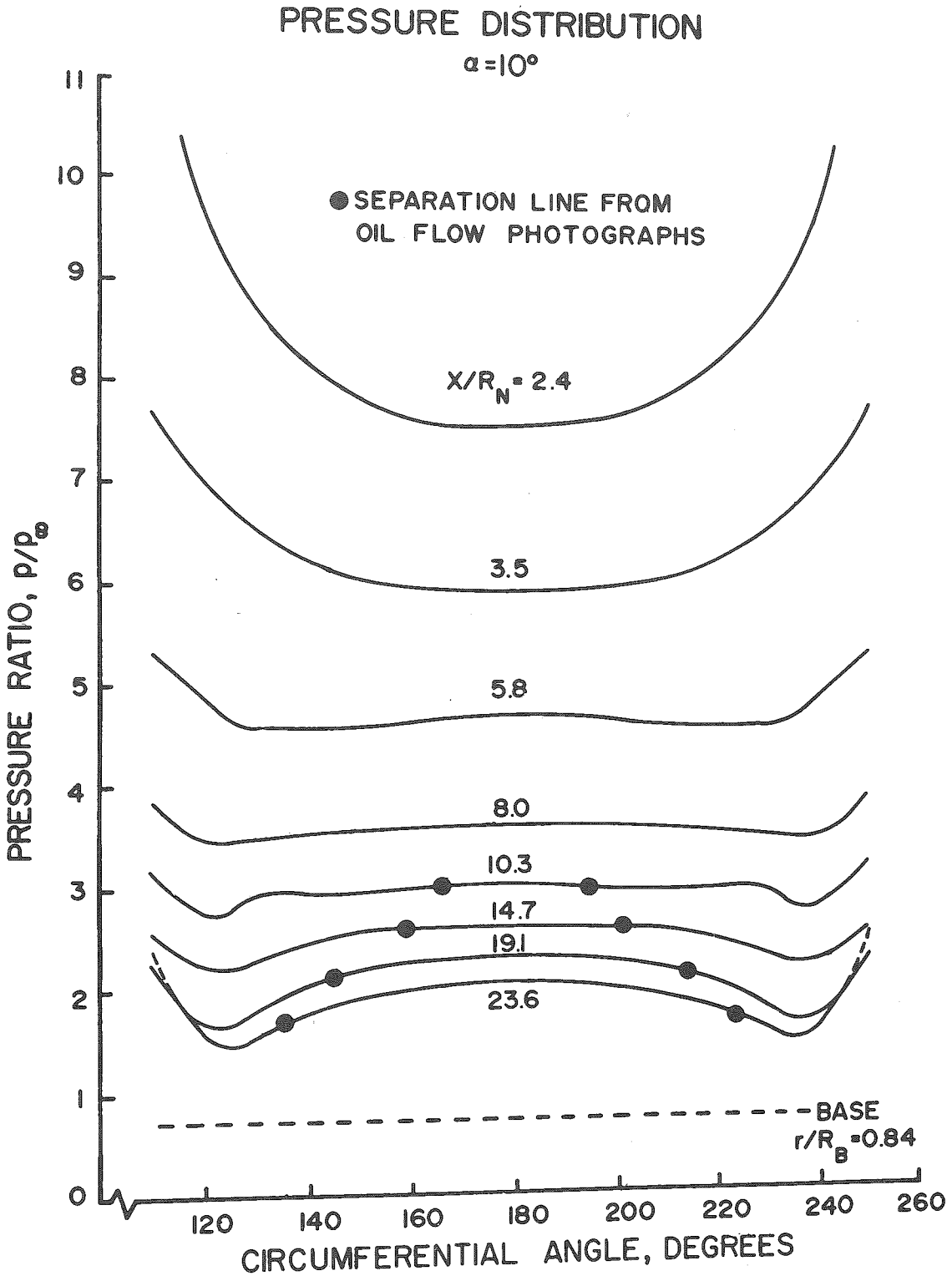

Figure 34. Circumferential Pressure Distributions, 30% Bluntness, α = 10 Degrees

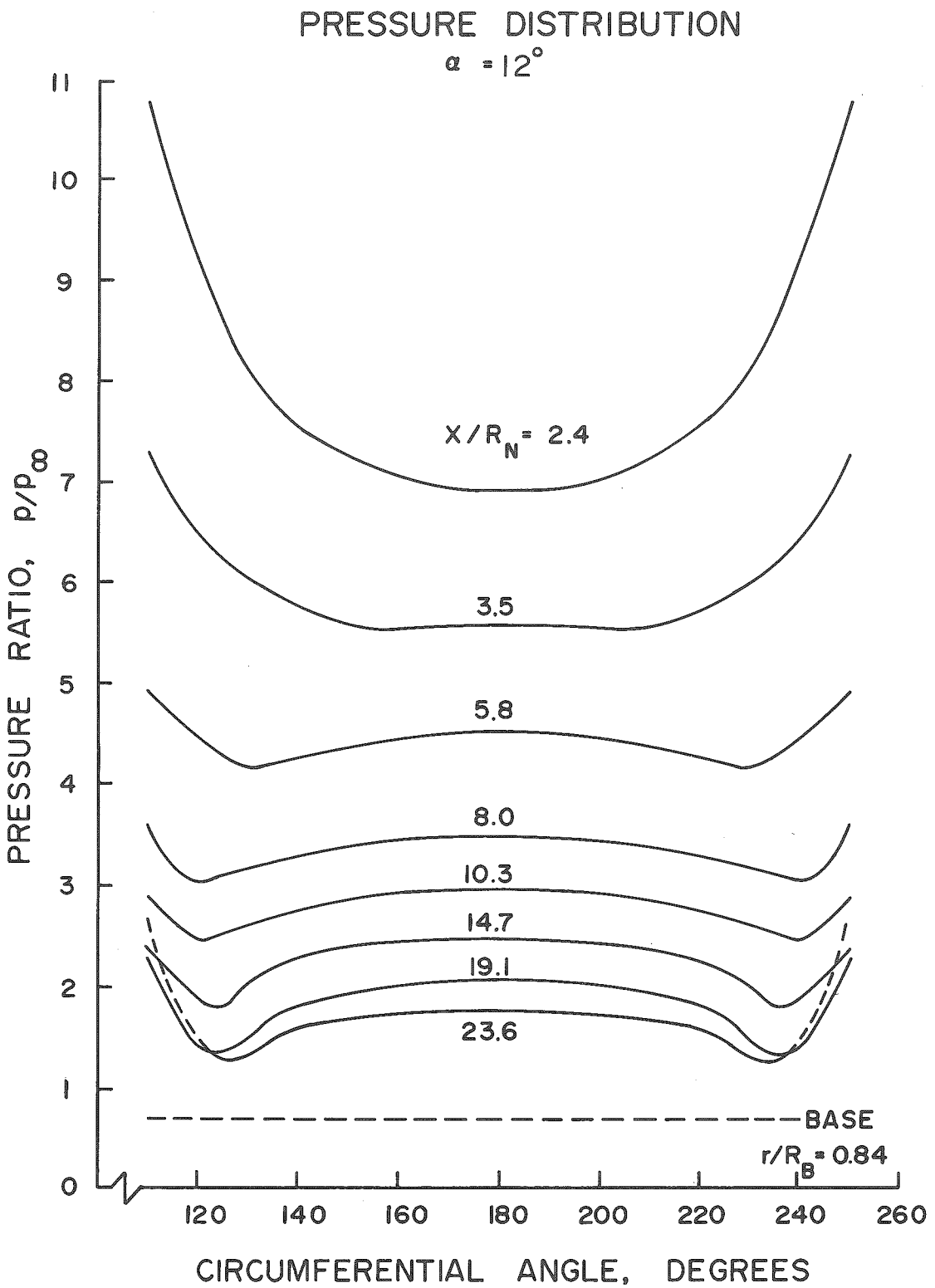

Figure 35. Circumferential Pressure Distributions, 30% Bluntness, α = 12 Degrees

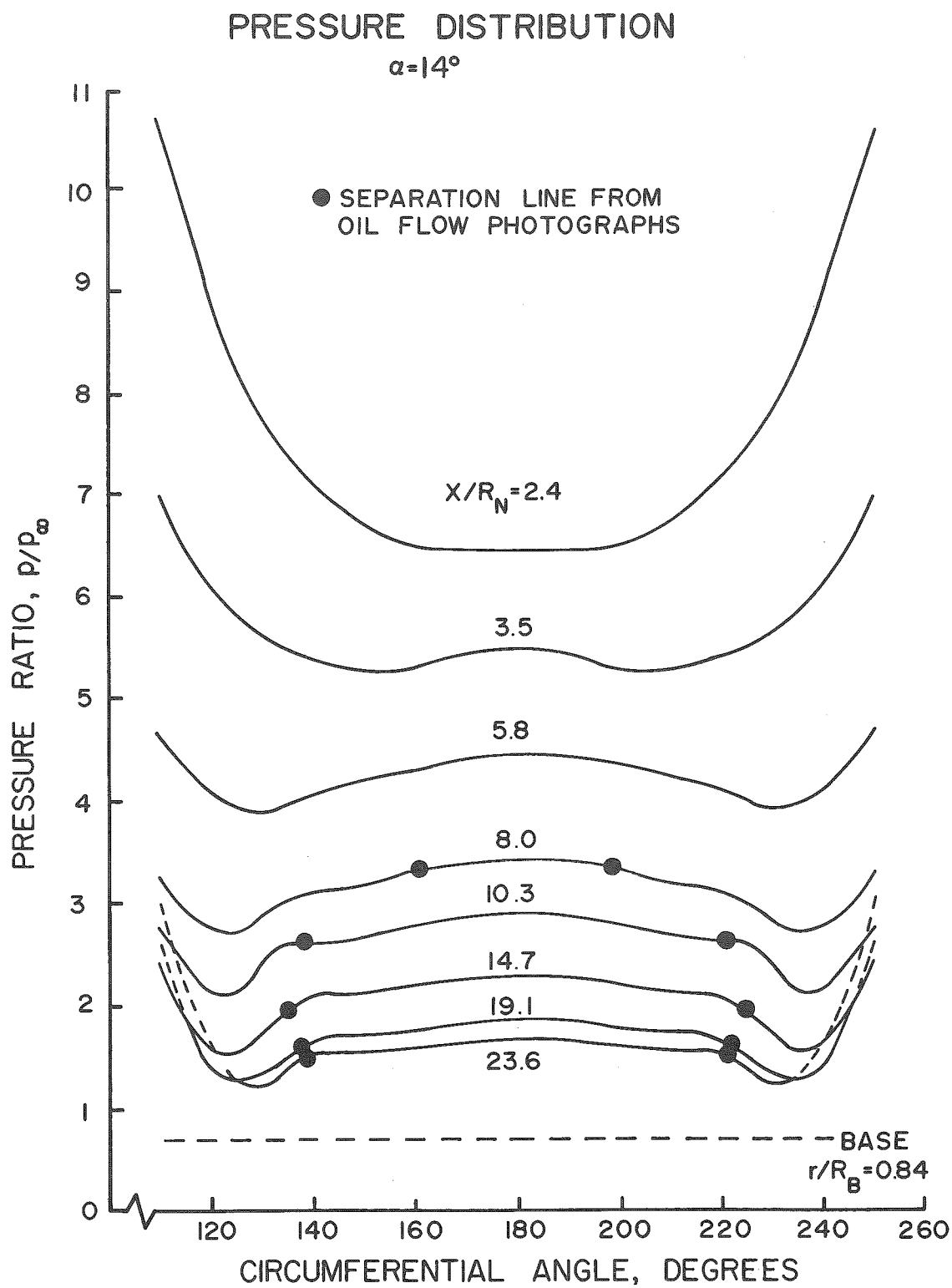

Figure 36. Circumferential Pressure Distributions, 30% Bluntness, α = 14 Degrees

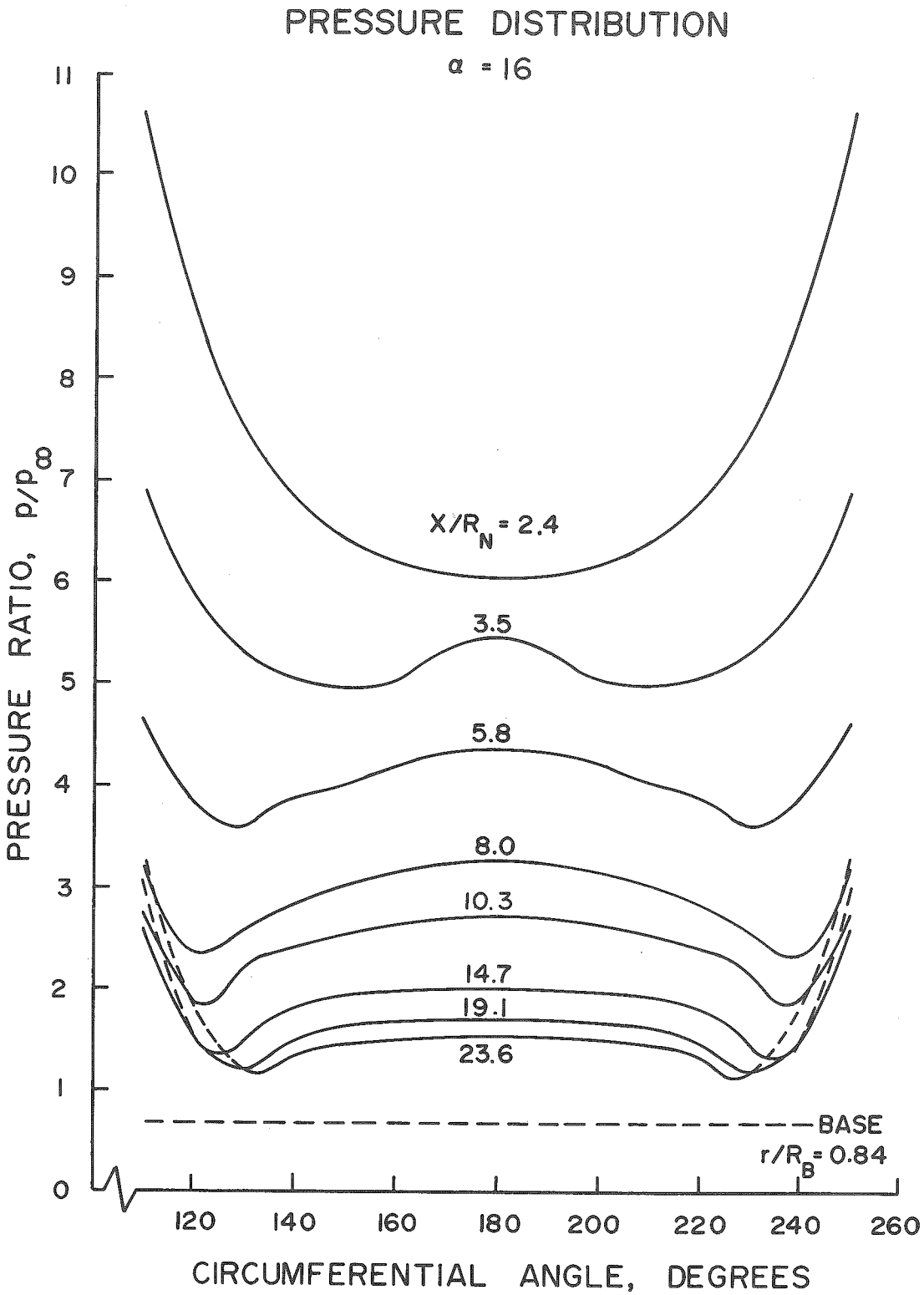

Figure 37. Circumferential Pressure Distributions, 30% Bluntness, α = 16 Degrees

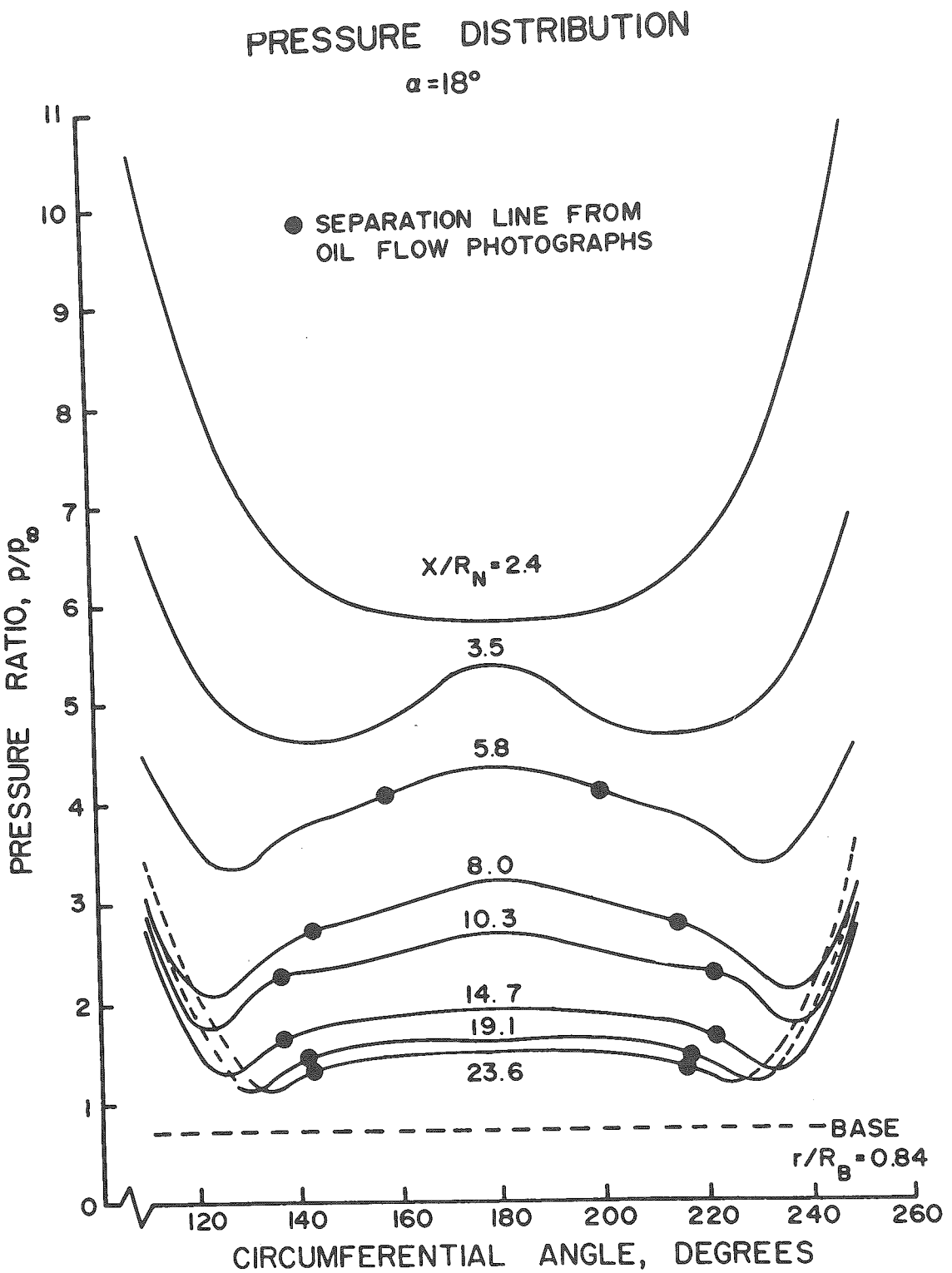

Figure 38. Circumferential Pressure Distributions, 30% Bluntness, α = 18 Degrees

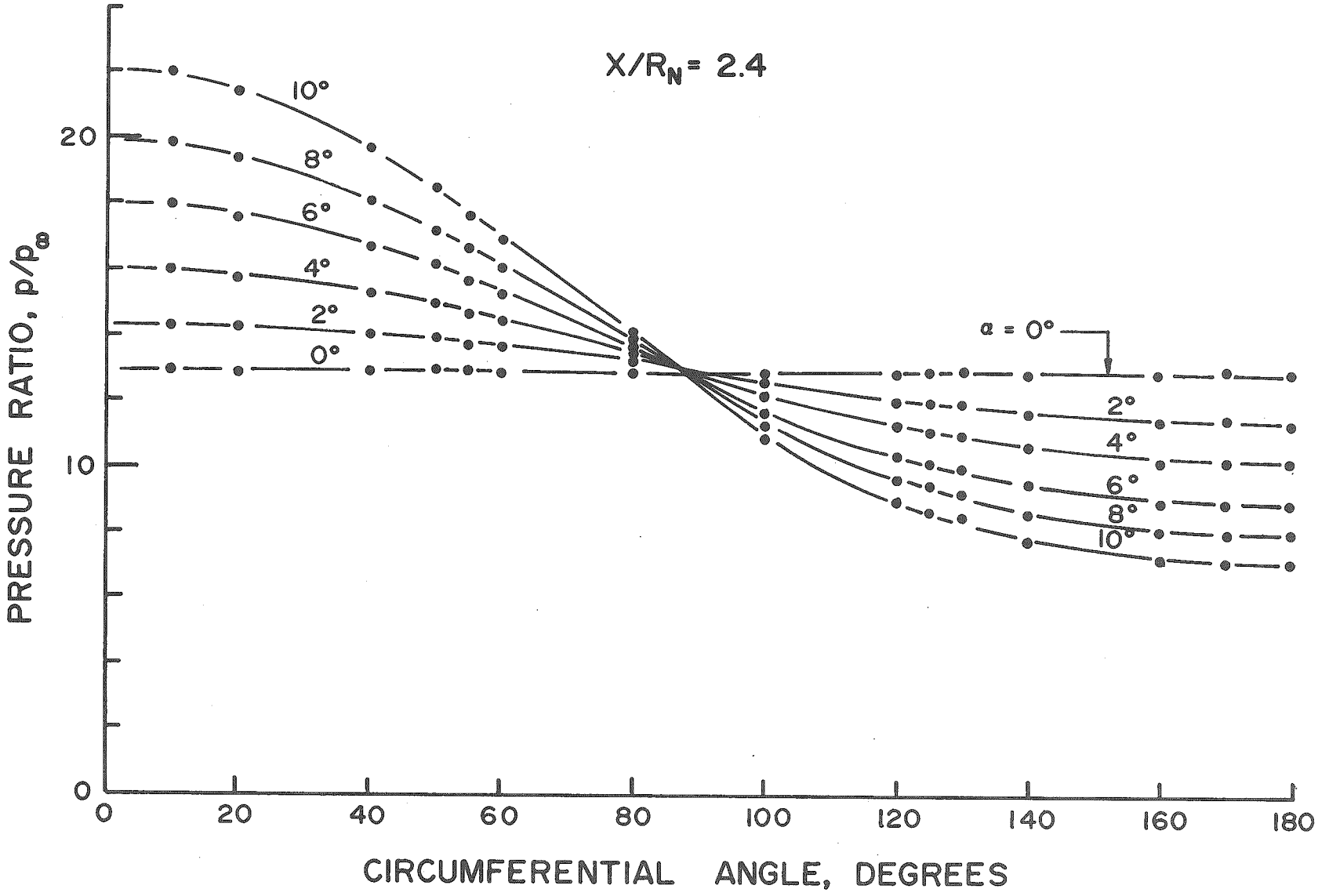

Figure 39. Circumferential Pressure Distributions, ϕ = 0° to 180°, X/R_N = 2.4

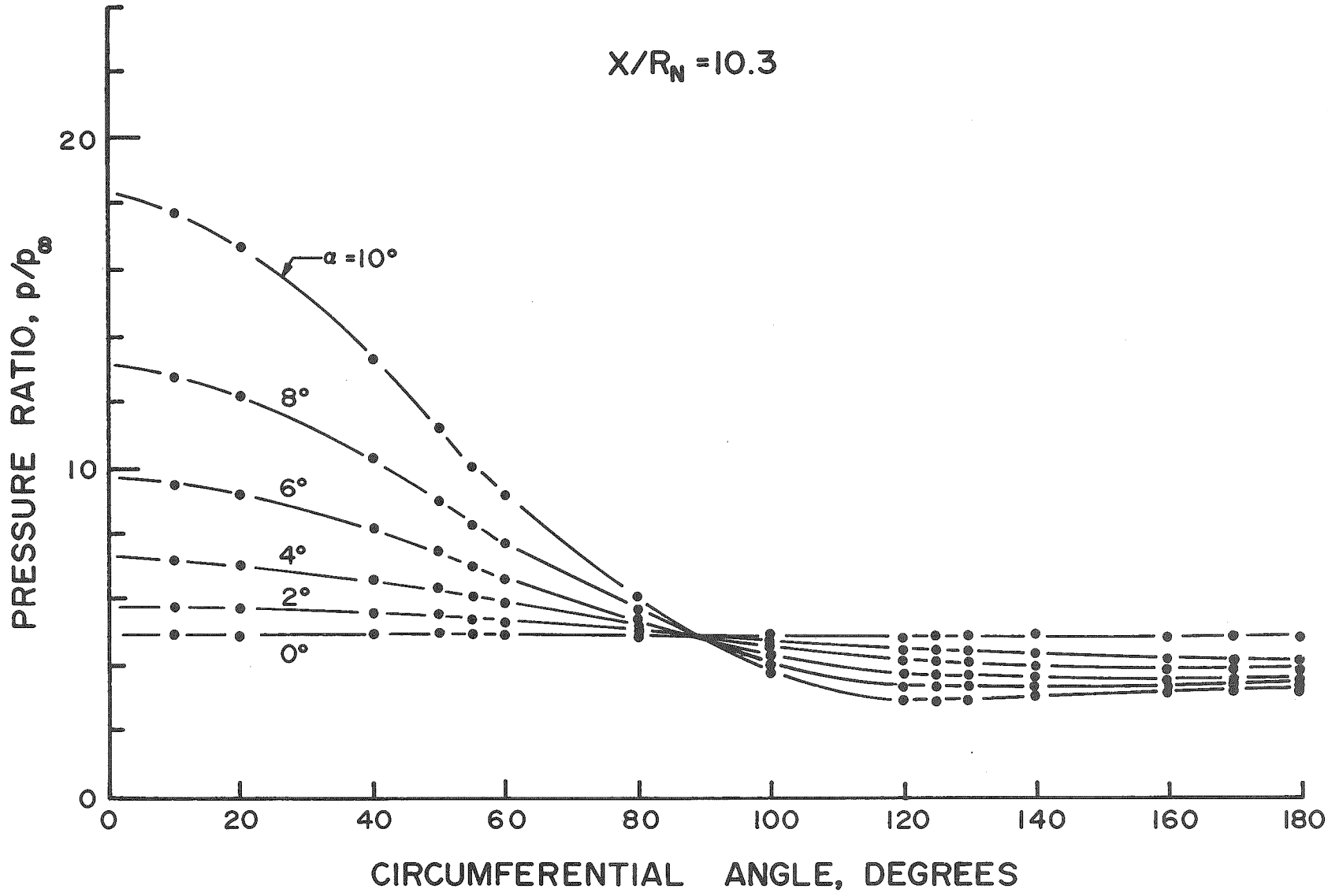

Figure 40. Circumferential Pressure Distributions, ϕ = 0° to 180°, X/R_N = 10.3

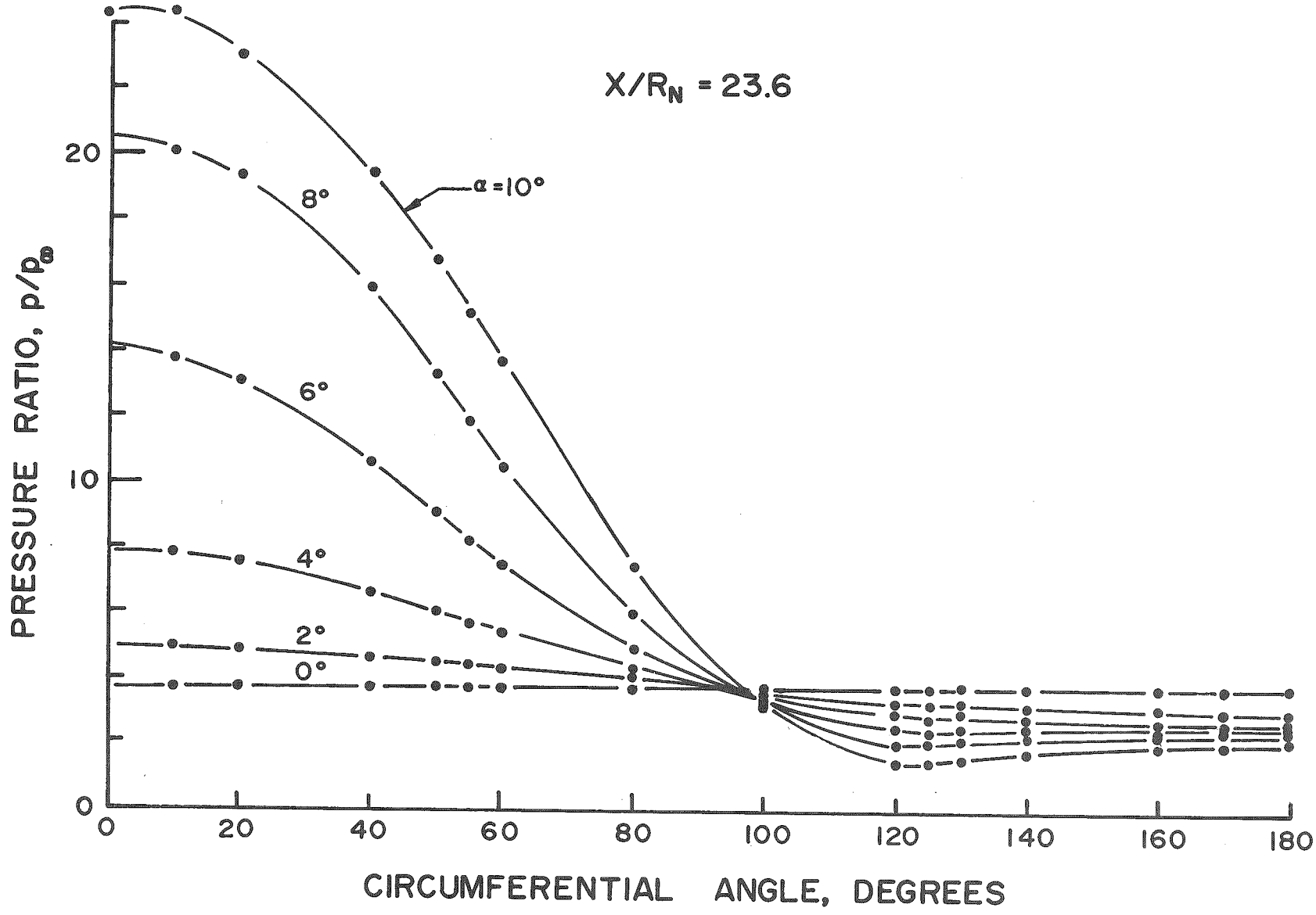

Figure 41. Circumferential Pressure Distributions, $\phi = 0°$ to $180°$, $X/R_N = 23.6$

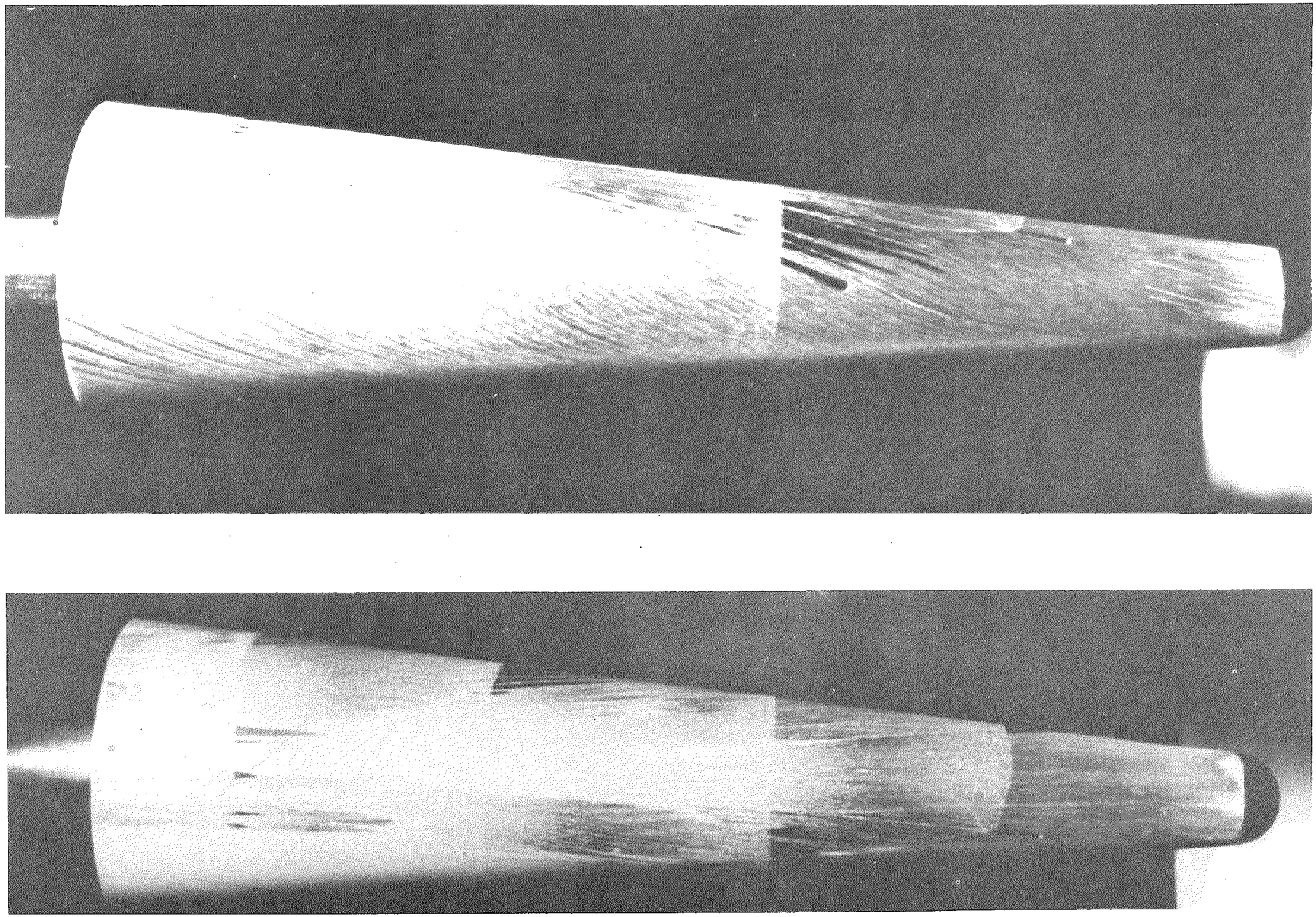

Figure 42. Oil Flow Photographs, Side and Leeward Views, 30% Bluntness, α = 4 Degrees

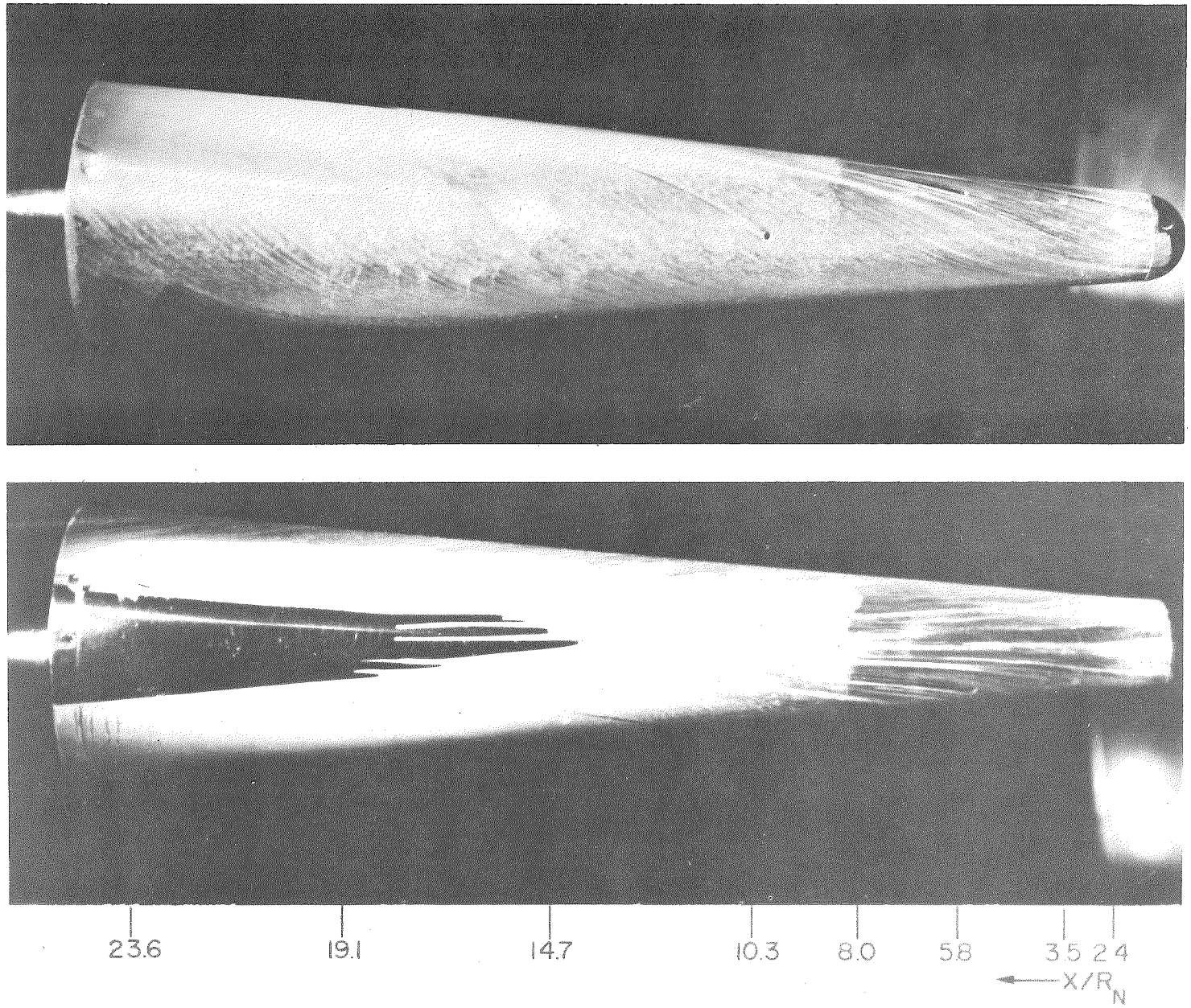

Figure 43. Oil Flow Photographs, Side and Leeward Views, 30% Bluntness, α = 6 Degrees

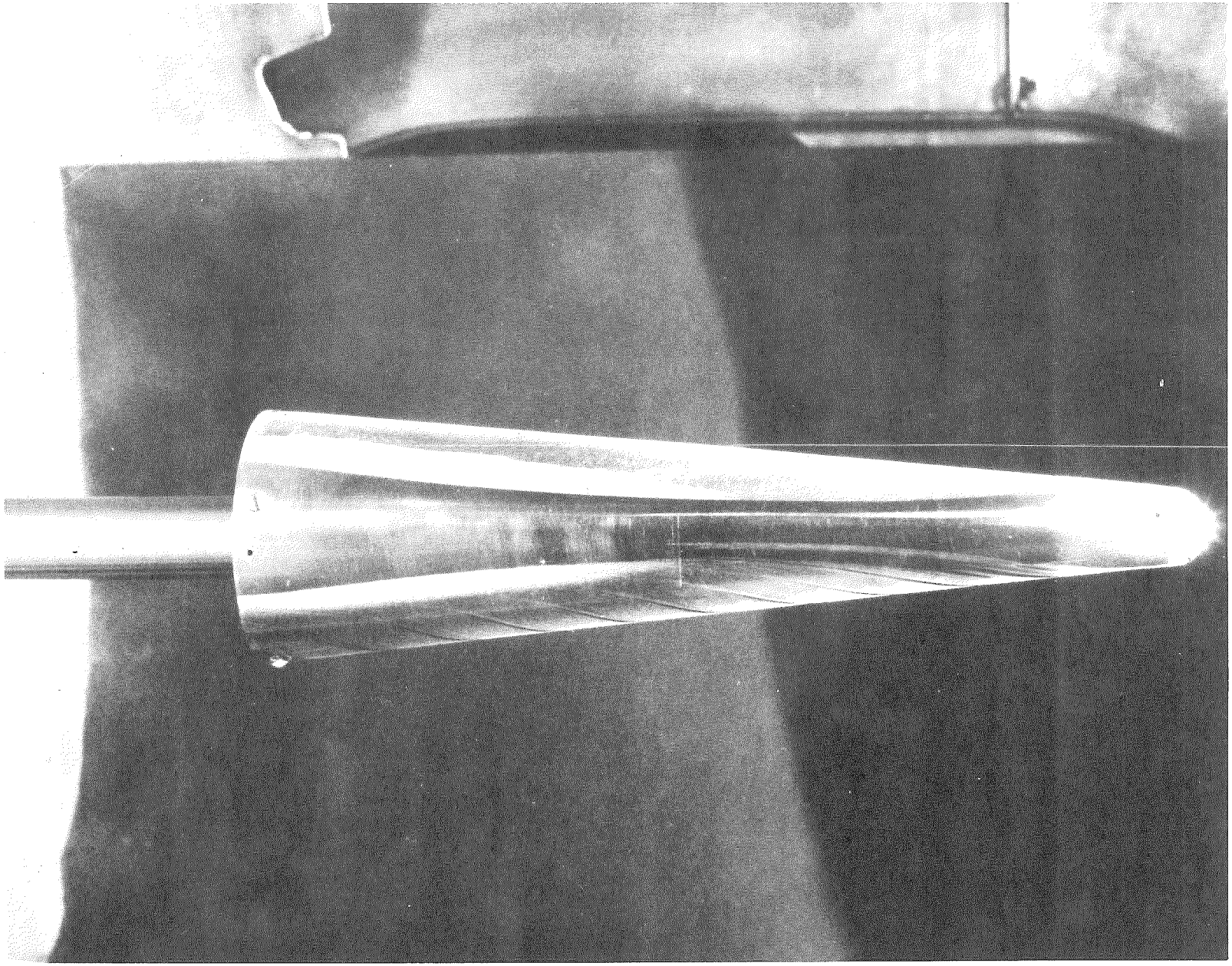

Figure 44. Oil Flow Photograph, Leeward View, 30% Bluntness, α = 8 Degrees

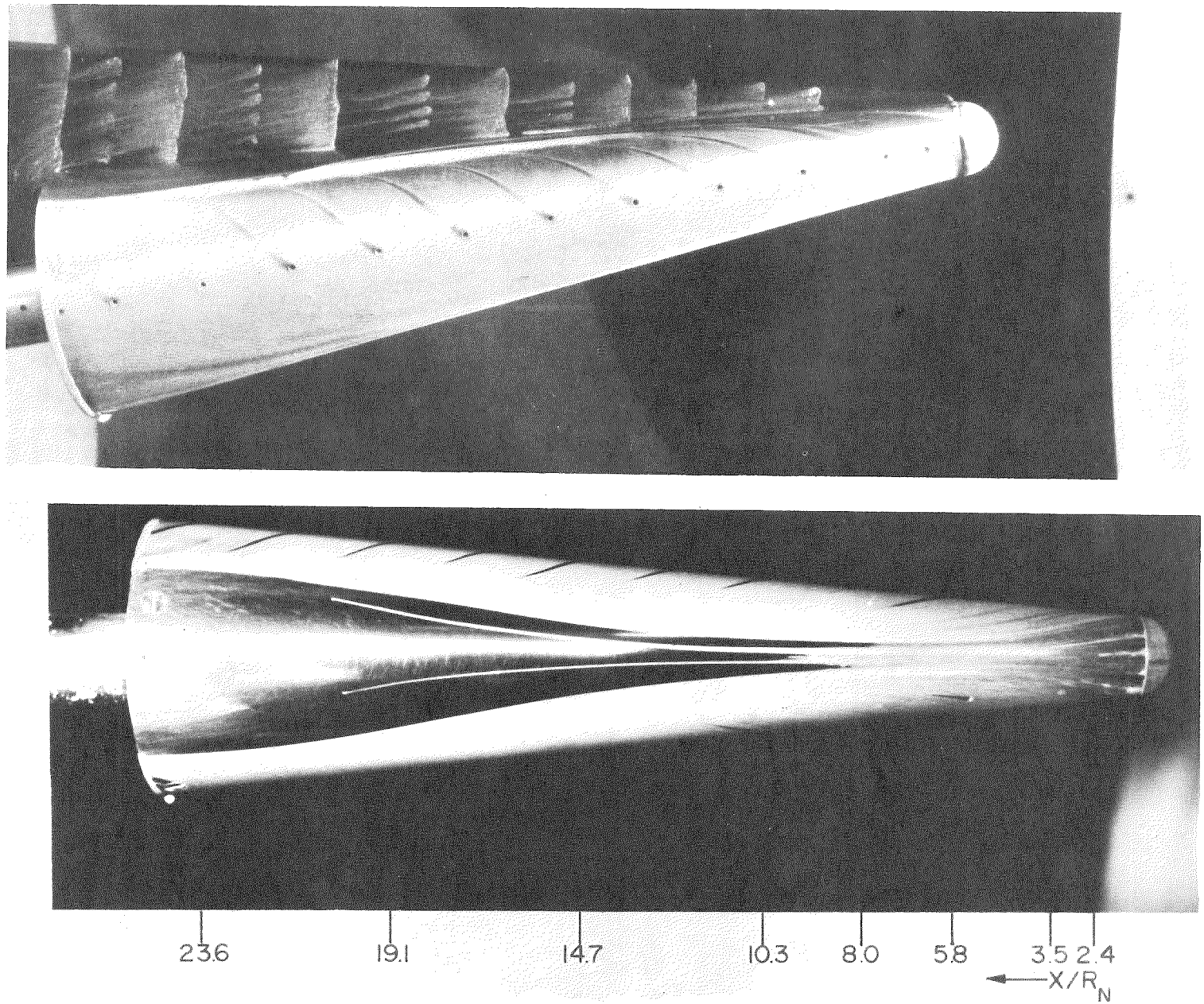

Figure 45. Oil Flow Photographs, Side and Leeward Views, 30% Bluntness, α = 10 Degrees

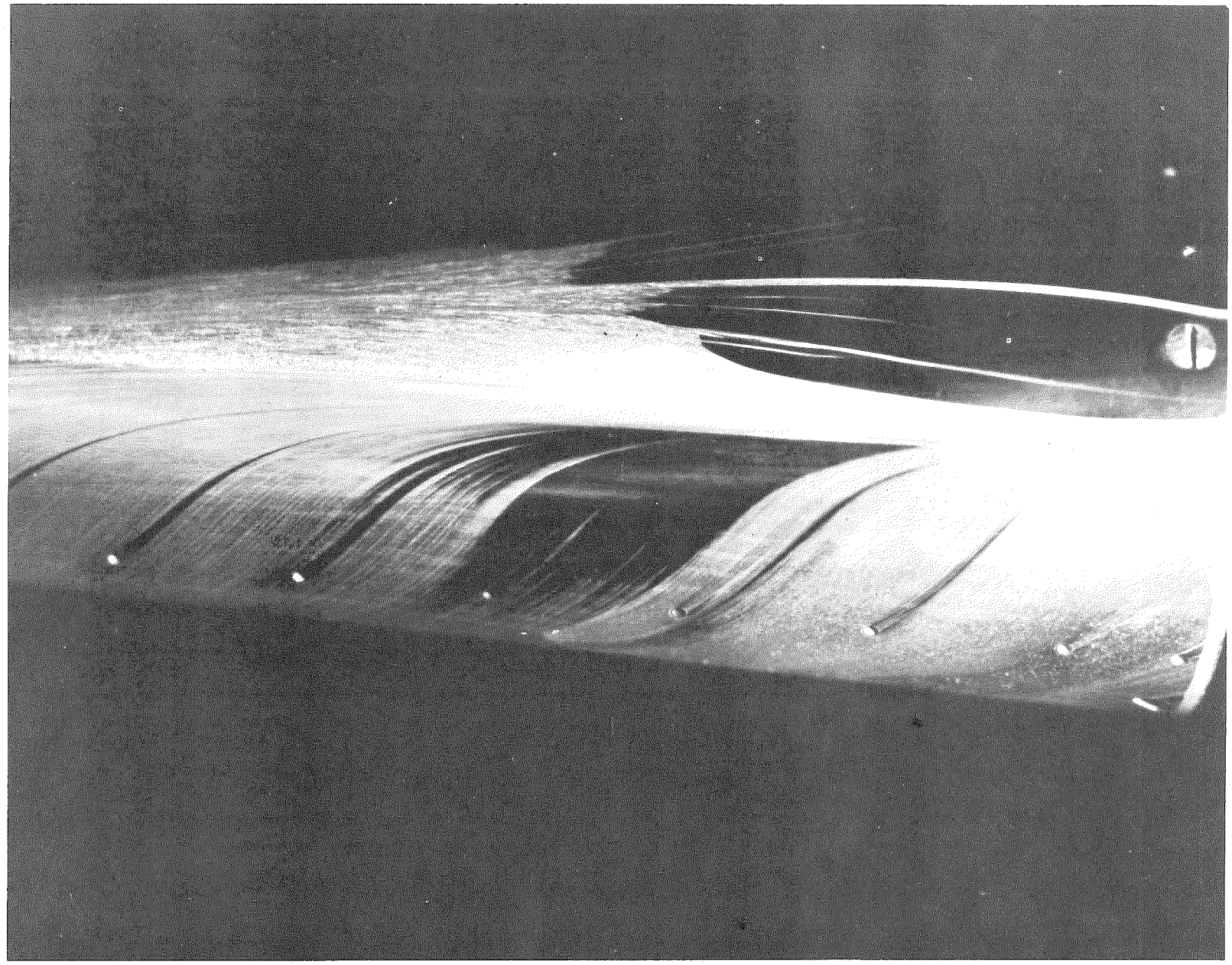

Figure 46. Oil Flow Photograph, Leeward and Side Region, 30% Bluntness, α = 10 Degrees

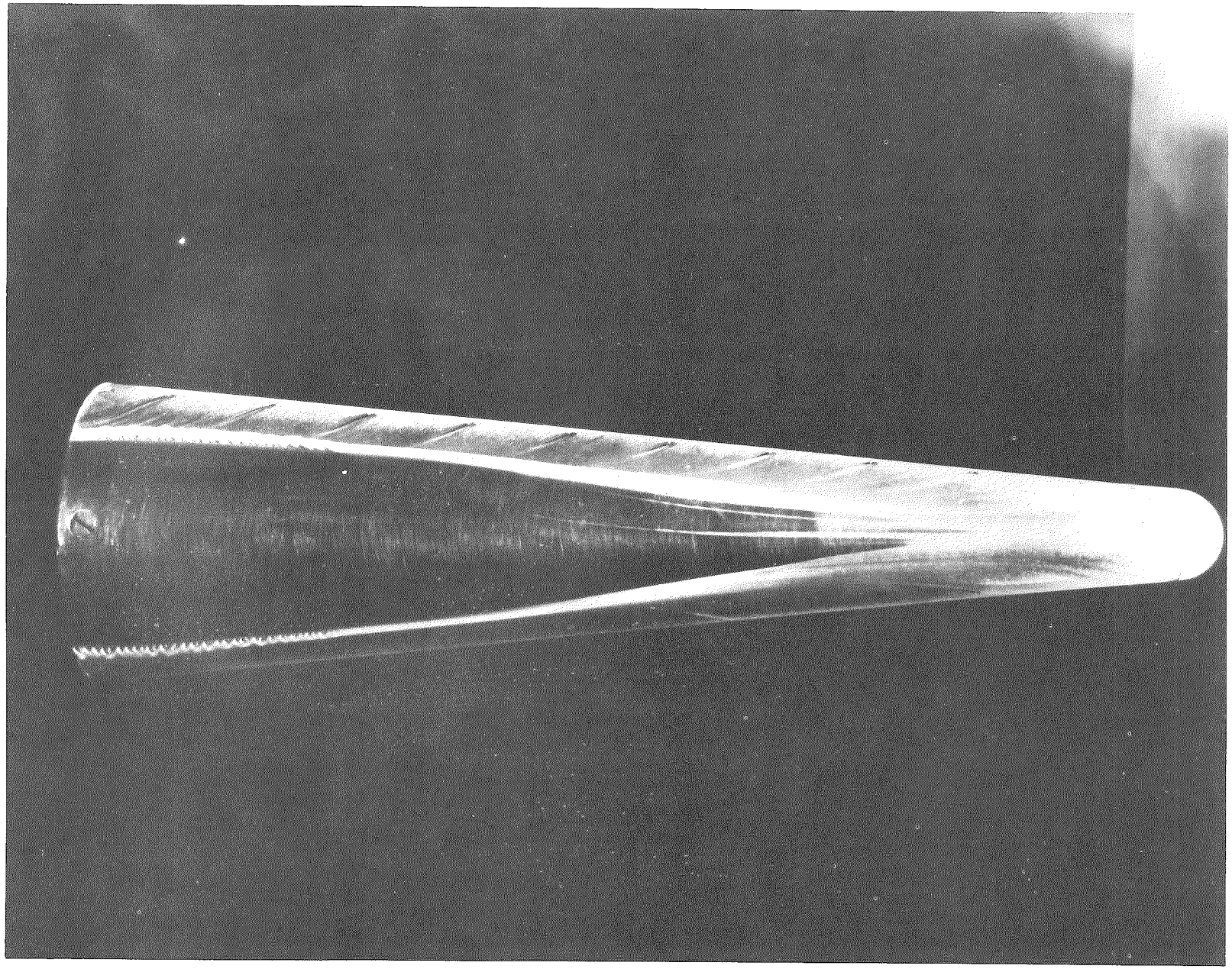

Figure 47. Oil Flow Photograph, Leeward View, 30% Bluntness, α = 12 Degrees

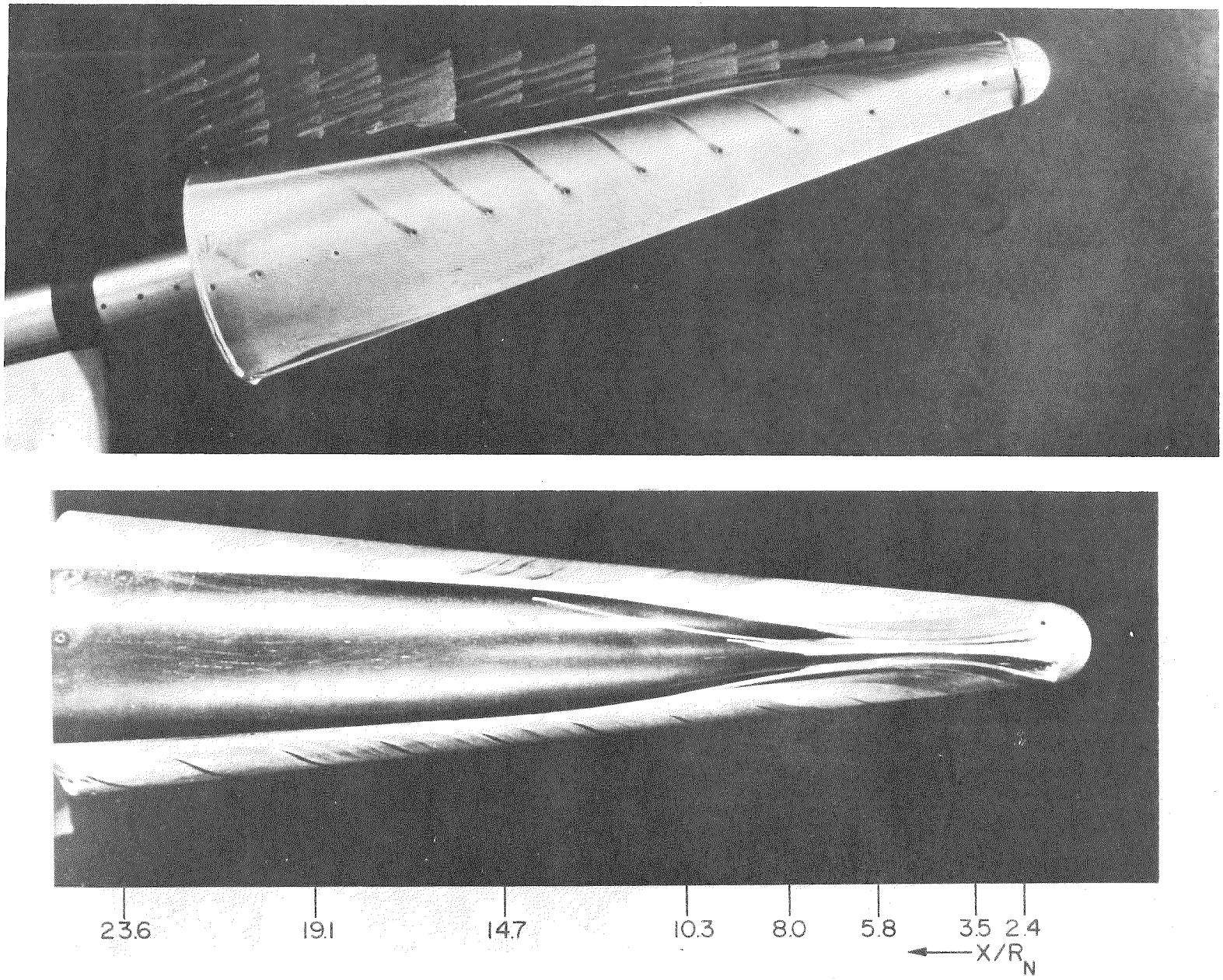

Figure 48. Oil Flow Photographs, Side and Leeward Views, 30% Bluntness, α = 14 Degrees

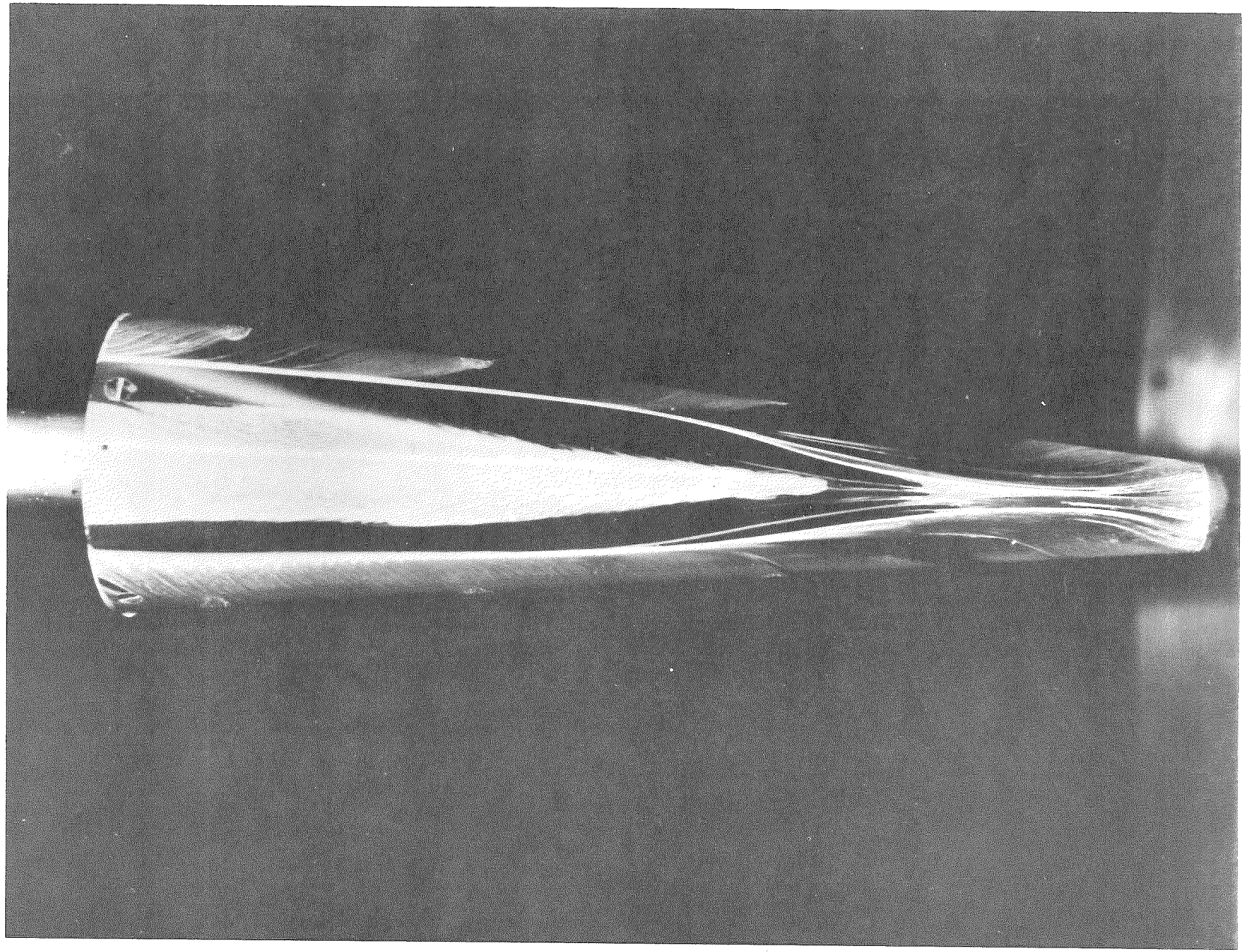

Figure 49. Oil Flow Photograph, Leeward View, 30% Bluntness, α = 14 Degrees

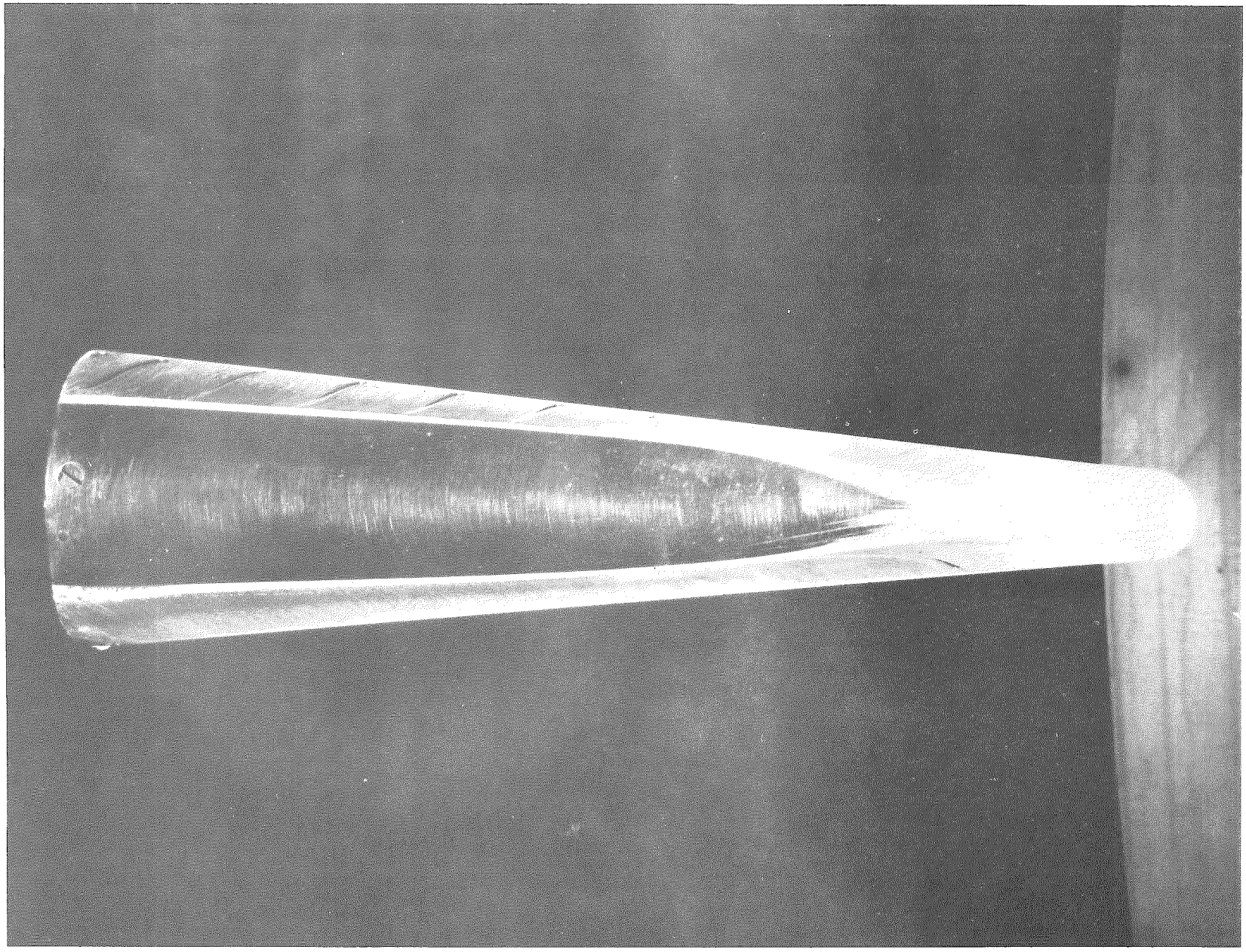

Figure 50. Oil Flow Photograph, Leeward View, 30% Bluntness, α = 16 Degrees

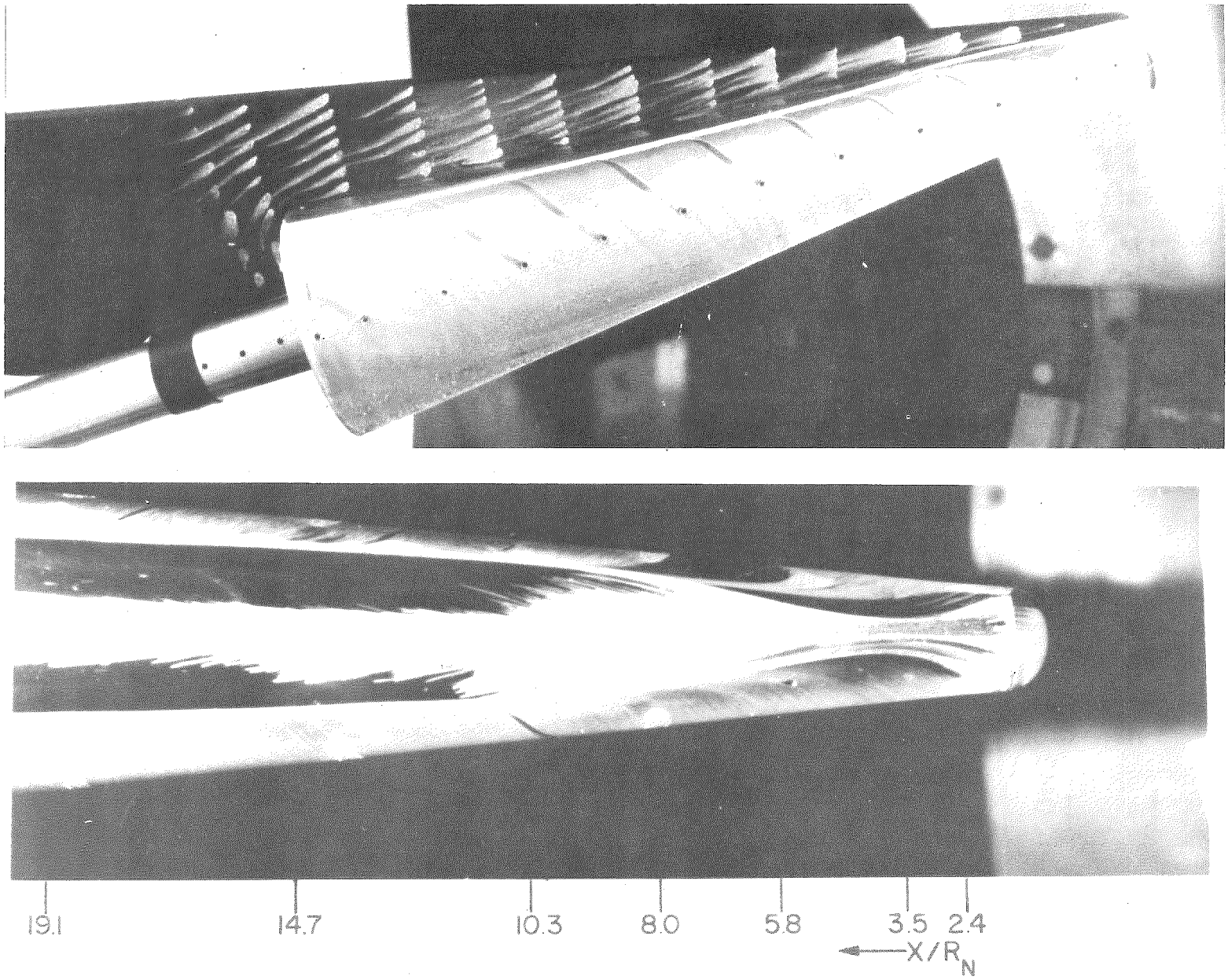

Figure 51. Oil Flow Photographs, Side and Leeward Views, 30% Bluntness, α = 18 Degrees

$X/R_N = 8$

$\alpha = 10°$

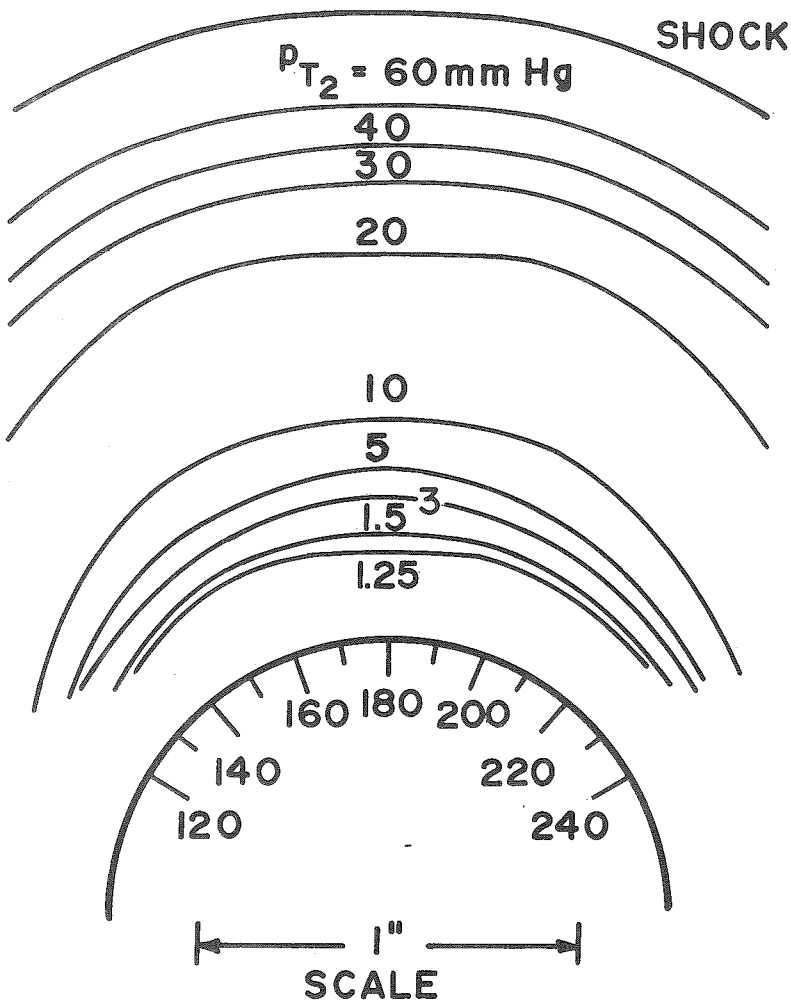

Figure 52. Blunt Cone Pitot Pressure Contours, $X/R_N = 8$, $\alpha = 10$ Degrees

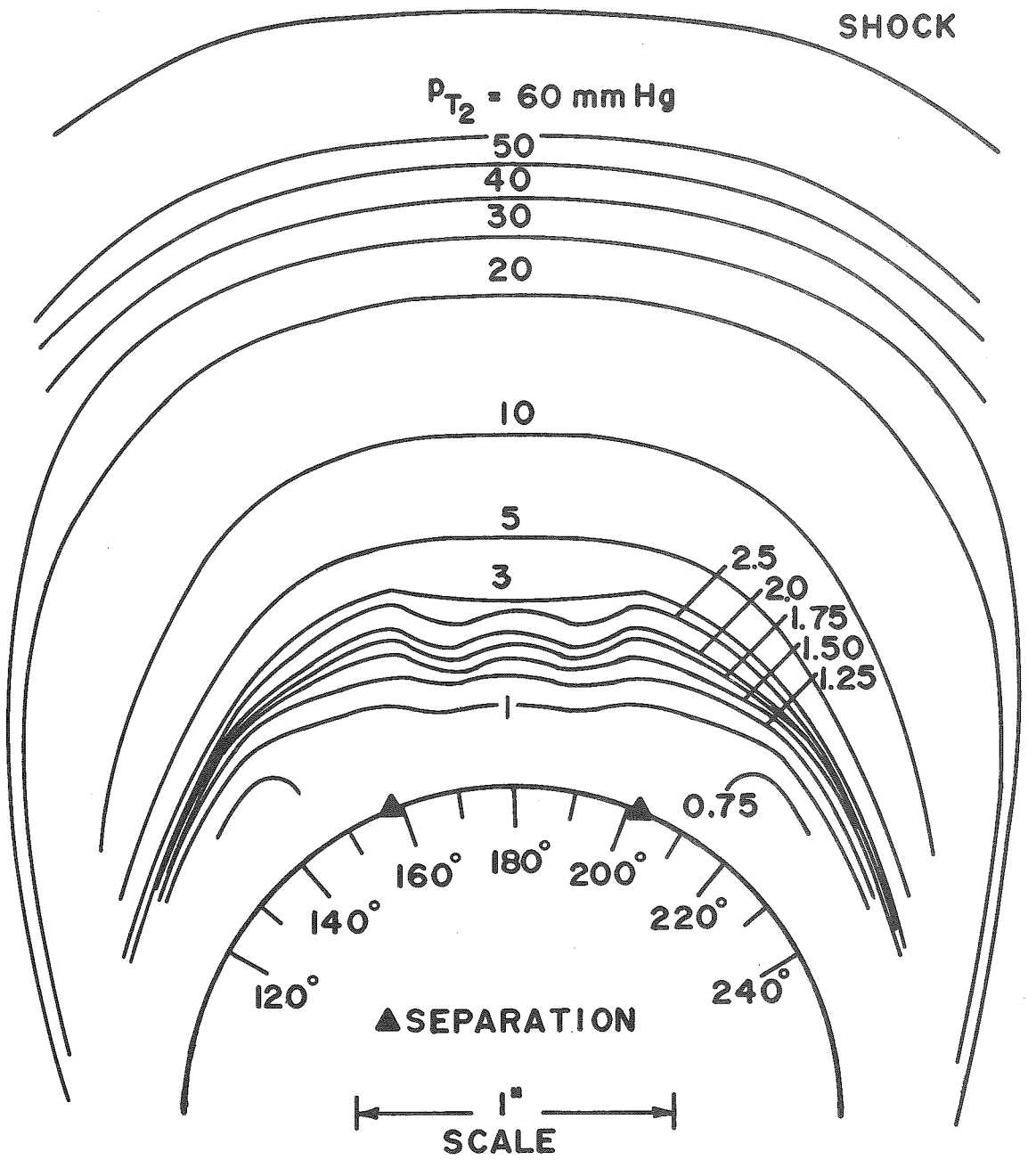

Figure 53. Blunt Cone Pitot Pressure Contours, $X/R_N = 14.7$, $\alpha = 10$ Degrees

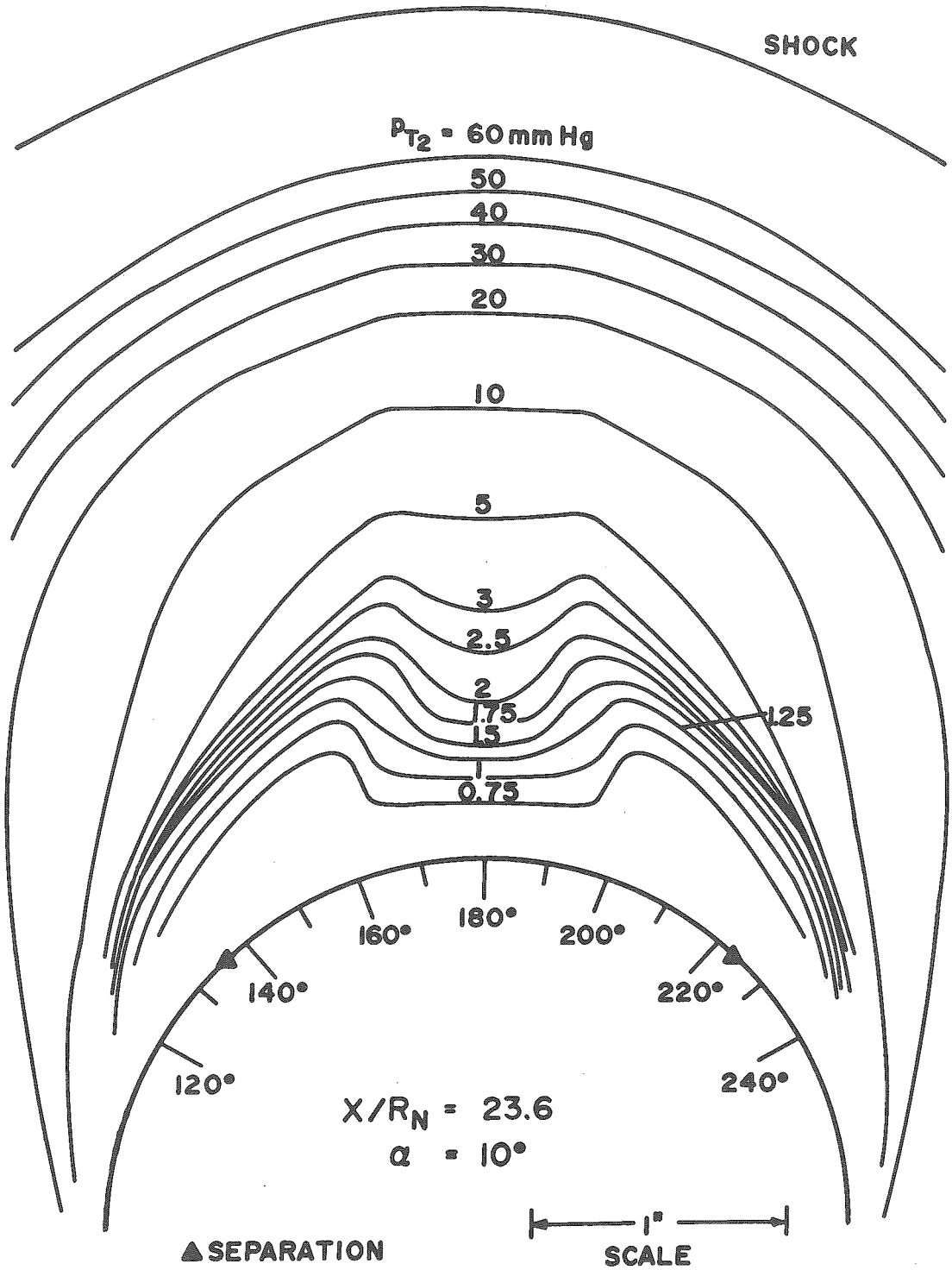

Figure 54. Blunt Cone Pitot Pressure Contours, X/R_N = 23.6, α = 10 Degrees

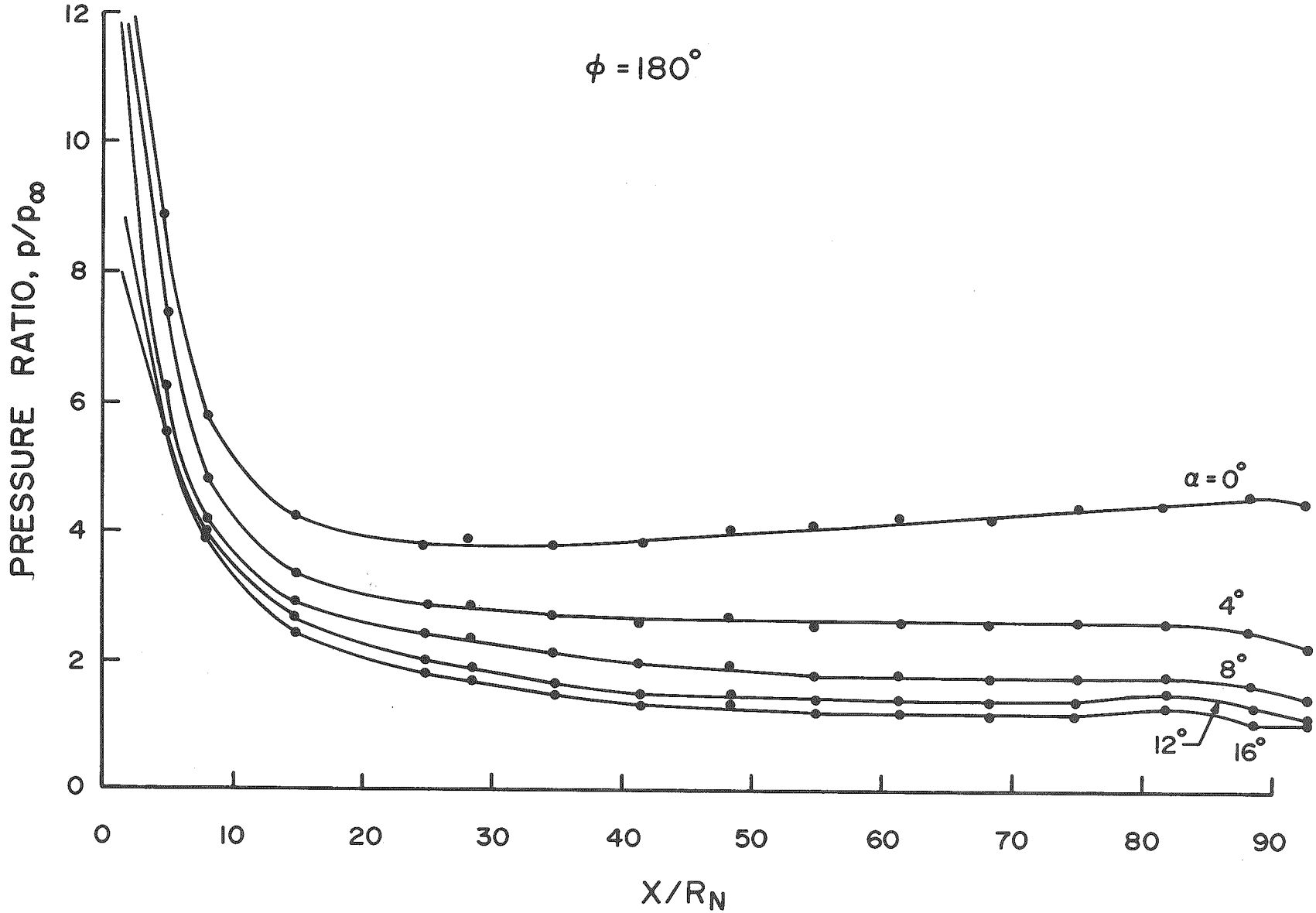

Figure 55. Pressure Distributions Along the Most Leeward Ray, 10% Bluntness

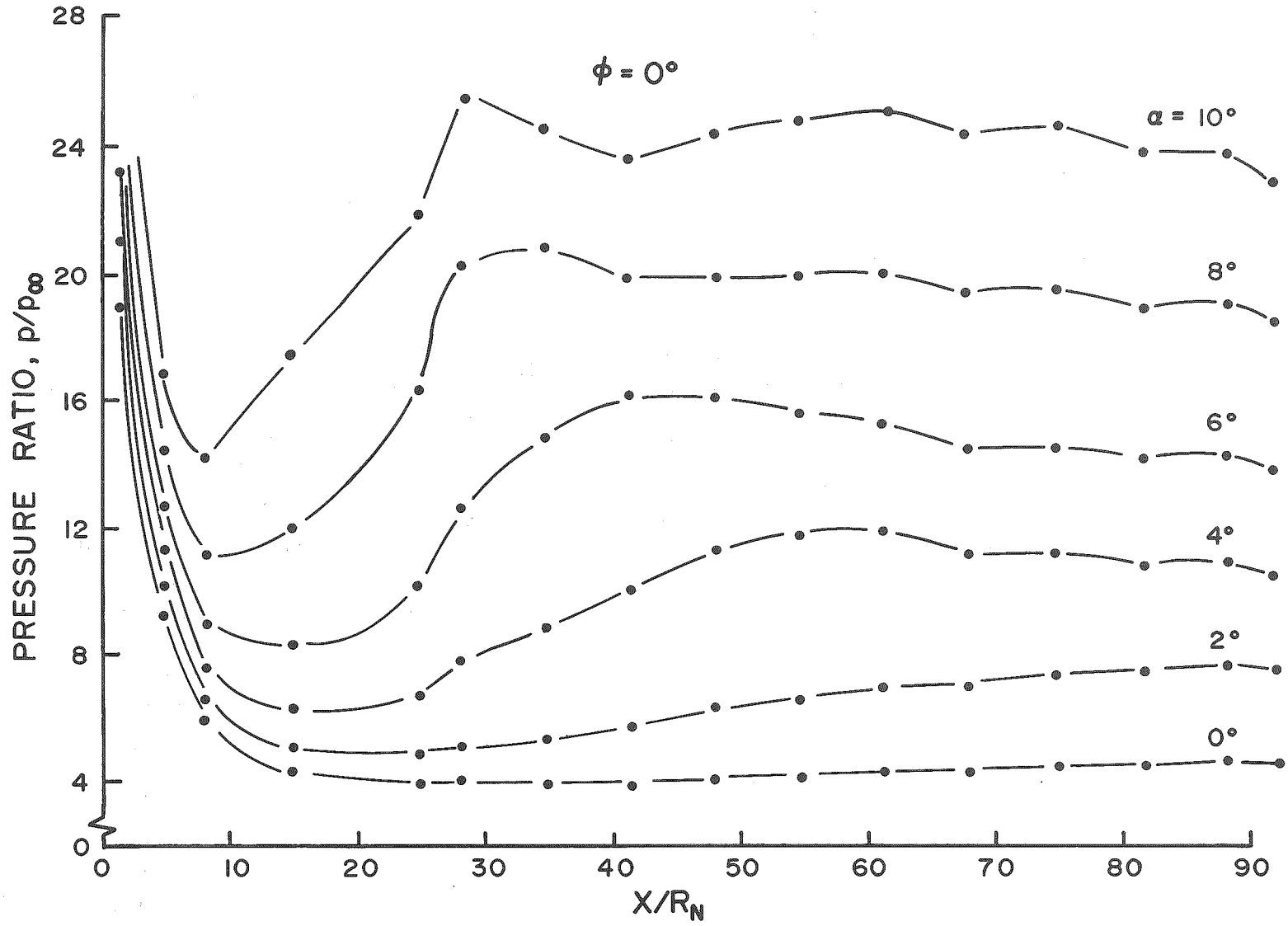

Figure 56. Pressure Distributions Along the Most Windward Ray, 10% Bluntness

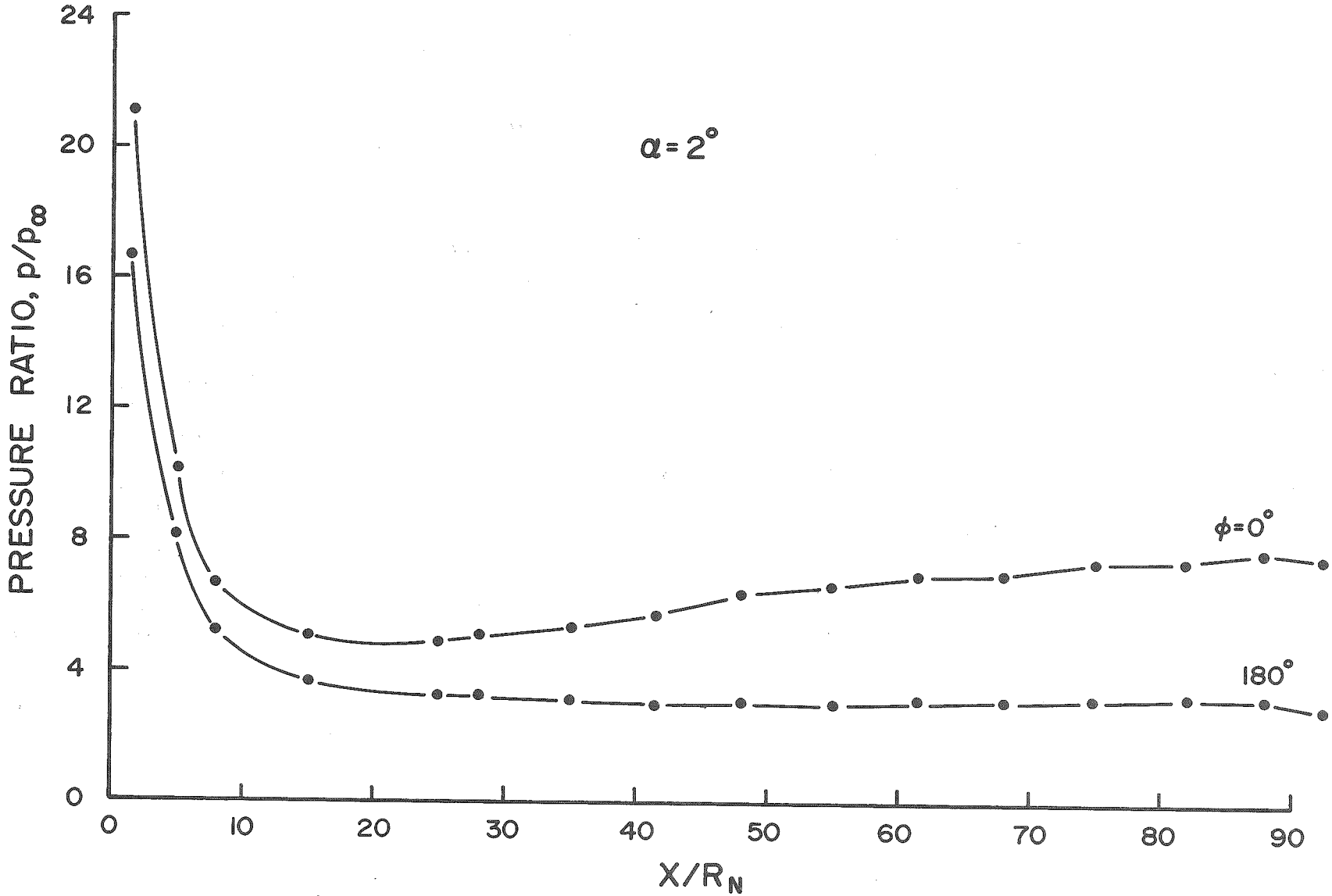

Figure 57. Longitudinal Pressure Distributions, 10% Bluntness, α = 2 Degrees

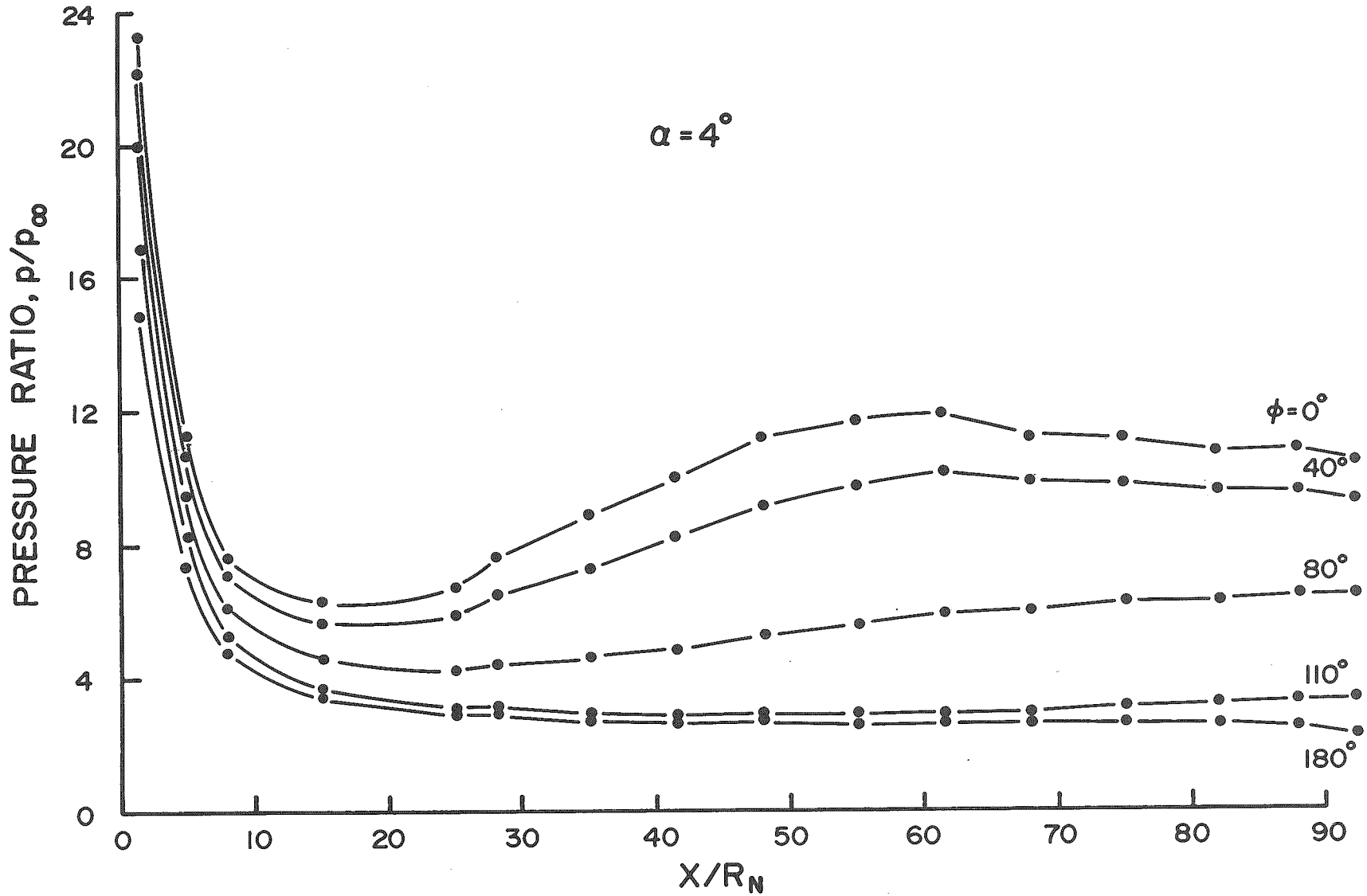

Figure 58. Longitudinal Pressure Distributions, 10% Bluntness, α = 4 Degrees

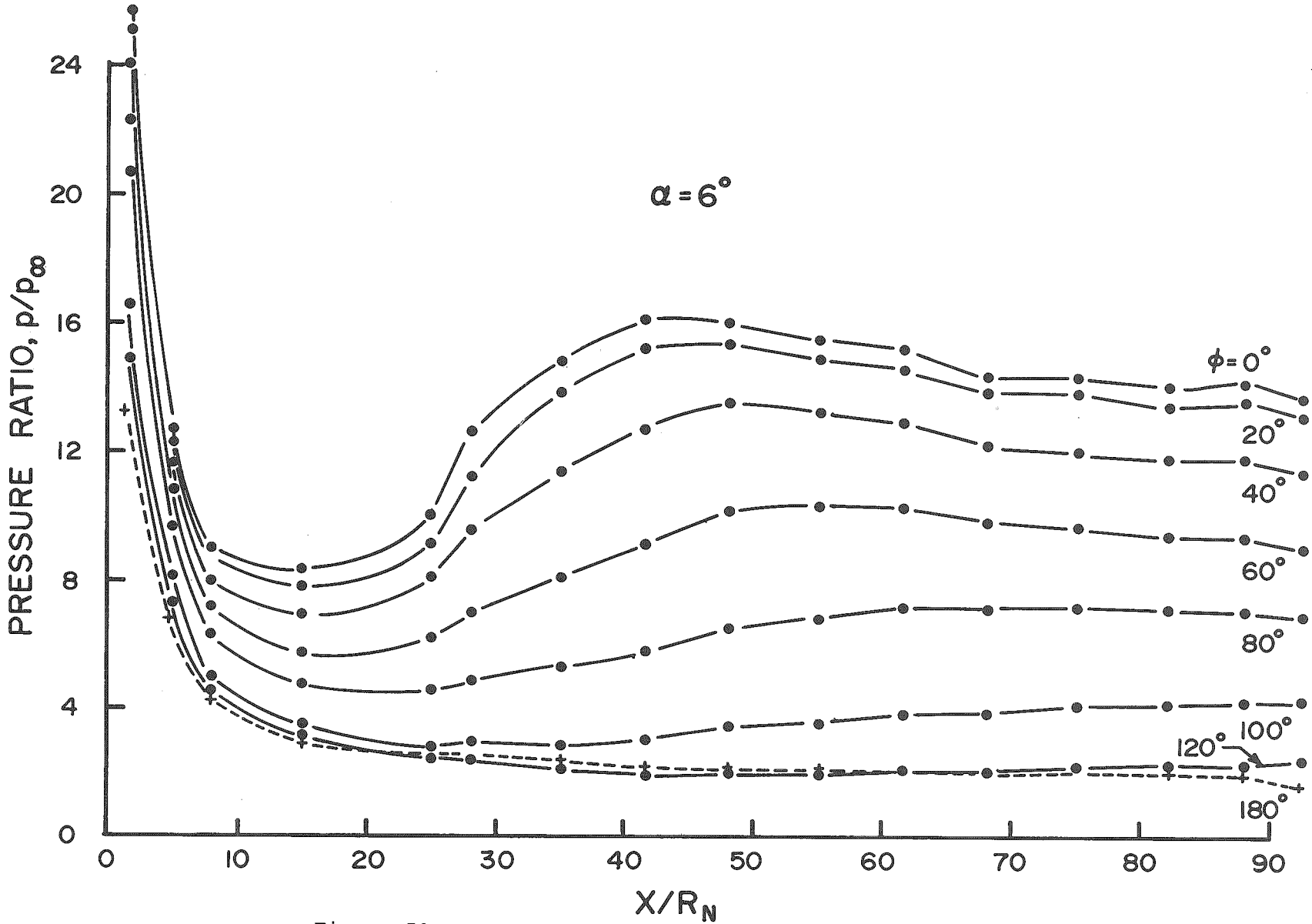

Figure 59. Longitudinal Pressure Distributions, 10% Bluntness, α = 6 Degrees

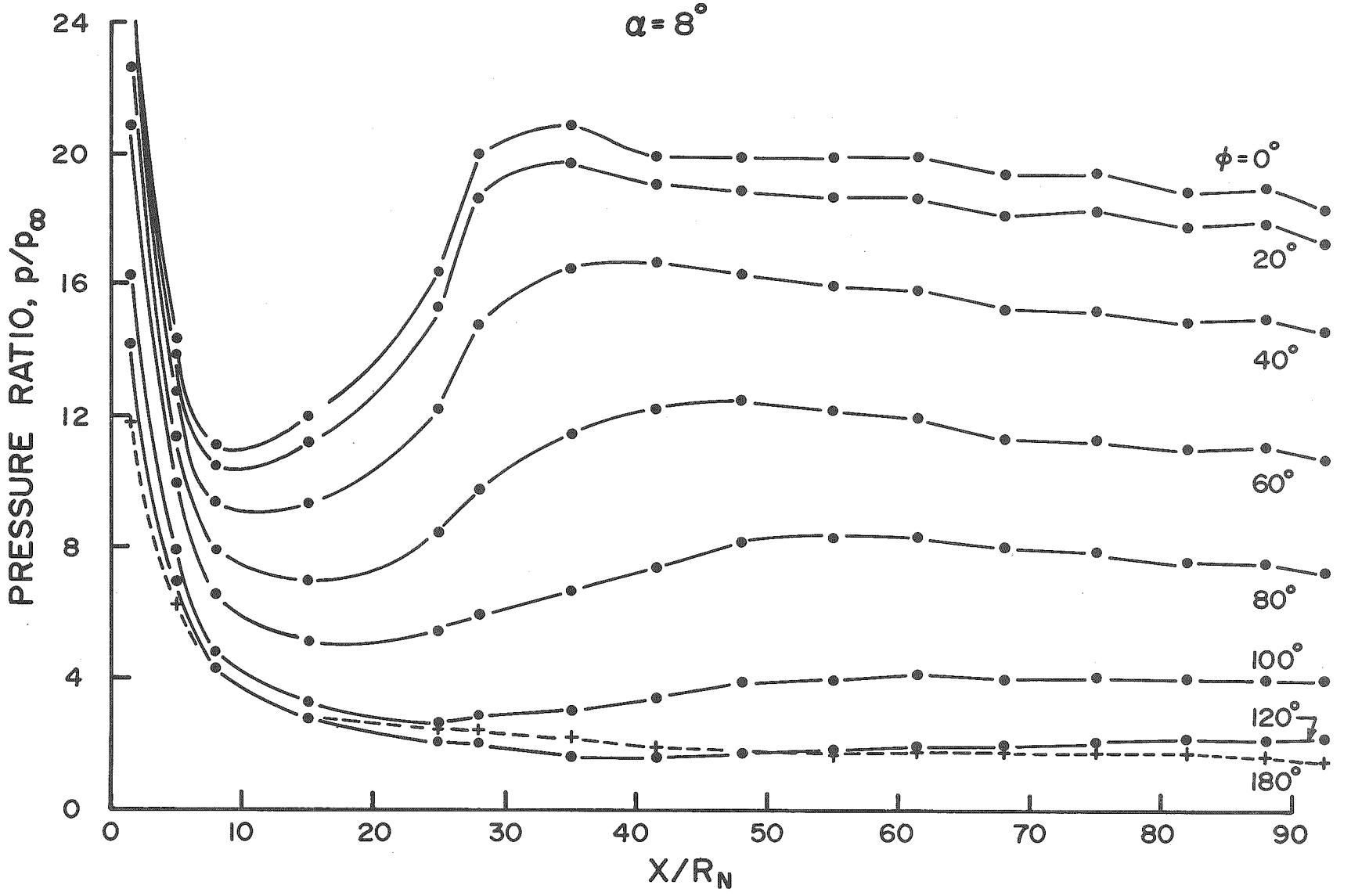

Figure 60. Longitudinal Pressure Distributions, 10% Bluntness, α = 8 Degrees

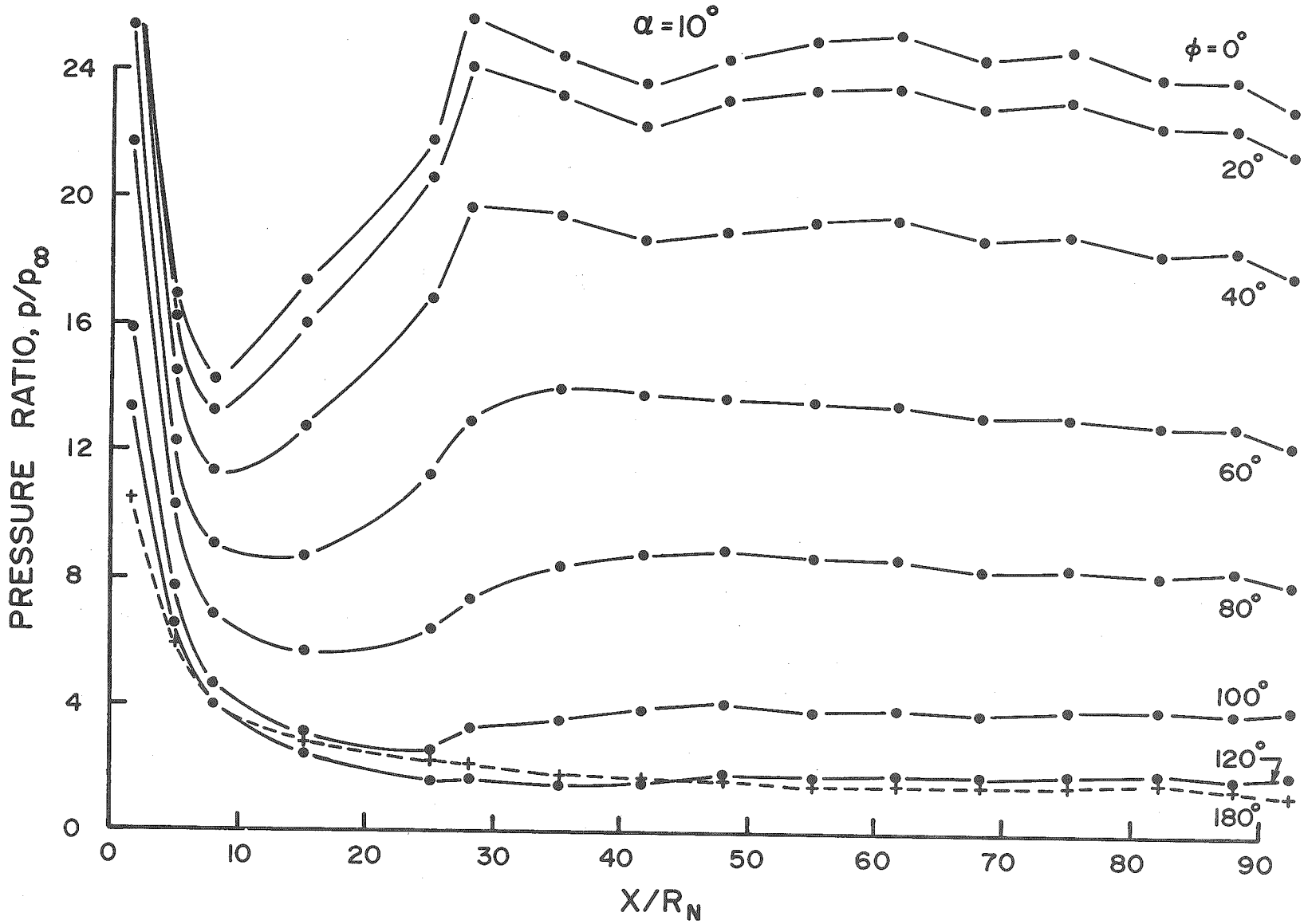

Figure 61. Longitudinal Pressure Distributions, 10% Bluntness, α = 10 Degrees

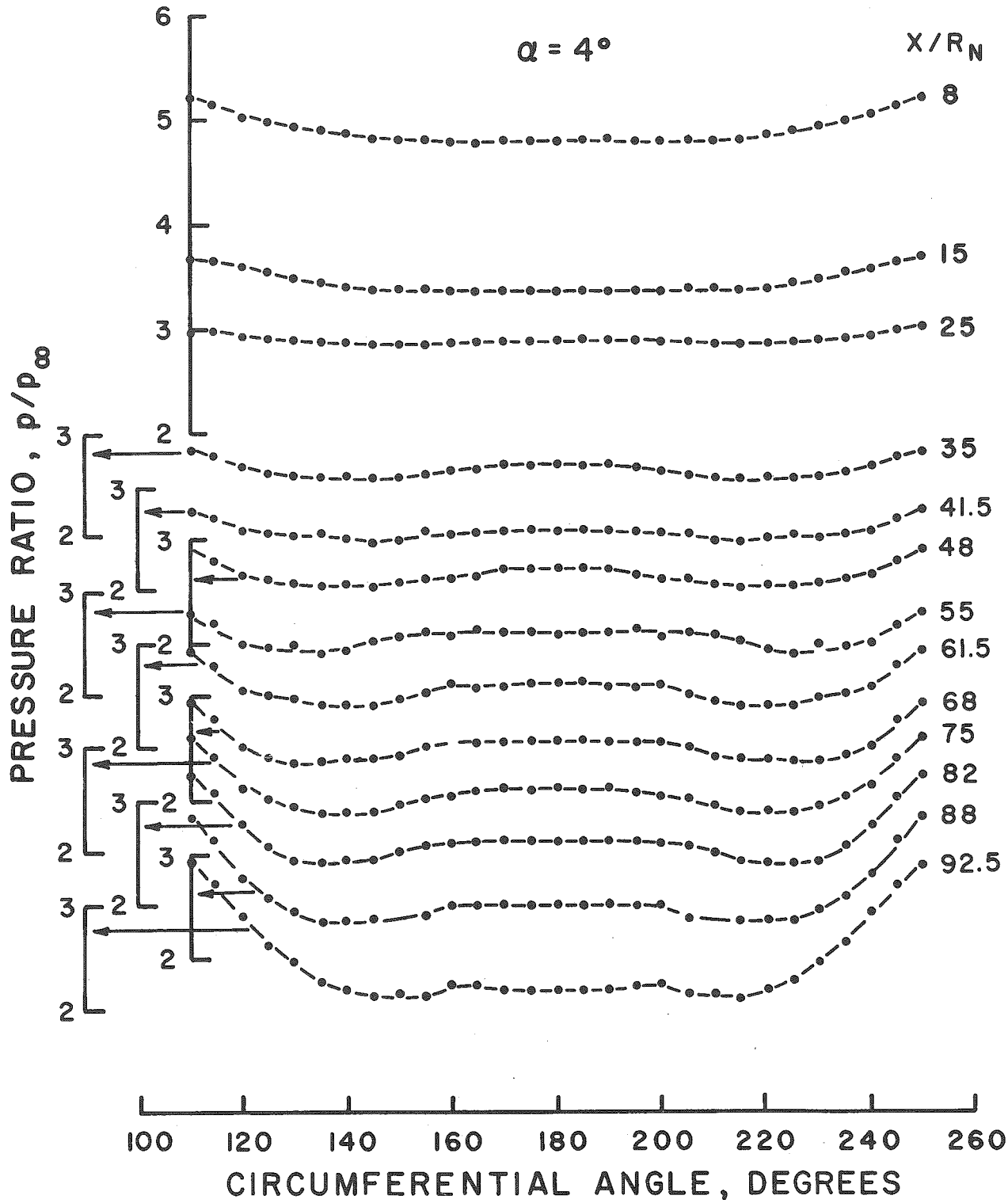

Figure 62. Circumferential Pressure Distributions, 10% Bluntness, α = 4 Degrees

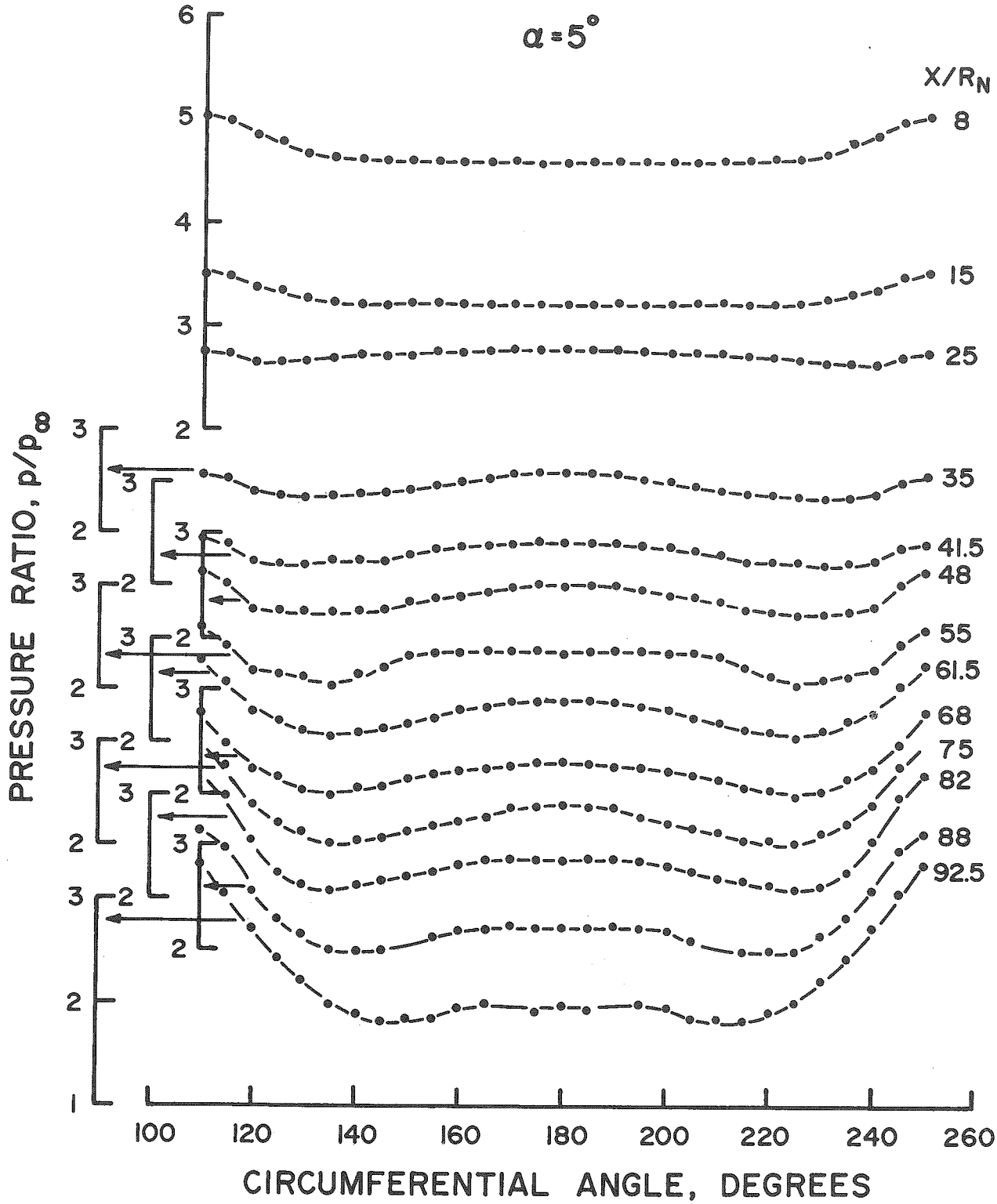

Figure 63. Circumferential Pressure Distributions, 10% Bluntness, α = 5 Degrees

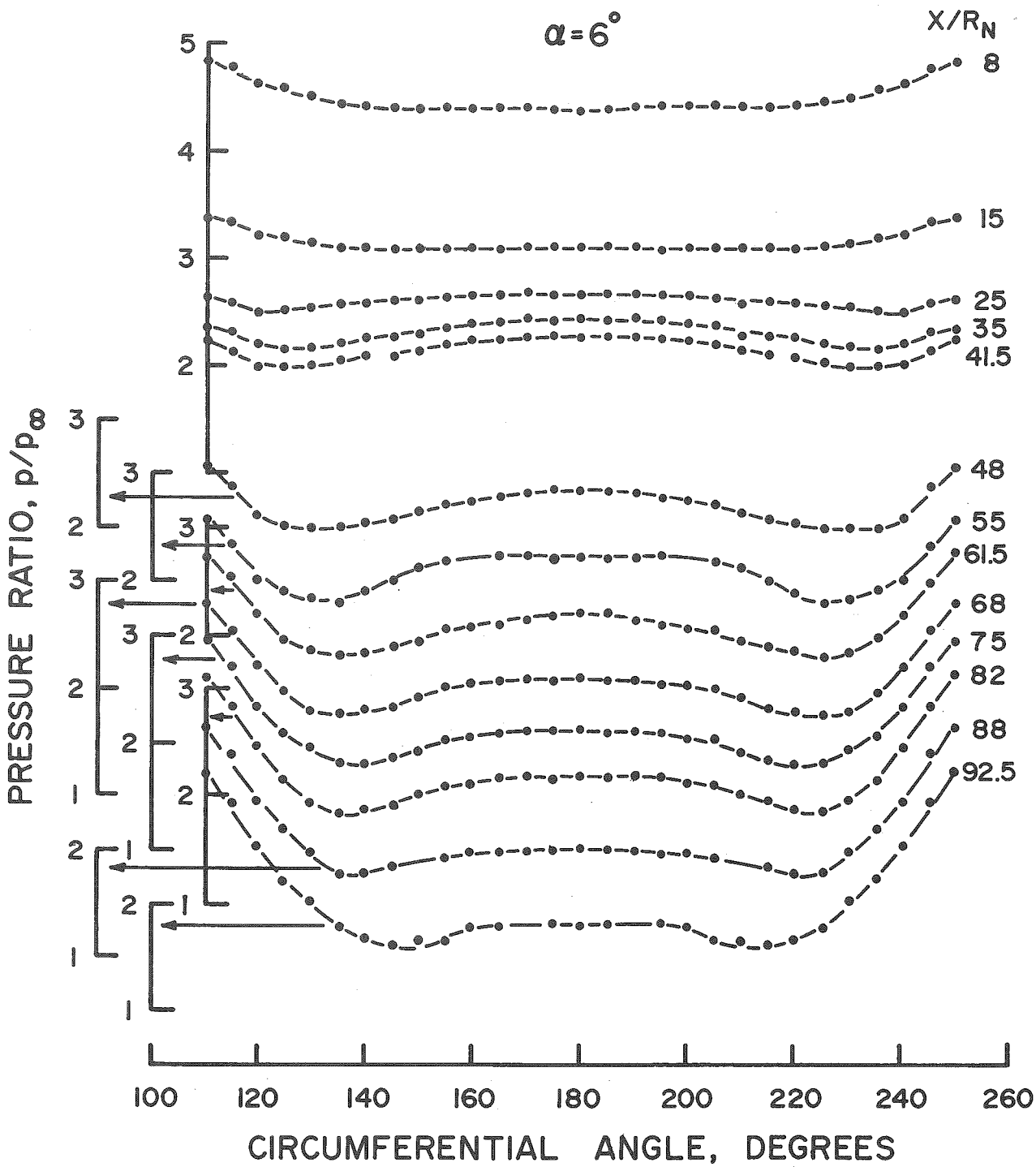

Figure 64. Circumferential Pressure Distributions, 10% Bluntness, α = 6 Degrees

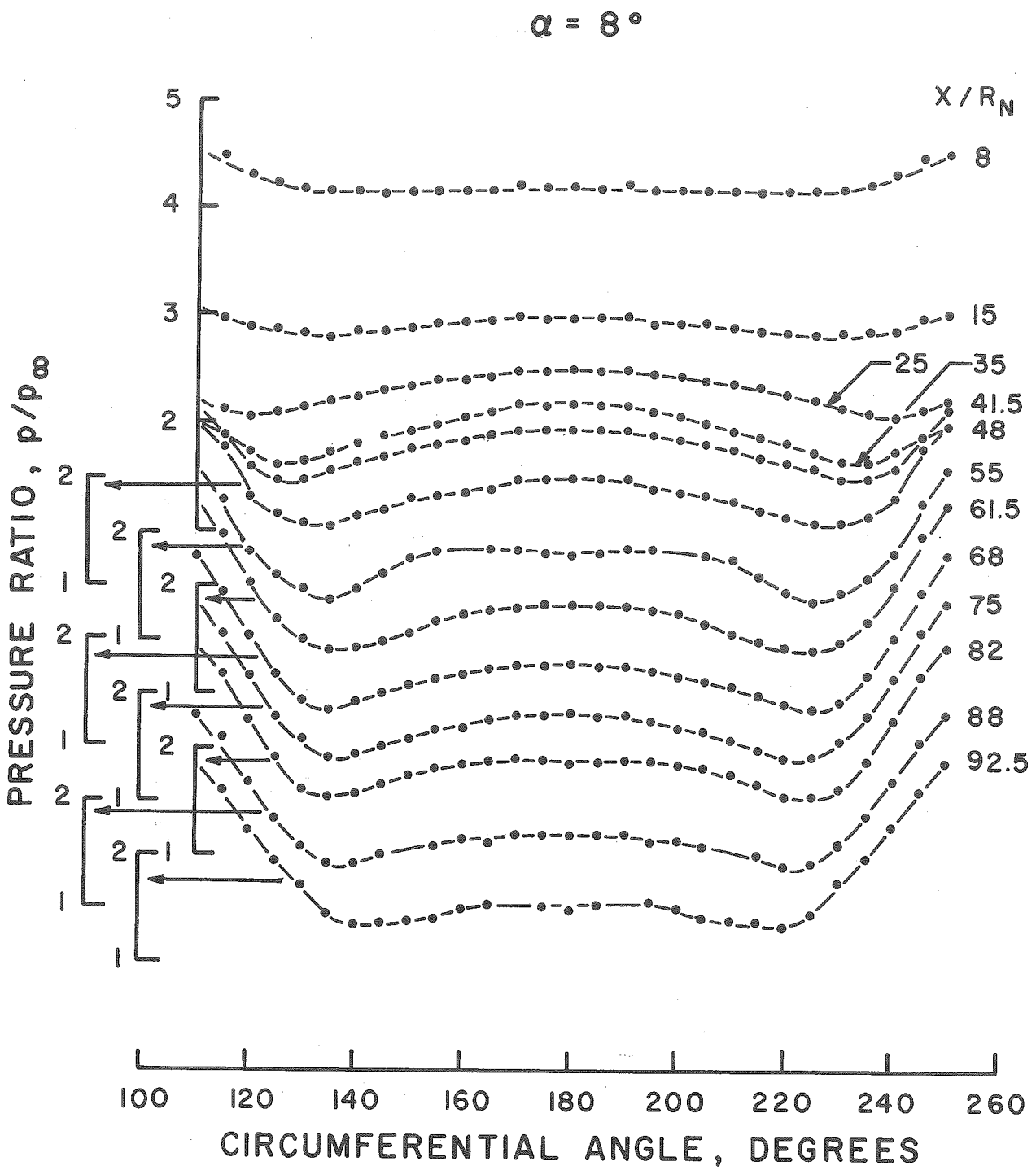

Figure 65. Circumferential Pressure Distributions, 10% Bluntness, α = 8 Degrees

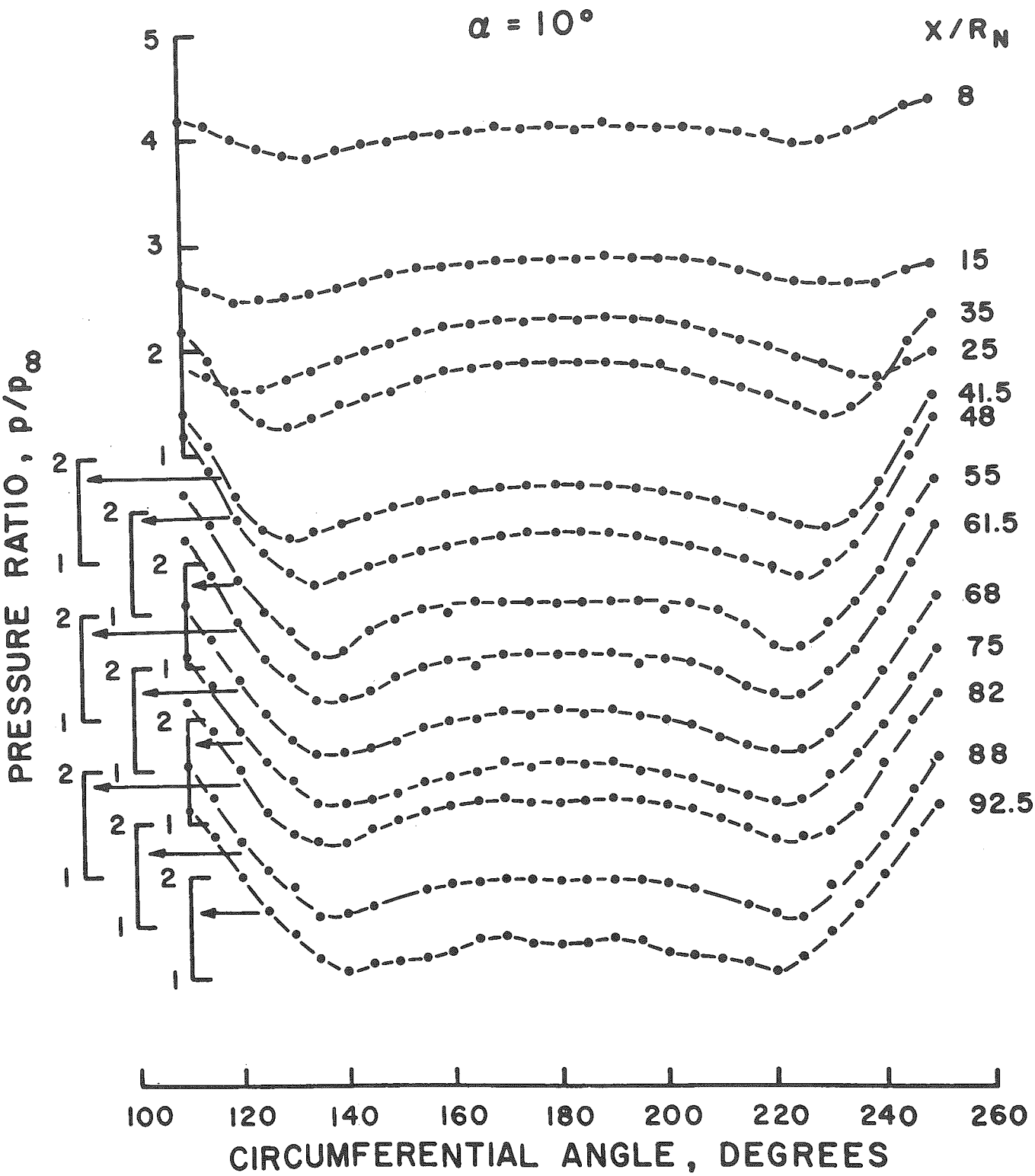

Figure 66. Circumferential Pressure Distributions, 10% Bluntness, α = 10 Degrees

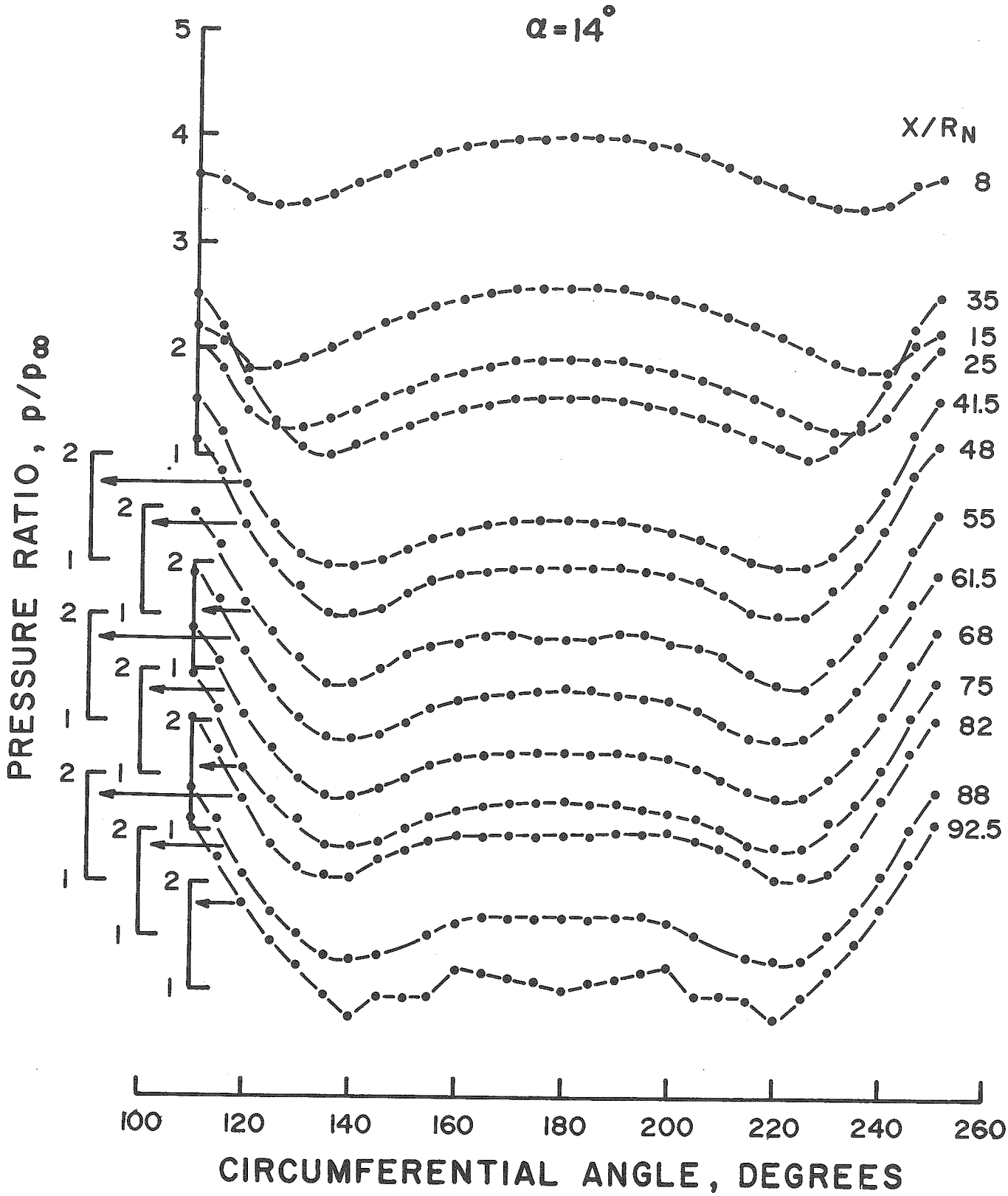

Figure 67. Circumferential Pressure Distributions, 10% Bluntness, α = 14 Degrees

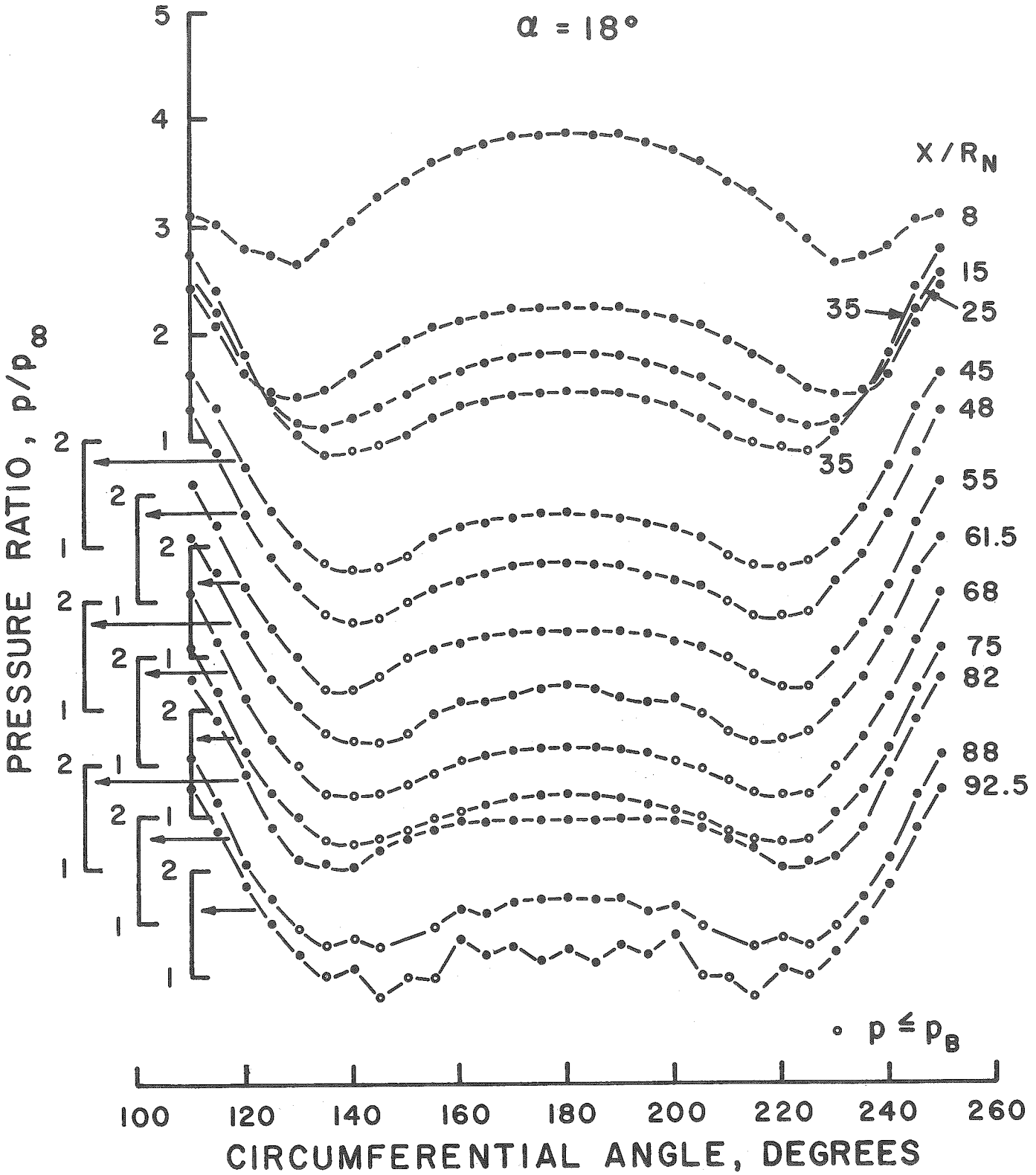

Figure 68. Circumferential Pressure Distributions, 10% Bluntness, α = 18 Degrees

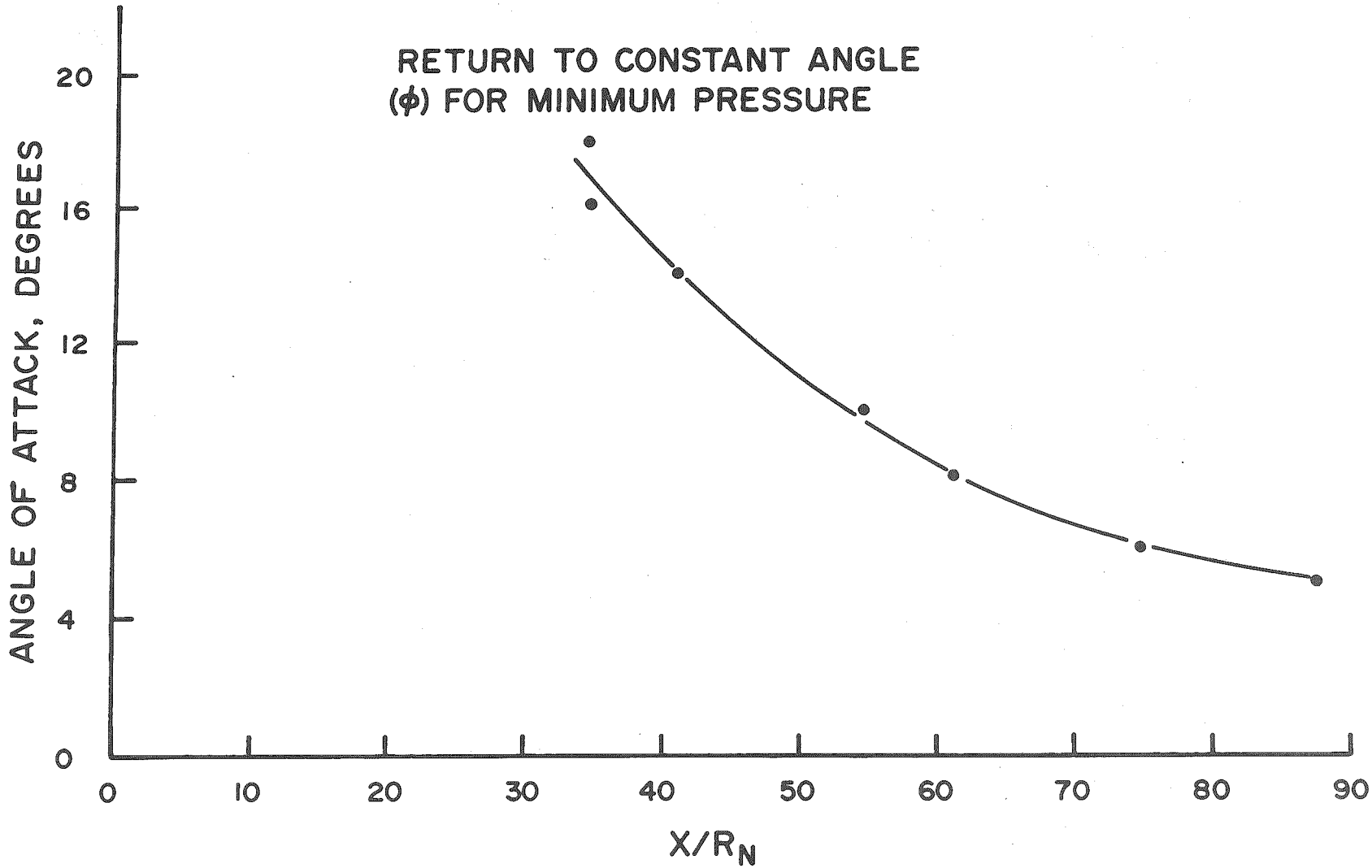

Figure 69. Distance to Return to Constant Angle (ϕ) for Minimum Pressure

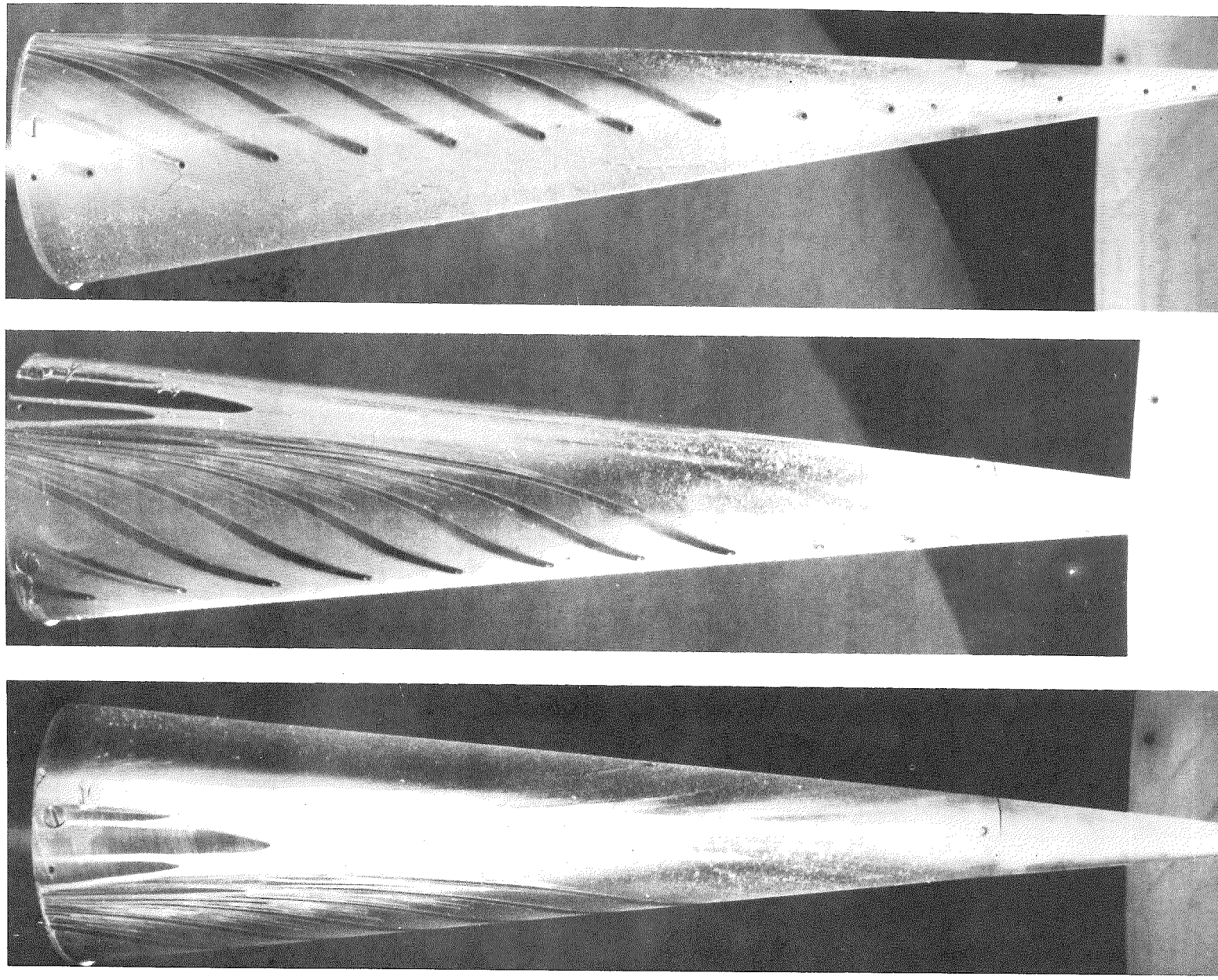

Figure 70. Oil Flow Photographs, Side and Leeward Views, 10% Bluntness, α = 4 Degrees

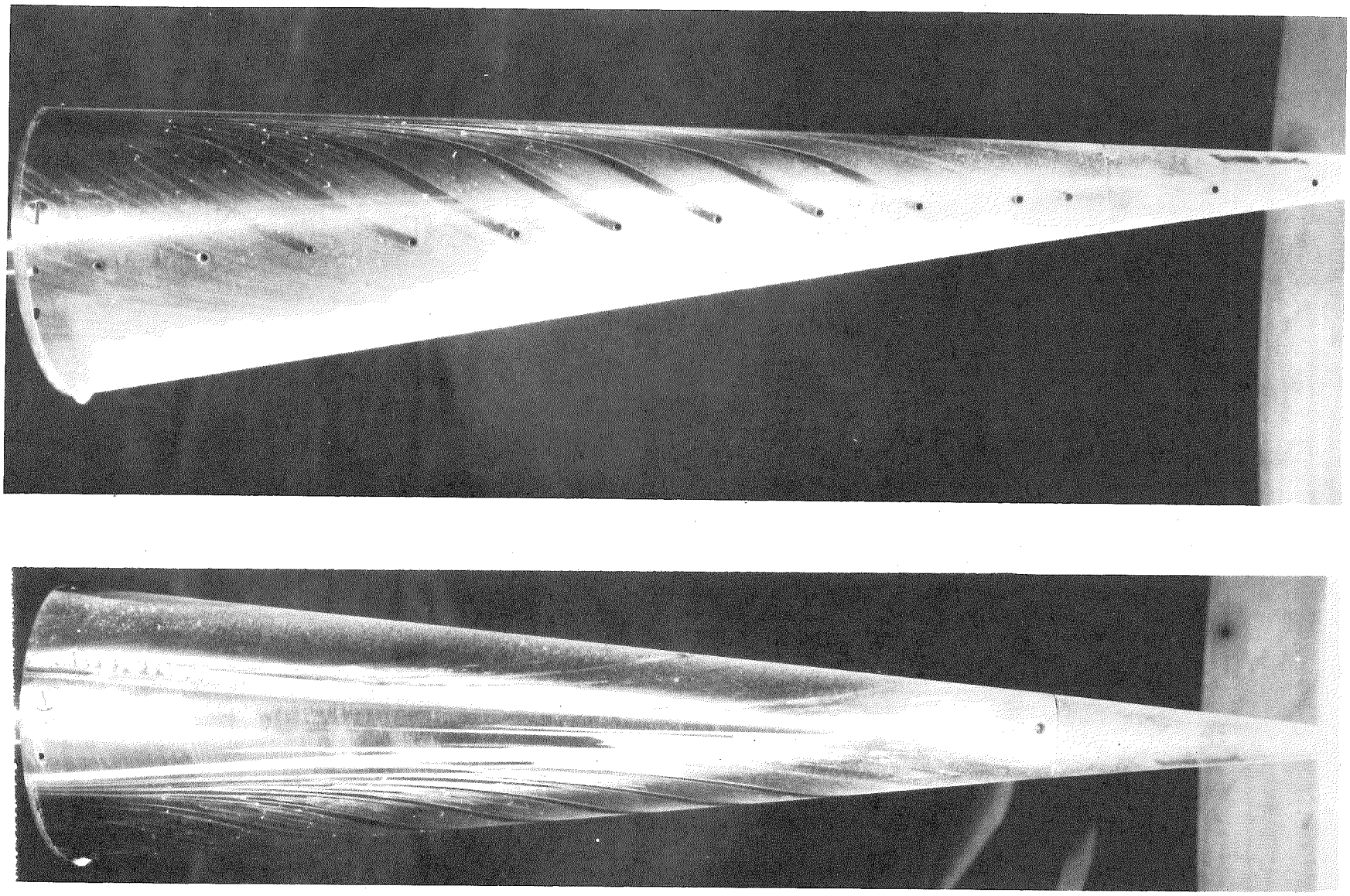

Figure 71. Oil Flow Photographs, Side and Leeward Views, 10% Bluntness, α = 4-1/2 Degrees

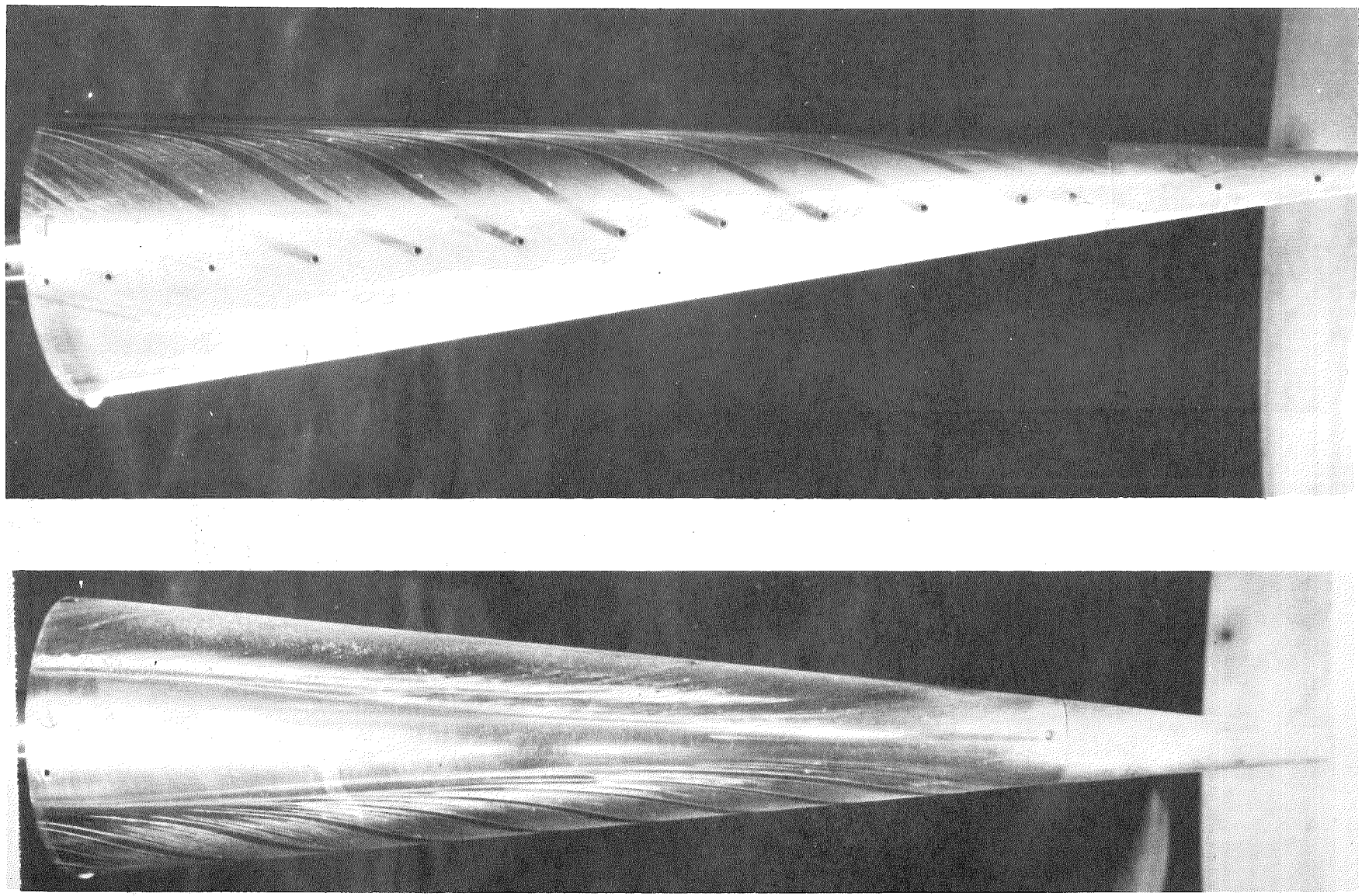

Figure 72. Oil Flow Photographs, Side and Leeward Views, 10% Bluntness, α = 5 Degrees

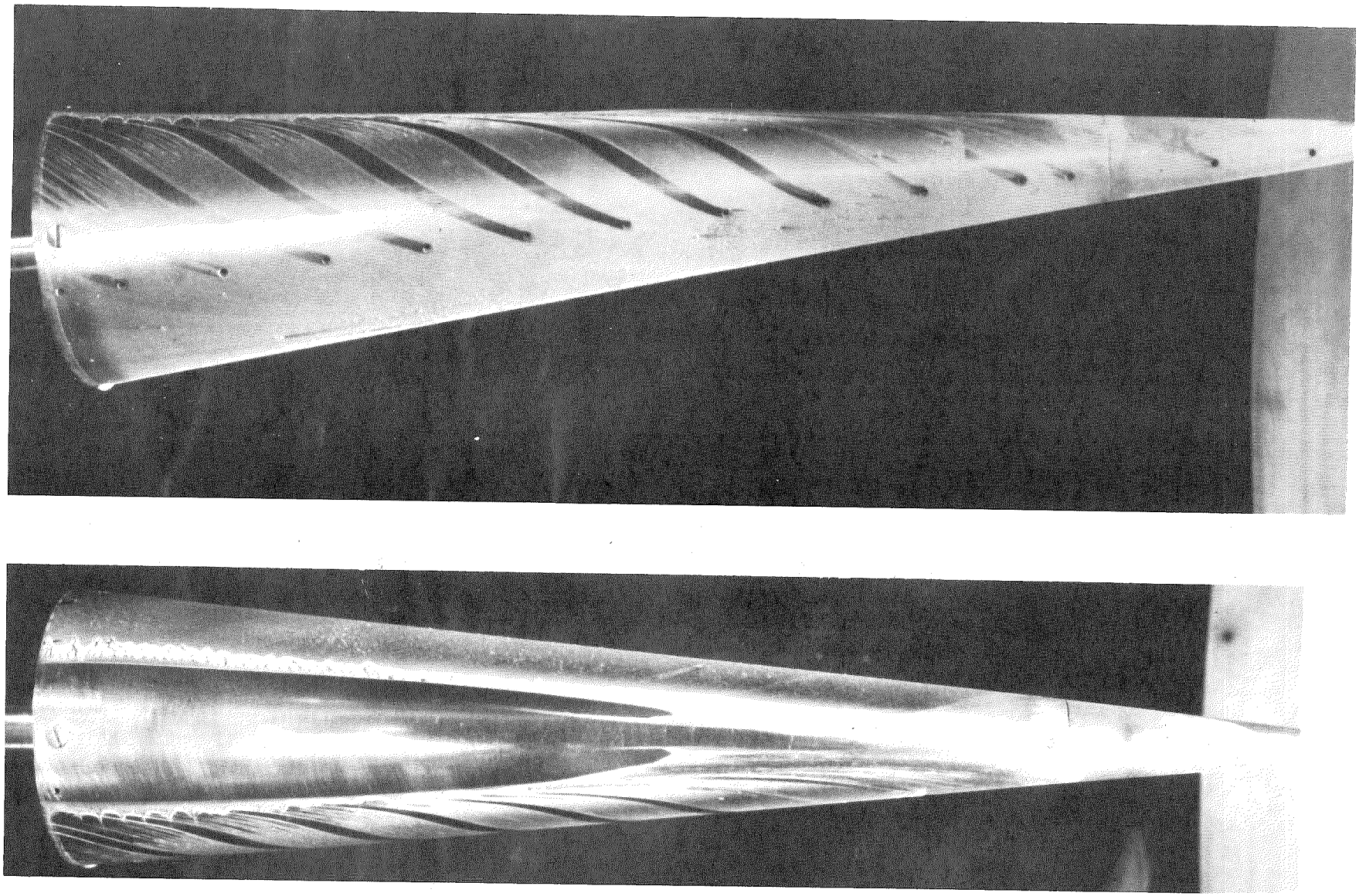

Figure 73. Oil Flow Photographs, Side and Leeward Views, 10% Bluntness, α = 6 Degrees

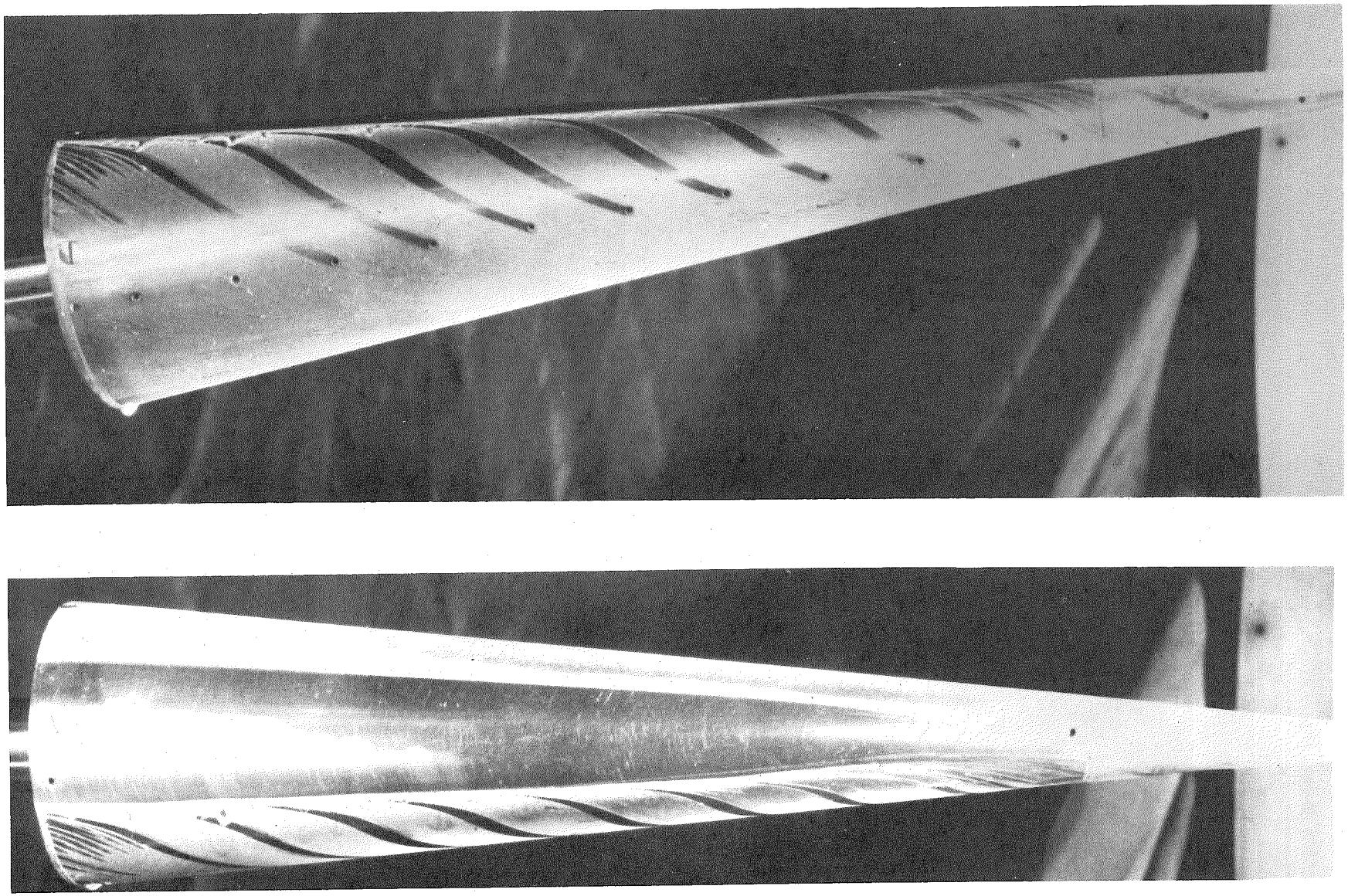

Figure 74. Oil Flow Photographs, Side and Leeward Views, 10% Bluntness, α = 8 Degrees

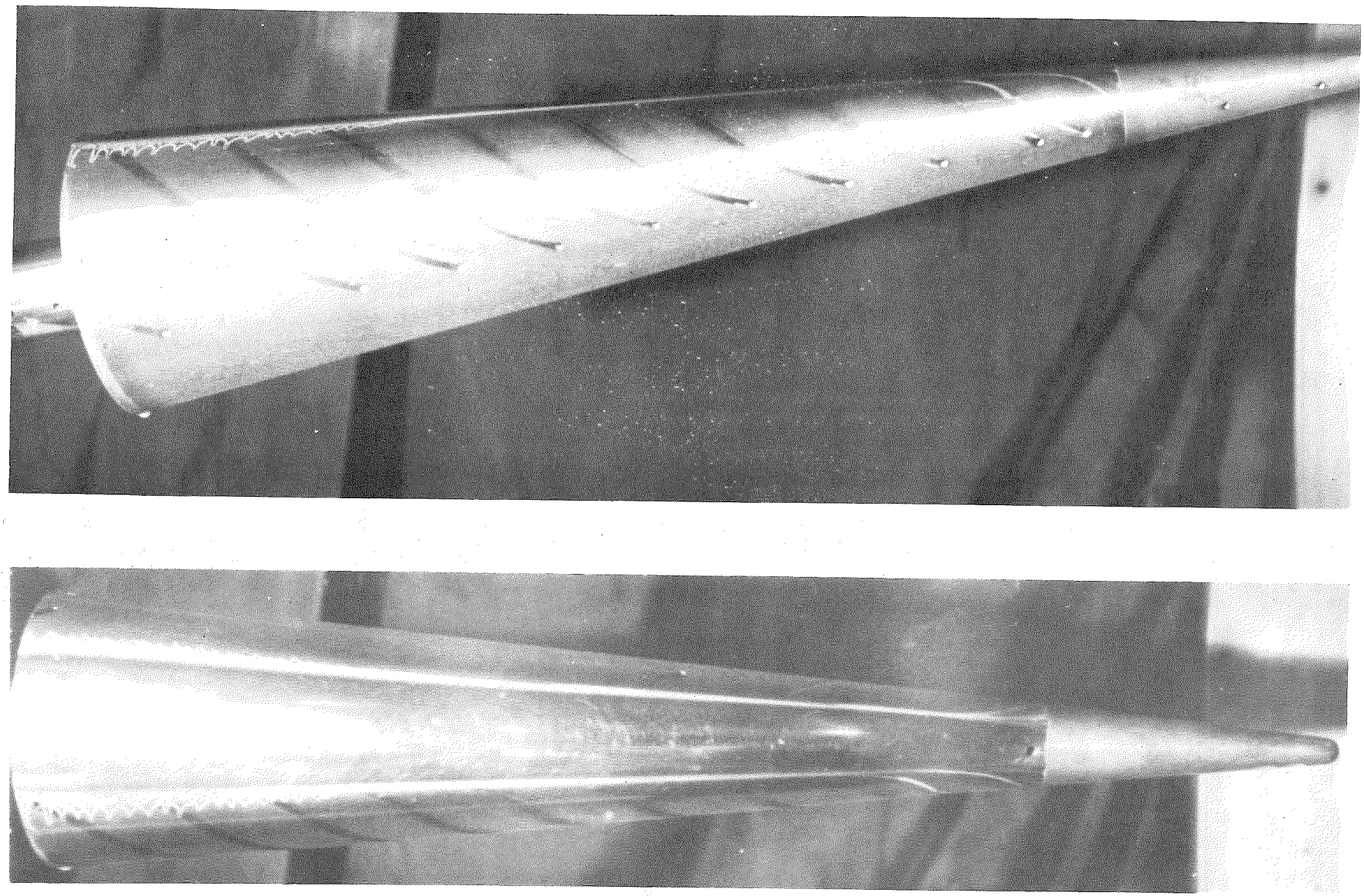

Figure 75. Oil Flow Photographs, Side and Leeward Views, 10% Bluntness, α = 10 Degrees

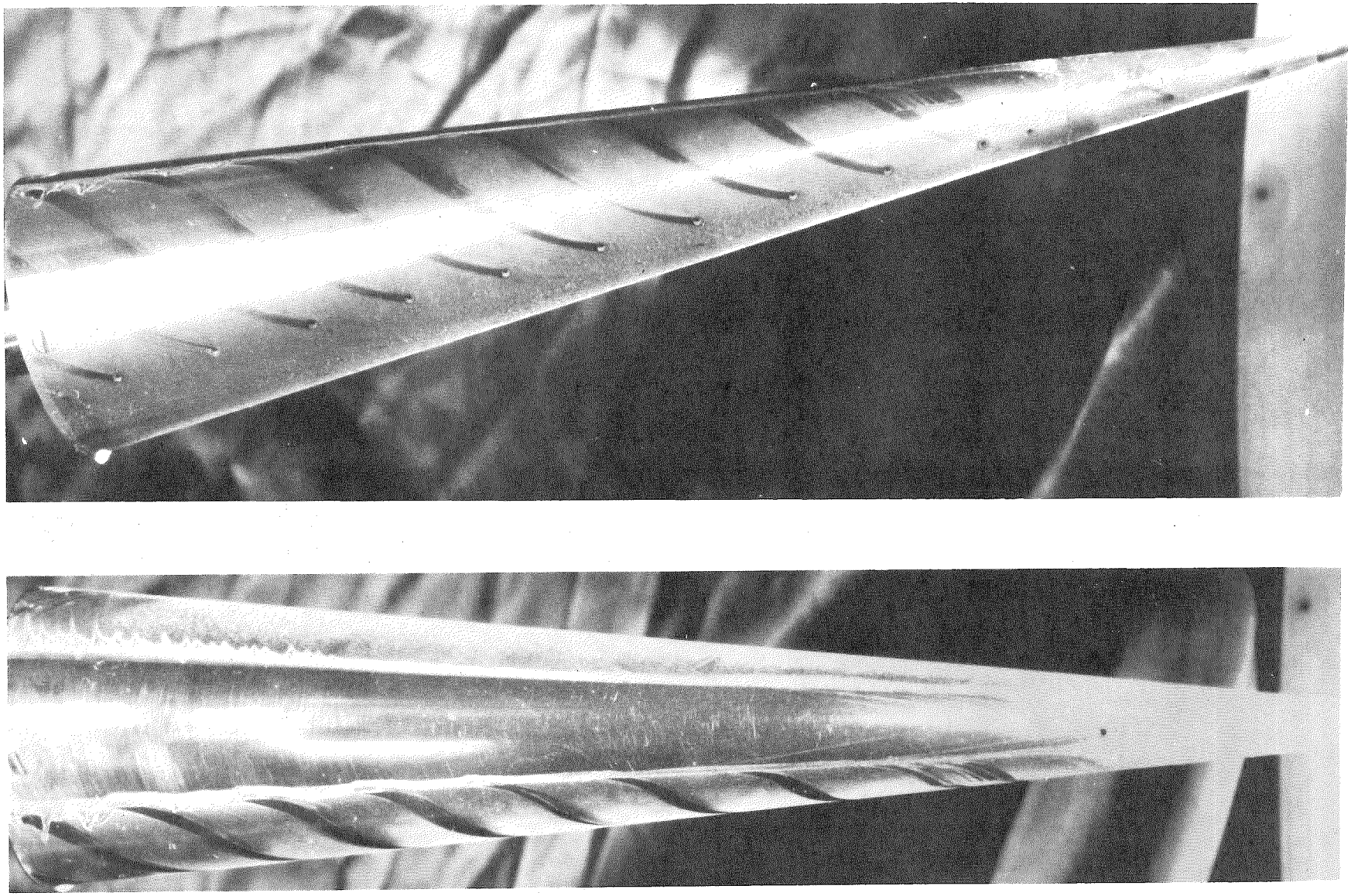

Figure 76. Oil Flow Photographs, Side and Leeward Views, 10% Bluntness, α = 12 Degrees

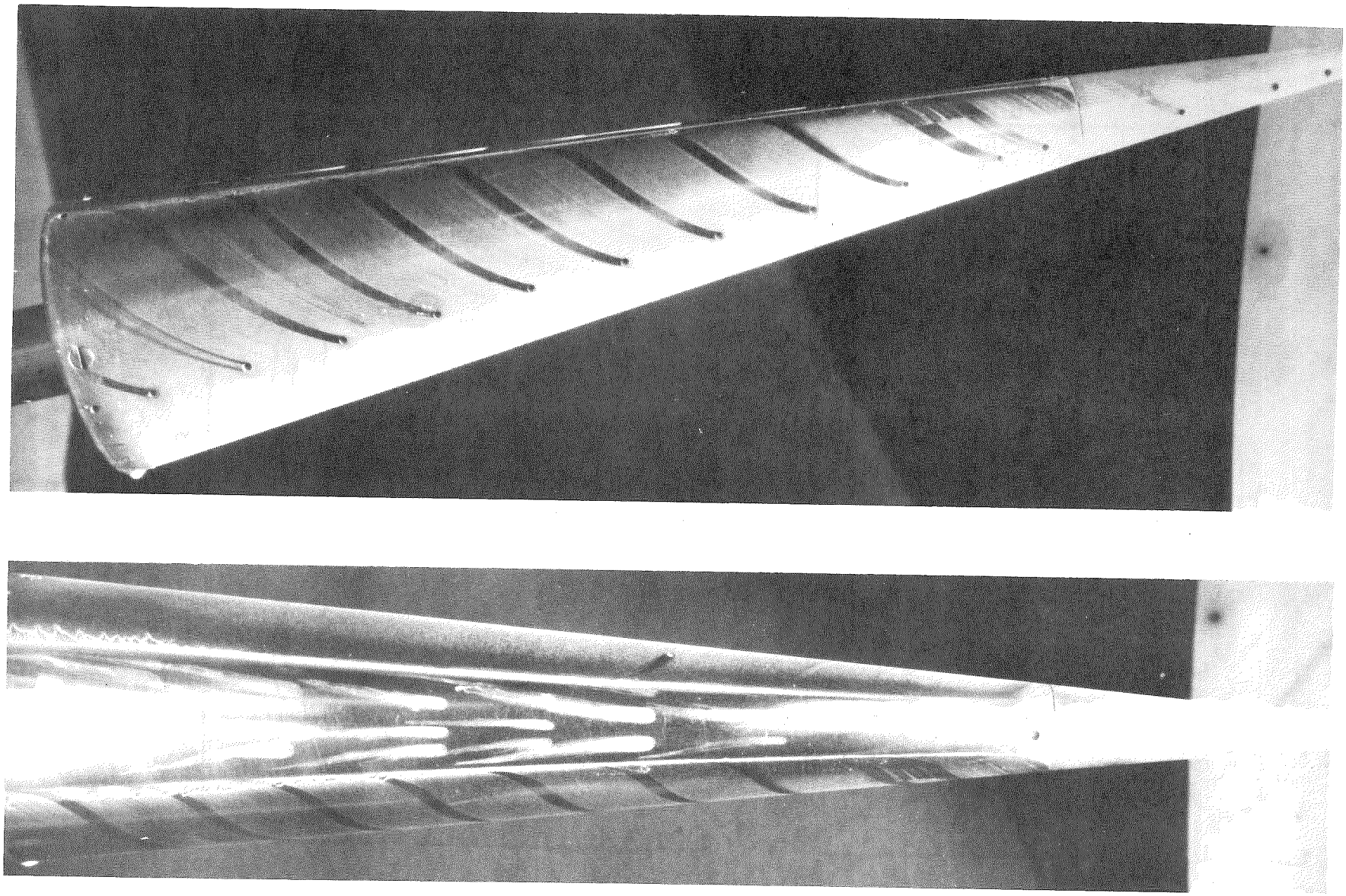

Figure 77. Oil Flow Photographs, Side and Leeward Views, 10% Bluntness, α = 14 Degrees

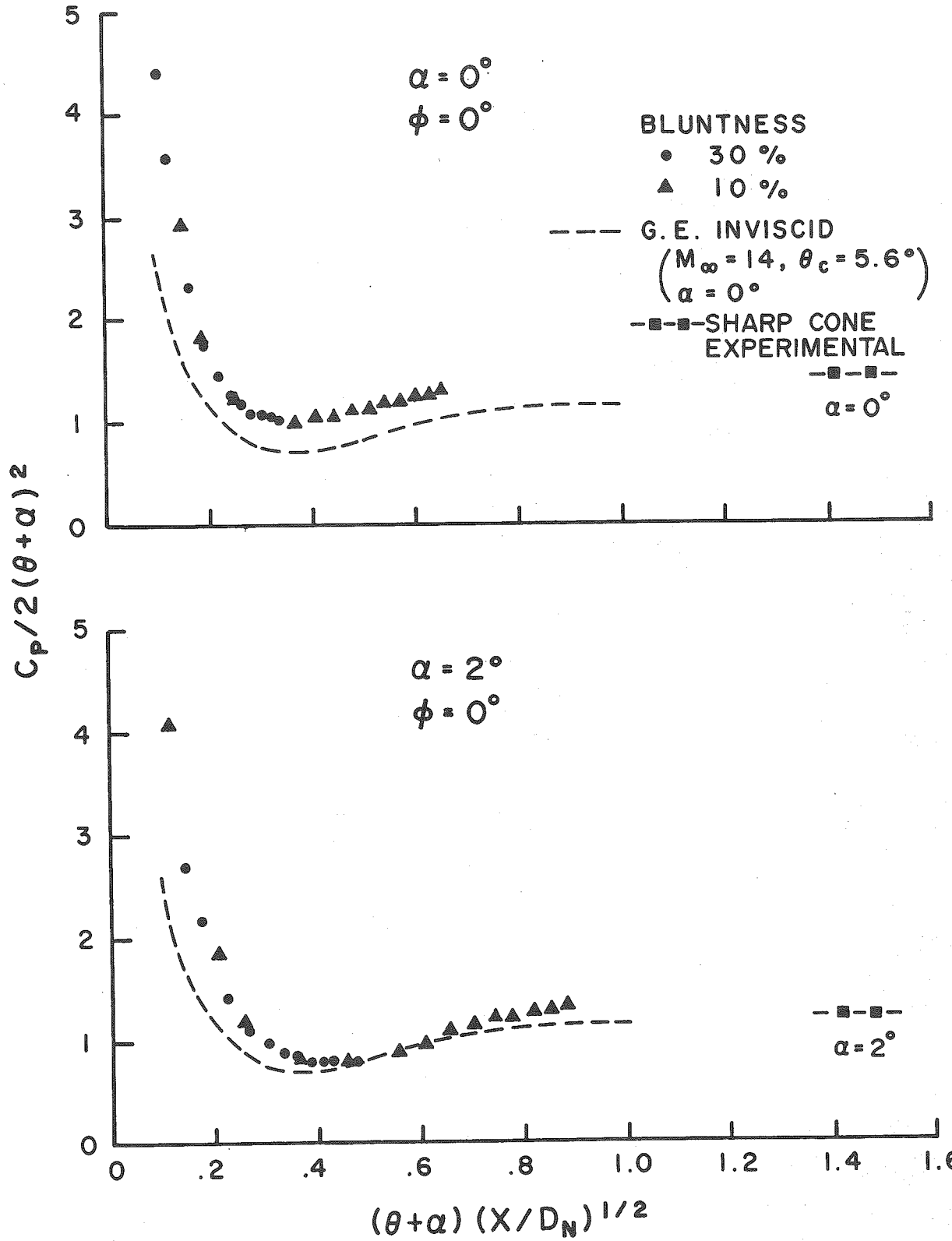

Figure 78. Blunt Cone Pressure Correlation, α = 0 and 2 Degrees

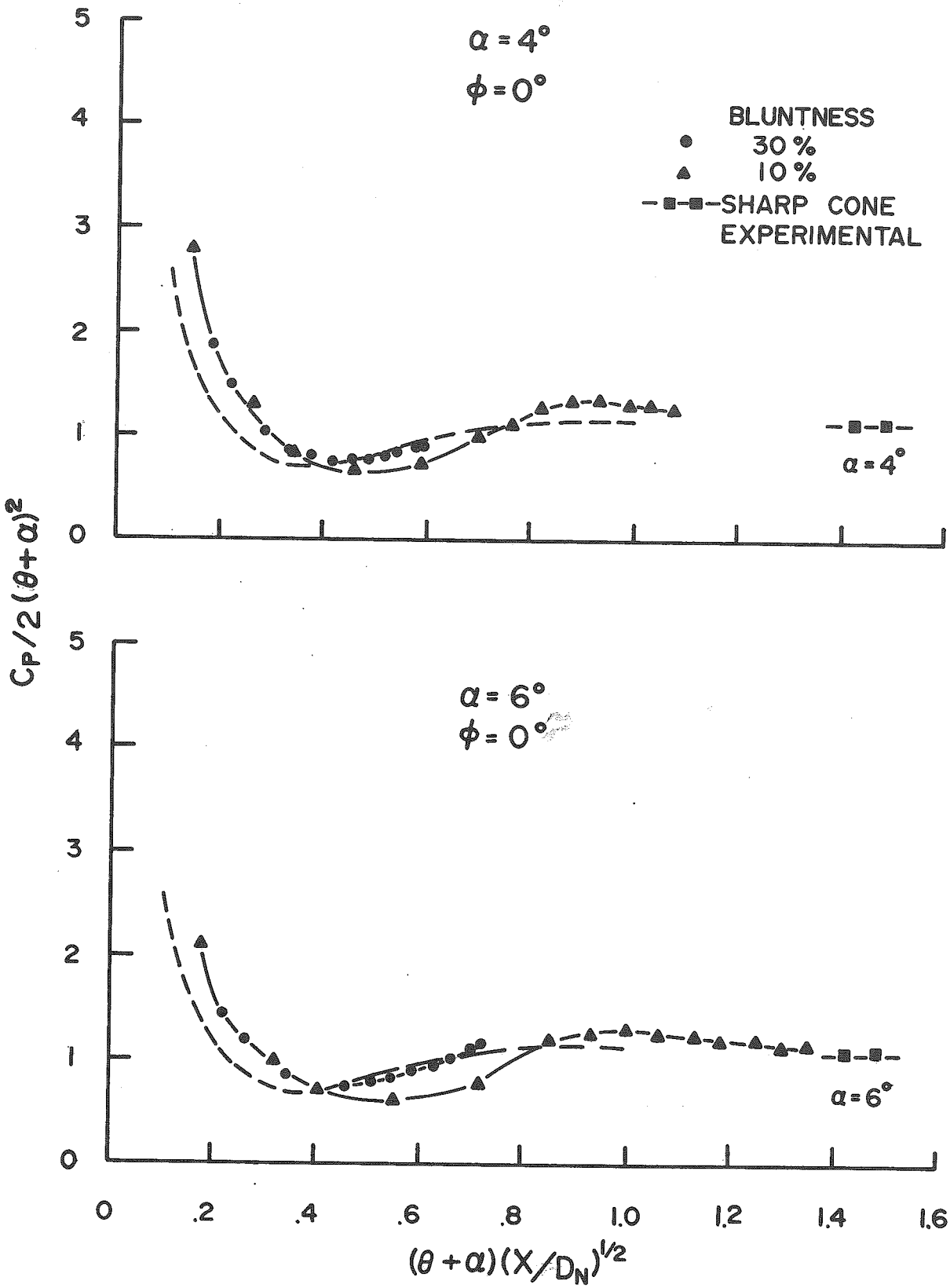

Figure 79. Blunt Cone Pressure Correlation, α = 4 and 6 Degrees

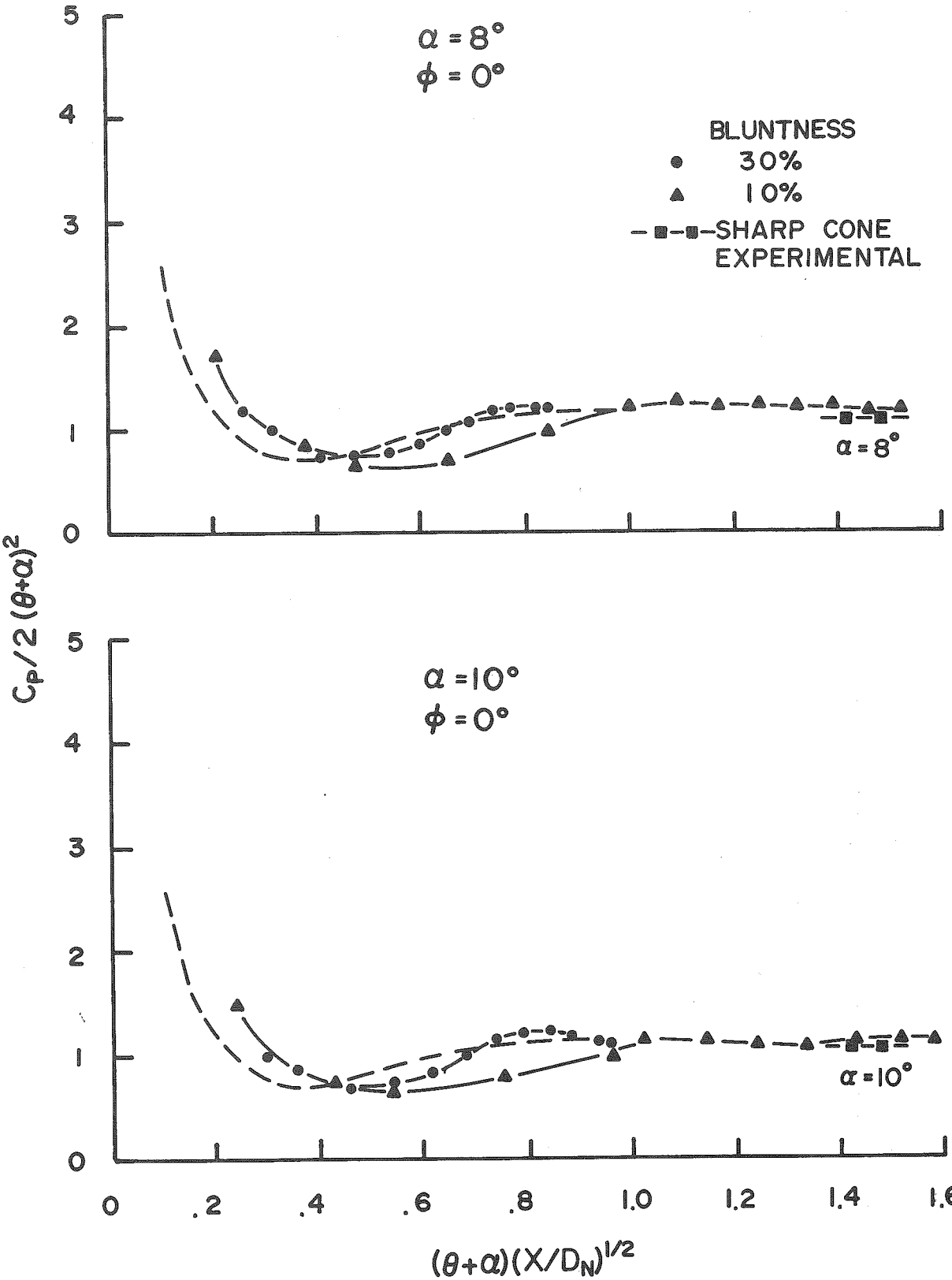

Figure 80. Blunt Cone Pressure Correlation, α = 8 and 10 Degrees

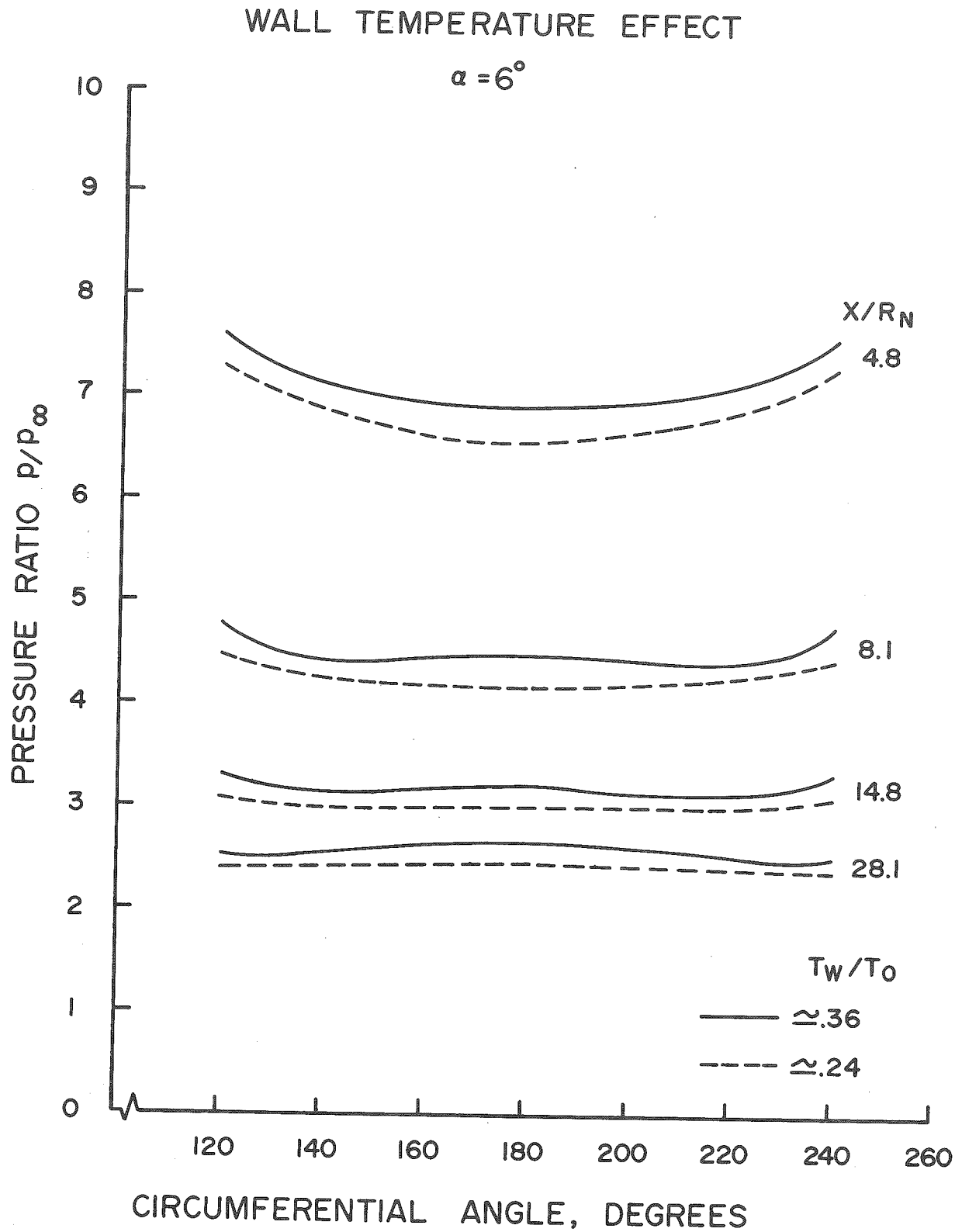

Figure 81(a). Circumferential Pressure Distributions for Two Wall Temperatures, 10% Bluntness

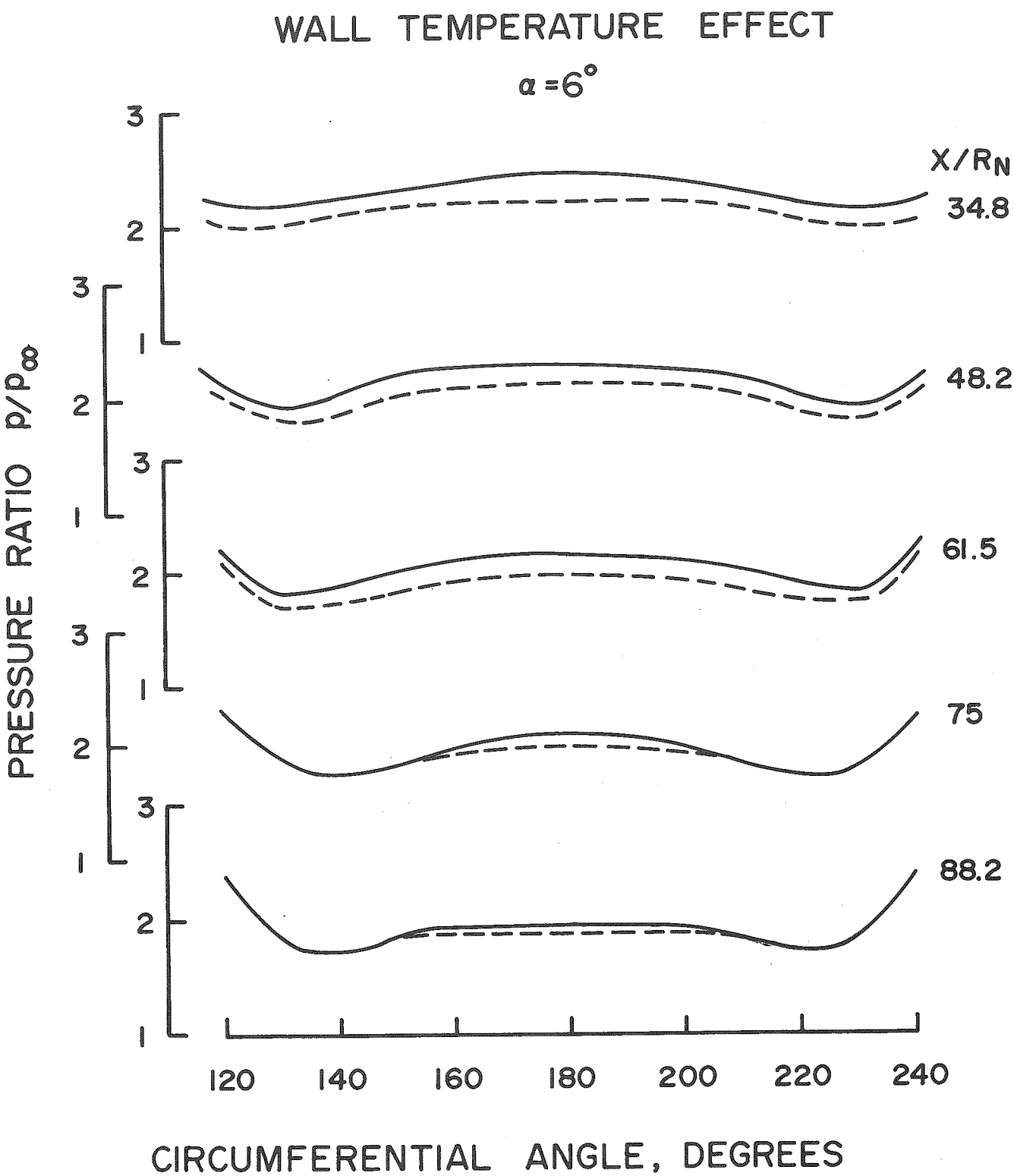

Figure 81(b). Circumferential Pressure Distributions for Two Wall Temperatures, 10% Bluntness

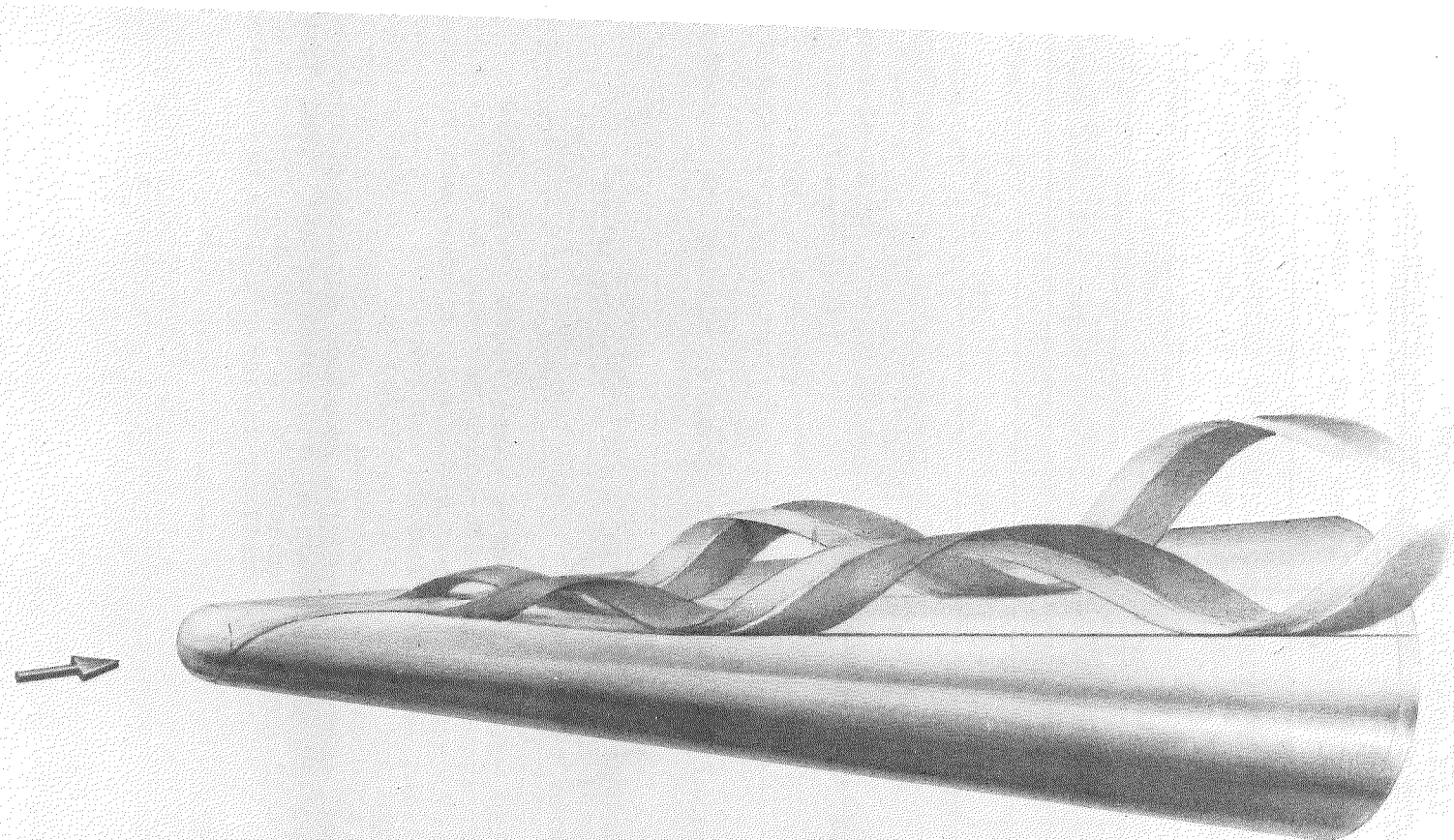

Figure 82. Conceptual Drawing of New Model of Boundary-Layer Separation on a Blunt Cone at Angle of Attack

UNCLASSIFIED
Security Classification

DOCUMENT CONTROL DATA - R & D

(Security classification of title, body of abstract and indexing annotation must be entered when the overall report is classified)

1. ORIGINATING ACTIVITY *(Corporate author)*
Aerospace Research Laboratories, AFSC
Wright-Patterson Air Force Base, Ohio 45433

2a. REPORT SECURITY CLASSIFICATION
Unclassified

2b. GROUP

3. REPORT TITLE
EXPERIMENTAL RESULTS OF LAMINAR BOUNDARY LAYER SEPARATION ON A SLENDER CONE AT ANGLE OF ATTACK AT $M_\infty = 14.2$

4. DESCRIPTIVE NOTES *(Type of report and inclusive dates)*
Scientific. Final.

5. AUTHOR(S) *(First name, middle initial, last name)*
Kenneth F. Stetson

6. REPORT DATE	7a. TOTAL NO. OF PAGES	7b. NO. OF REFS
August 1971	108	23

8a. CONTRACT OR GRANT NO.	9a. ORIGINATOR'S REPORT NUMBER(S)
In-house b. PROJECT NO. 7065-00-22 c. DoD Element 61102F d. DoD Subelement 681307	9b. OTHER REPORT NO(S) *(Any other numbers that may be assigned this report)* ARL 71-0127

10. DISTRIBUTION STATEMENT
Approved for public release; distribution unlimited.

11. SUPPLEMENTARY NOTES	12. SPONSORING MILITARY ACTIVITY
TECH OTHER	Fluid Dynamics Facilities Rsch Lab Aerospace Research Laboratories Wright-Patterson AFB, Ohio

13. ABSTRACT

Wind tunnel experiments with a 5.6 degree half angle cone at $M_\infty = 14.2$ indicated that the three-dimensional separation bubble concept was not the correct flow field model for these data. Based on data consisting of surface pressure measurements, pitot pressure surveys, and surface oil flow patterns, a new model for hypersonic three-dimensional separation is proposed. This model contains symmetrical supersonic helical vortices with an attachment line on the most leeward ray. The vortices are in contact with the surface (at least up to $\alpha = 18°$) and there is no subsonic reverse flow or singular points associated with the vortex pattern.

DD FORM 1 NOV 65 1473

UNCLASSIFIED
Security Classification